CMS

CMS-HIG-19-001

arXiv:2103.04956v1 [hep-ex] 8 Mar 2021

# Measurements of production cross sections of the Higgs boson in the four-lepton final state in proton-proton collisions at $\sqrt{s} = 13\,\text{TeV}$

The CMS Collaboration*

## Abstract

Production cross sections of the Higgs boson are measured in the $\text{H} \rightarrow \text{ZZ} \rightarrow 4\ell$ ($\ell = \text{e}, \mu$) decay channel. A data sample of proton-proton collisions at a center-of-mass energy of 13 TeV, collected by the CMS detector at the LHC and corresponding to an integrated luminosity of $137\,\text{fb}^{-1}$ is used. The signal strength modifier $\mu$, defined as the ratio of the Higgs boson production rate in the $4\ell$ channel to the standard model (SM) expectation, is measured to be $\mu = 0.94 \pm 0.07\,\text{(stat)}^{+0.09}_{-0.08}\,\text{(syst)}$ at a fixed value of $m_\text{H} = 125.38\,\text{GeV}$. The signal strength modifiers for the individual Higgs boson production modes are also reported. The inclusive fiducial cross section for the $\text{H} \rightarrow 4\ell$ process is measured to be $2.84^{+0.23}_{-0.22}\,\text{(stat)}^{+0.26}_{-0.21}\,\text{(syst)}\,\text{fb}$, which is compatible with the SM prediction of $2.84 \pm 0.15\,\text{fb}$ for the same fiducial region. Differential cross sections as a function of the transverse momentum and rapidity of the Higgs boson, the number of associated jets, and the transverse momentum of the leading associated jet are measured. A new set of cross section measurements in mutually exclusive categories targeted to identify production mechanisms and kinematical features of the events is presented. The results are in agreement with the SM predictions.

*See Appendix A for the list of collaboration members

# 1 Introduction

The discovery of the Higgs boson (H) in 2012 by the ATLAS and CMS collaborations [1–3] has been a major step towards the understanding of the electroweak symmetry breaking mechanism [4–9]. Further studies by the two experiments [10–13] have shown that the properties of the new particle are consistent with the standard model (SM) expectations for the H boson.

The $H \to ZZ \to 4\ell$ decay channel ($\ell = e, \mu$) has a large signal-to-background ratio thanks to a low background rate and the complete reconstruction of the final state decay products, capitalizing on the excellent lepton momentum resolution of the CMS detector. The measurements performed using this decay channel with the LHC Run 1 data set at center-of-mass energies of 7 and 8 TeV, and the Run 2 data set at 13 TeV include the determination of the mass, the spin and the parity of the H boson [14–19], its width [20–23], the inclusive and differential fiducial cross sections [18, 24–28], and the tensor structure of the H boson interaction with a pair of neutral gauge bosons in both on-shell and off-shell regions [17, 19, 21, 29, 30].

This paper presents the measurement of production cross sections in granular kinematic regions of the H boson in the $H \to ZZ \to 4\ell$ decay channel. A data sample of proton-proton (pp) collisions at a center-of-mass energy of $\sqrt{s} = 13$ TeV, collected by the CMS detector at the LHC and corresponding to an integrated luminosity of $137\,\text{fb}^{-1}$ is used. The inclusive signal strength modifier, defined as the ratio of the H boson production rate in the $4\ell$ channel to the SM expectation, and signal strength modifiers for the individual H boson production modes are measured. The measurements of the inclusive and differential fiducial cross sections are also presented, and their compatibility with the SM predictions is tested. The present analysis is similar to that previously performed by the CMS Collaboration [18], but is based on a larger data sample.

In addition, measurements of the H boson cross sections within the simplified template cross section (STXS) framework [31–33] are also presented. The main goals of the STXS framework are to increase the reinterpretability of the precision H boson measurements and to minimize the theory dependence. This is achieved by defining exclusive kinematic regions in the H boson production phase space. These kinematic regions, referred to as bins, are defined in different stages corresponding to increasing degrees of granularity. This paper presents results in the STXS stage 0 where the bins correspond closely to the different H boson production mechanisms. Previous measurements of cross sections in stage 0 production bins in the $H \to 4\ell$ decay channel were already presented by the CMS Collaboration [18]. In the STXS framework, additional stages are defined by further splitting of the bins enhancing the sensitivity to possible signature of physics beyond the SM at high transverse momentum of the H boson. Measurements of stage 0, stage 1, and stage 1.1 cross sections in the $H \to 4\ell$ decay channel were recently published by the ATLAS Collaboration [27]. The most recent refinement of STXS binning is referred to as STXS stage 1.2. This paper presents a first set of the cross section measurements in the STXS stage 1.2 bins in the $H \to 4\ell$ decay channel.

The paper is organized as follows. A brief introduction of the CMS detector is given in Section 2. The data, as well as the simulated signal and background samples, are described in Section 3. The event reconstruction and selection, the kinematic discriminants, and the categorization of the H boson candidate events are described in Sections 4, 5, and 6, respectively. The background estimation is detailed in Section 7 while the signal modeling is described in Section 8. The experimental and theoretical systematic uncertainties are described in Section 9 and the results are presented in Section 10. Concluding remarks are given in Section 11.

## 2 The CMS detector

The central feature of the CMS apparatus is a superconducting solenoid of 6 m internal diameter, providing a magnetic field of 3.8 T. Within the solenoid volume are a silicon pixel and strip tracker, a lead tungstate crystal electromagnetic calorimeter (ECAL), and a brass and scintillator hadron calorimeter (HCAL), each composed of a barrel and two endcap sections. Forward calorimeters extend the pseudorapidity $\eta$ coverage provided by the barrel and endcap detectors. Muons are detected in gas-ionization chambers embedded in the steel flux-return yoke outside the solenoid.

Events of interest are selected using a two-tiered trigger system. The first level, composed of custom hardware processors, uses information from the calorimeters and muon detectors to select events at a rate of around 100 kHz within a fixed latency of about 4 $\mu$s [34]. The second level, known as the high-level trigger, consists of a farm of processors running a version of the full event reconstruction software optimized for fast processing, and reduces the event rate to around 1 kHz before data storage [35].

The candidate vertex with the largest value of summed physics-object squared transverse momentum $p_T^2$ is taken to be the primary pp interaction vertex (PV). The physics objects are the jets, clustered using the jet finding algorithm [36, 37] with the tracks assigned to candidate vertices as inputs, and the associated missing transverse momentum, taken as the negative vector sum of the $p_T$ of those jets.

The electron momentum is estimated by combining the energy measurement in the ECAL with the momentum measurement in the tracker. The momentum resolution for electrons with $p_T \approx$ 45 GeV from Z $\to$ ee decays ranges from 1.7% to 4.5%. It is generally better in the barrel region than in the endcaps, and also depends on the bremsstrahlung energy emitted by the electron as it traverses the material in front of the ECAL [38]. The ECAL consists of 75 848 lead tungstate crystals, which provide coverage of $|\eta| < 1.48$ in the barrel region and $1.48 < |\eta| < 3.00$ in the two endcap regions (EE). Preshower detectors consisting of two planes of silicon sensors interleaved with a total of $3X_0$ of lead are located in front of each EE detector.

Muons are measured in the pseudorapidity range $|\eta| < 2.4$, with detection planes made using three technologies: drift tubes, cathode strip chambers, and resistive plate chambers. The single muon trigger efficiency exceeds 90% over the full $\eta$ range, and the efficiency to reconstruct and identify muons is greater than 96%. Matching muons to tracks measured in the silicon tracker results in a relative transverse momentum resolution, for muons with $p_T$ up to 100 GeV, of 1% in the barrel and 3% in the endcaps. The $p_T$ resolution in the barrel is better than 7% for muons with $p_T$ up to 1 TeV [39].

A more detailed description of the CMS detector, together with a definition of the coordinate system used and the relevant kinematic variables, can be found in Ref. [40].

## 3 Data and simulated samples

This analysis is based on the pp collision data collected by the CMS detector at the LHC in 2016, 2017, and 2018 with integrated luminosities of 35.9, 41.5, and 59.7 fb$^{-1}$, respectively [41–43]. The collision events are selected by high-level trigger algorithms that require the presence of leptons passing loose identification and isolation requirements. The main triggers select either a pair of electrons or muons, or an electron and a muon. The minimal transverse momentum of the leading and subleading leptons changed throughout the years to account for the different data-taking conditions and is summarized in Table 1.

Table 1: The minimal $p_{\mathrm{T}}$ of the leading/subleading leptons for the main di-electron (e/e), di-muon ($\mu/\mu$), and electron-muon (e/$\mu$, $\mu$/e) high-level trigger algorithms used in the H $\rightarrow 4\ell$ analysis in 2016, 2017, and 2018.

|  | e/e (GeV) | $\mu/\mu$ (GeV) | e/$\mu$, $\mu$/e (GeV) |
|---|---|---|---|
| 2016 | 17/12 | 17/8 | 17/8, 8/23 |
| 2017 | 23/12 | 17/8 | 23/8, 12/23 |
| 2018 | 23/12 | 17/8 | 23/8, 12/23 |

To maximize the coverage of the H $\rightarrow 4\ell$ phase space, triggers requiring three leptons with relaxed transverse momenta thresholds and no isolation requirement are also used, as are isolated single-electron and single-muon triggers. The overall trigger efficiency for simulated signal events that pass the full event selection (described in Section 4) is larger than 99%. The trigger efficiency is derived from data using a sample of $4\ell$ events collected by the single-lepton triggers and a method based on the "tag and probe" technique. One of the four leptons is matched to a candidate reconstructed by the single-lepton trigger and the remaining three leptons in the event are used as probes. The probe leptons are combined in an attempt to reconstruct any of the triggers used in the analysis. The efficiency in data is found to be in agreement with the expectation from the simulation.

Monte Carlo (MC) simulation samples for the signals and the relevant background processes are used to evaluate the signal shape, estimate backgrounds, optimize the event selection, and evaluate the acceptance and systematic uncertainties. The SM H boson signals are simulated at next-to-leading order (NLO) in perturbative QCD (pQCD) with the POWHEG 2.0 [44–46] generator for the five main production processes: gluon fusion (ggH) [47], vector boson fusion (VBF) [48], associated production with a vector boson (VH, where V is a W or a Z boson) [49], and associated production with a pair of top quarks (t$\bar{\mathrm{t}}$H) [50]. The ZH production occurs in two ways, q$\overline{\mathrm{q}} \rightarrow$ ZH and a much smaller contribution from gg $\rightarrow$ ZH, which is simulated at leading order (LO) using JHUGEN 7.3.0 [51–55]. In addition to the five main production processes, the contributions due to H boson production in association with a single top quark (q$_{\mathrm{t}}$H) and either a quark (q$_{\mathrm{t}}$Hq) or a W boson (q$_{\mathrm{t}}$HW) are simulated at LO using JHUGEN 7.0.2 and MADGRAPH5_aMC@NLO 2.2.2 [56], respectively. The associated production with a pair of bottom quarks (b$\bar{\mathrm{b}}$H) is simulated at LO with JHUGEN 7.0.2. In all cases, the decay of the H boson to four leptons is modeled with JHUGEN 7.0.2. The theoretical predictions used for the various production and decay modes can be found in Refs. [57–79] and are summarized in Ref. [32].

The ZZ background contribution from quark-antiquark annihilation is simulated at NLO pQCD with POWHEG 2.0 [80], while the gg $\rightarrow$ ZZ process is generated at LO with MCFM 7.0.1 [81]. The WZ background and the triboson backgrounds ZZZ, WZZ, and WWZ are modeled at NLO using MADGRAPH5_aMC@NLO 2.4.2. The smaller t$\bar{\mathrm{t}}$Z, t$\bar{\mathrm{t}}$WW, and t$\bar{\mathrm{t}}$ZZ background processes are simulated at LO with MADGRAPH5_aMC@NLO 2.4.2. The events containing Z bosons with associated jets (Z+jets) are simulated at NLO with MADGRAPH5_aMC@NLO 2.4.2 and the t$\bar{\mathrm{t}}$ background is simulated at NNLO with POWHEG 2.0. The reducible background determination does not rely on the MC but is based on data, as described in Section 7.2.

All signal and background event generators are interfaced with PYTHIA 8.230 [82] using the CUETP8M1 tune [83] for the 2016 data-taking period and the CP5 tune [84] for the 2017 and 2018 data-taking periods, to simulate the multi-parton interaction and hadronization effects. The NNPDF3.0 set of parton distribution functions (PDFs) is used [85]. The generated events are processed through a detailed simulation of the CMS detector based on GEANT4 [86, 87]

and are reconstructed with the same algorithms that are used for data. The simulated events include overlapping pp interactions (pileup) and have been reweighted so that the distribution of the number of interactions per LHC bunch crossing in simulation matches that observed in data.

# 4 Event reconstruction and selection

The particle-flow (PF) algorithm [88] aims to reconstruct and identify each individual particle (PF candidate) in an event, with an optimized combination of information from the various elements of the CMS detector. The energy of photons is obtained from the ECAL measurement. The energy of electrons is determined from a combination of the electron momentum at the PV as determined by the tracker, the energy of the corresponding ECAL cluster, and the energy sum of all bremsstrahlung photons spatially compatible with originating from the electron track. The energy of muons is obtained from the curvature of the corresponding track. The energy of charged hadrons is determined from a combination of their momentum measured in the tracker and the matching ECAL and HCAL energy deposits, corrected for the response function of the calorimeters to hadronic showers. Finally, the energy of neutral hadrons is obtained from the corresponding ECAL and HCAL energies.

The missing transverse momentum vector $\vec{p}_T^{\text{miss}}$ is computed as the negative vector sum of the transverse momenta of all the PF candidates in an event, and its magnitude is denoted as $p_T^{\text{miss}}$ [89]. The $\vec{p}_T^{\text{miss}}$ is modified to account for corrections to the energy scale of the reconstructed jets in the event.

Muons with $p_T^\mu > 5\,\text{GeV}$ are reconstructed within the geometrical acceptance, corresponding to the region $|\eta^\mu| < 2.4$, by combining information from the silicon tracker and the muon system [90]. The matching between the inner and outer tracks proceeds either outside-in, starting from a track in the muon system, or inside-out, starting from a track in the silicon tracker. Inner tracks that match segments in only one or two stations of the muon system are also considered because they may belong to very low-$p_T$ muons that do not have sufficient energy to penetrate the entire muon system. The muons are selected among the reconstructed muon track candidates by applying minimal requirements on the track in both the muon system and the inner tracker system, and taking into account the compatibility with small energy deposits in the calorimeters.

To discriminate between prompt muons from Z boson decay and those arising from electroweak (EW) decays of hadrons within jets, an isolation requirement of $\mathcal{I}^\mu < 0.35$ is imposed, where the relative isolation is defined as

$$\mathcal{I}^\mu \equiv \left( \sum p_T^{\text{charged}} + \max\left[0, \sum p_T^{\text{neutral}} + \sum p_T^\gamma - p_T^{\mu,\text{PU}}\right] \right) / p_T^\mu. \tag{1}$$

In Eq. (1), $\sum p_T^{\text{charged}}$ is the scalar sum of the transverse momenta of charged hadrons originating from the chosen PV of the event. The quantities $\sum p_T^{\text{neutral}}$ and $\sum p_T^\gamma$ are the scalar sums of the transverse momenta for neutral hadrons and photons, respectively. The isolation sums involved are all restricted to a volume bound by a cone of angular radius $\Delta R = 0.3$ around the muon direction at the PV, where the angular distance between two particles $i$ and $j$ is $\Delta R(i,j) = \sqrt{(\eta^i - \eta^j)^2 + (\phi^i - \phi^j)^2}$. Since the isolation variable is particularly sensitive to energy deposits from pileup interactions, a $p_T^{\mu,\text{PU}}$ contribution is subtracted, defined as $p_T^{\mu,\text{PU}} \equiv 0.5 \sum_i p_T^{i,\text{PU}}$, where $i$ runs over the charged hadron PF candidates not originating from the PV, and the factor of 0.5 corrects for the different fraction of charged and neutral particles in the cone [91].

Electrons with $p_T^e > 7\,\text{GeV}$ are reconstructed within the geometrical acceptance, corresponding to the pseudorapidity region $|\eta^e| < 2.5$ [38]. Electrons are identified using a multivariate discriminant which includes observables sensitive to the presence of bremsstrahlung along the electron trajectory, the geometrical and momentum-energy matching between the electron trajectory and the associated cluster in the ECAL, the shape of the electromagnetic shower in the ECAL, and variables that discriminate against electrons originating from photon conversions. Instead of an additional isolation requirement, similar to the one for muons, the electron multivariate discriminant also includes the isolation sums described above ($\sum p_T^{\text{charged}}$, $\sum p_T^{\text{neutral}}$, and $\sum p_T^\gamma$) but computed around the electron direction. The inclusion of isolation sums helps suppressing electrons originating from electroweak decays of hadrons within jets [92] and has a better performance than a simple requirement on the relative isolation observable. The package XGBOOST [93] is used for the training and optimization of the multivariate discriminant employed for electron identification and isolation. The training is performed with simulated events that are not used at any other stage of the analysis. Events are divided into six regions defined by two transverse momentum ranges (7–10 GeV and >10 GeV) and three pseudorapidity regions: central barrel ($|\eta^e| < 0.8$), outer barrel ($0.8 < |\eta^e| < 1.479$), and endcaps ($1.479 < |\eta^e| < 2.5$). Separate training is performed for the three different data-taking periods and selection requirements are determined such that the signal efficiency remains the same for all three periods.

The effect of the final-state radiation (FSR) from leptons is recovered as follows. Photons reconstructed by the PF algorithm within $|\eta^\gamma| < 2.4$ are considered as FSR candidates if they satisfy the conditions $p_T^\gamma > 2\,\text{GeV}$ and $\mathcal{I}^\gamma < 1.8$, where the photon relative isolation $\mathcal{I}^\gamma$ is defined as for the muon in Eq. (1). Every such photon is associated to the closest selected lepton in the event. Photons that do not satisfy the requirements $\Delta R(\gamma, \ell)/(p_T^\gamma)^2 < 0.012\,\text{GeV}^{-2}$ and $\Delta R(\gamma, \ell) < 0.5$ are discarded. The lowest-$\Delta R(\gamma, \ell)/(p_T^\gamma)^2$ photon candidate of every lepton, if any, is retained. The photons thus identified are excluded from the isolation computation of the muons selected in the event.

In order to suppress muons from in-flight decays of hadrons and electrons from photon conversions, leptons are rejected if the ratio of their impact parameter in three dimensions, computed with respect to the PV position, to their uncertainty is greater or equal to four.

The momentum scale and resolution of electrons and muons are calibrated in bins of $p_T^\ell$ and $\eta^\ell$ using the decay products of known dilepton resonances as described in Refs. [38, 39].

A "tag and probe" technique [94] based on samples of Z boson events in data and simulation is used to measure the efficiency of the reconstruction and selection for prompt electrons and muons in several bins of $p_T^\ell$ and $\eta^\ell$. The difference in the efficiencies measured in simulation and data is used to rescale the yields of selected events in the simulated samples.

For each event, hadronic jets are clustered from the reconstructed particles using the infrared- and collinear-safe anti-$k_T$ algorithm [36, 37] with a distance parameter of 0.4. The jet momentum is determined as the vectorial sum of all particle momenta in the jet, and is found from simulation to be within 5 to 10% of the true momentum over the whole $p_T$ spectrum and detector acceptance. Additional pp interactions within the same or nearby bunch crossings can contribute extra tracks and calorimetric energy depositions to the jet. To mitigate this effect, tracks identified as originating from pileup vertices are discarded and an offset correction is applied to correct for the remaining contributions. Jet energy corrections are derived from simulation to match that of particle level jets on average. In situ measurements of the momentum balance in dijet, photon + jet, Z+ jet, and multijet events are used to account for any residual differences in jet energy scale in data and simulation [95]. Jet energies in simulation are

smeared to match the resolution in data. The jet energy resolution amounts typically to 16% at 30 GeV, 8% at 100 GeV, and 4% at 1 TeV. Additional selection criteria are applied to remove jets potentially dominated by anomalous contributions from various subdetector components or reconstruction failures. To be considered in the analysis, jets must satisfy the conditions $p_T^{jet} > 30$ GeV and $|\eta^{jet}| < 4.7$, and be separated from all selected lepton candidates and any selected FSR photons by $\Delta R(\ell/\gamma, jet) > 0.4$. Jets are also required to pass the tight identification criteria and the tight working point of pileup jet identification described in Ref. [91].

For event categorization, jets are tagged as $q_b$ jets using the DeepCSV algorithm [96], which combines information about impact parameter significance, secondary vertex, and jet kinematics. Data to simulation scale factors for the $q_b$ tagging efficiency are applied as a function of jet $p_T$, $\eta$, and flavor.

The event selection is designed to extract signal candidates from events containing at least four well-identified and isolated leptons, each originating from the PV and possibly accompanied by an FSR photon candidate. In what follows, unless otherwise stated, FSR photons are included in invariant mass computations.

First, Z candidates are formed with pairs of leptons of the same flavor and opposite-charge ($e^+e^-$, $\mu^+\mu^-$) that pass the requirement $12 < m_{\ell^+\ell^-} < 120$ GeV. They are then combined into ZZ candidates, wherein we denote as $Z_1$ the Z candidate with an invariant mass closest to the nominal Z boson mass [97], and as $Z_2$ the other one. The flavors of the involved leptons define three mutually exclusive subchannels: 4e, 4$\mu$, and 2e2$\mu$.

To be considered for the analysis, ZZ candidates have to pass a set of kinematic requirements that improve the sensitivity to H boson decays. The $Z_1$ invariant mass must be larger than 40 GeV. All leptons must be separated in angular space by at least $\Delta R(\ell_i, \ell_j) > 0.02$. At least two leptons are required to have $p_T > 10$ GeV and at least one is required to have $p_T > 20$ GeV. In the 4$\mu$ and 4e subchannels, where an alternative $Z_a Z_b$ candidate can be built out of the same four leptons, we discard candidates with $m_{Z_b} < 12$ GeV if $Z_a$ is closer to the nominal Z boson mass than $Z_1$ is. This rejects events that contain an on-shell Z and a low-mass dilepton resonance. To further suppress events with leptons originating from hadron decays in jet fragmentation or from the decay of low-mass resonances, all four opposite-charge lepton pairs that can be built with the four leptons (irrespective of flavor) are required to satisfy the condition $m_{\ell^+\ell'^-} > 4$ GeV, where selected FSR photons are disregarded in the invariant mass computation. Finally, the four-lepton invariant mass $m_{4\ell}$ must be larger than 70 GeV, which defines the mass range of interest for the subsequent steps of the analysis.

In events where more than one ZZ candidate passes the above selection, the candidate with the highest value of $\mathcal{D}_{bkg}^{kin}$ (defined in Section 5) is retained, except if two candidates consist of the same four leptons, in which case the candidate with the $Z_1$ mass closest to the nominal Z boson mass is retained.

## 5 Kinematic discriminants

The full kinematic information from each event using either the H boson decay products and/or the associated particles in the H boson production is extracted by means of matrix element calculations and is used to form several kinematic discriminants. These computations rely on the MELA package [51–53, 55] and exploit the JHUGEN matrix elements for the signal and the MCFM matrix elements for the background. Both the H boson decay kinematics and the kinematics of the associated production of H + 1 jet, H + 2 jets, VBF, ZH, and WH are explored.

The full event kinematics is described by decay observables $\vec{\Omega}^{H\to4\ell}$ or observables describing the associated production $\vec{\Omega}^{H+jj}$, which may or may not include the $H \to 4\ell$ decay kinematic information depending on the use case. The definition of these observables can be found in Refs. [51–53].

Two types of kinematic discriminants are exploited in the $H \to 4\ell$ analysis. First we construct the three categorization discriminants in order to classify signal events into exclusive categories defined in Section 6.2. Categorization discriminants are designed to increase the purity of the targeted production mechanism in a dedicated event category. In addition, we define another set of three kinematic discriminants that are taken as an observable in the two-dimensional likelihood fits carried out to extract the results, as described in Section 10. These kinematic discriminants are designed to separate the targeted H boson production mechanism from its dominant background.

Categorization discriminants are calculated following the prescription in Refs. [18, 21, 98]. The discriminants sensitive to the VBF signal topology with two associated jets, the VBF signal topology with one associated jet, and the VH (either ZH or WH) signal topology with two associated jets are:

$$
\mathcal{D}_{\text{2jet}}^{\text{VBF}} = \left[ 1 + \frac{\mathcal{P}_{\text{Hjj}}(\vec{\Omega}^{H+jj}|m_{4\ell})}{\mathcal{P}_{\text{VBF}}(\vec{\Omega}^{H+jj}|m_{4\ell})} \right]^{-1} \quad \mathcal{D}_{\text{1jet}}^{\text{VBF}} = \left[ 1 + \frac{\mathcal{P}_{\text{Hj}}(\vec{\Omega}^{H+j}|m_{4\ell})}{\int d\eta^j \mathcal{P}_{\text{VBF}}(\vec{\Omega}^{H+jj}|m_{4\ell})} \right]^{-1}
$$
$$
\mathcal{D}_{\text{2jet}}^{\text{WH}} = \left[ 1 + \frac{\mathcal{P}_{\text{Hjj}}(\vec{\Omega}^{H+jj}|m_{4\ell})}{\mathcal{P}_{\text{WH}}(\vec{\Omega}^{H+jj}|m_{4\ell})} \right]^{-1} \quad \mathcal{D}_{\text{2jet}}^{\text{ZH}} = \left[ 1 + \frac{\mathcal{P}_{\text{Hjj}}(\vec{\Omega}^{H+jj}|m_{4\ell})}{\mathcal{P}_{\text{ZH}}(\vec{\Omega}^{H+jj}|m_{4\ell})} \right]^{-1} ,
$$
(2)

where $\mathcal{P}_{\text{VBF}}$, $\mathcal{P}_{\text{Hjj}}$, $\mathcal{P}_{\text{Hj}}$, and $\mathcal{P}_{\text{VH}}$ are the probabilities for the VBF process, the ggH process in association with two jets (combination of $gg/qg/qq'$ parton collisions producing $H + 2$ jets), the ggH process in association with one jet ($H + 1$ jet), and the VH process, respectively. The quantity $\int d\eta^j \mathcal{P}_{\text{VBF}}$ is the integral of the two-jet VBF matrix element probability over the $\eta^j$ values of the unobserved jet, with the constraint that the total transverse momentum of the $H + 2$ jets system is zero. The discriminant $\mathcal{D}_{\text{2jet}}^{\text{VH}}$, used for event categorization, is defined as the maximum value of the two discriminants, $\mathcal{D}_{\text{2jet}}^{\text{VH}} = \max(\mathcal{D}_{\text{2jet}}^{\text{ZH}}, \mathcal{D}_{\text{2jet}}^{\text{WH}})$.

A set of three discriminants used in the likelihood fits is calculated as in Refs. [17, 18]. The discriminant sensitive to the $gg/q\overline{q} \to 4\ell$ process exploits the kinematics of the four-lepton decay system. It is used in most of the event categories described in Section 6 to separate signal from background and is defined as:

$$
\mathcal{D}_{\text{bkg}}^{\text{kin}} = \left[ 1 + \frac{\mathcal{P}_{\text{bkg}}^{q\overline{q}}(\vec{\Omega}^{H\to4\ell}|m_{4\ell})}{\mathcal{P}_{\text{sig}}^{gg}(\vec{\Omega}^{H\to4\ell}|m_{4\ell})} \right]^{-1} ,
$$
(3)

where $\mathcal{P}_{\text{sig}}^{gg}$ is the probability for the signal and $\mathcal{P}_{\text{bkg}}^{q\overline{q}}$ is the probability for the dominant $q\overline{q} \to 4\ell$ background process, calculated using the LO matrix elements. In the VBF-2jet-tagged and VH-hadronic-tagged event categories (defined in Section 6.2), the background includes the QCD production of $ZZ/Z\gamma^*/\gamma^*\gamma^* \to 4\ell$ in association with two jets, the EW background from the vector boson scattering (VBS), as well as the triboson (VVV) production process. We therefore use dedicated production-dependent discriminants based on the kinematics of the four-lepton decay and information from the associated jets (noted with VBF+ dec or VH+ dec), defined

as:

$$\mathcal{D}_{\text{bkg}}^{\text{VBF+dec}} = \left[ 1 + \frac{c^{\text{VBF}}(m_{4\ell})[\mathcal{P}_{\text{bkg}}^{\text{EW}}(\vec{\Omega}^{\text{H+jj}}|m_{4\ell}) + \mathcal{P}_{\text{bkg}}^{\text{QCD}}(\vec{\Omega}^{\text{H+jj}}|m_{4\ell})]}{\mathcal{P}_{\text{sig}}^{\text{EW}}(\vec{\Omega}^{\text{H+jj}}|m_{4\ell})} \right]^{-1} \qquad (4)$$

$$\mathcal{D}_{\text{bkg}}^{\text{VH+dec}} = \left[ 1 + \frac{c^{\text{VH}}(m_{4\ell})[\mathcal{P}_{\text{bkg}}^{\text{EW}}(\vec{\Omega}^{\text{H+jj}}|m_{4\ell}) + \mathcal{P}_{\text{bkg}}^{\text{QCD}}(\vec{\Omega}^{\text{H+jj}}|m_{4\ell})]}{\mathcal{P}_{\text{sig}}^{\text{EW}}(\vec{\Omega}^{\text{H+jj}}|m_{4\ell})} \right]^{-1}, \qquad (5)$$

where $\mathcal{P}_{\text{sig}}^{\text{EW}}$ is the probability for the VBF and VH signal, $\mathcal{P}_{\text{bkg}}^{\text{EW}}$ is the probability for the VBS and VVV background processes, and $\mathcal{P}_{\text{bkg}}^{\text{QCD}}$ is the probability for $\text{ZZ}/\text{Z}\gamma^*/\gamma^*\gamma^* \to 4\ell$ QCD production in association with two jets. The quantity $c^p(m_{4\ell})$ for category $p$ is the $m_{4\ell}$-dependent parameter that allows to change the relative normalization of the EW probabilities, separately for the VBF and VH topologies. For each slice of $m_{4\ell}$, the distributions of the signal and background discriminants are plotted, and the $c^p(m_{4\ell})$ value is determined in such a way that the two distributions cross at 0.5. This procedure allows rescaling of the distributions for the linear-scale binning of the templates used in the likelihood fits described in Section 10.

# 6 Event categorization

In order to improve the sensitivity to the H boson production mechanisms, the selected events are classified into mutually exclusive categories based on the features of the reconstructed objects associated with the H $\to 4\ell$ candidates. Event categorization is organized in two steps with increasing granularity of the categories. First step is primarily designed to separate the ggH, VBF, VH, and $t\bar{t}$H processes. There is little sensitivity to $b\bar{b}$H or $q_t$H, even though these production modes are considered explicitly in the analysis. The reconstructed event categories from the first step are further subdivided (as discussed in Section 6.2) in order to study each production mechanism in more detail. This subdivision is carried out by matching the recommended binning of the framework of STXS described in the following section.

## 6.1 STXS production bins

The STXS framework has been adopted by the LHC experiments as a common framework for studies of the H boson. It has been developed to define fine-grained measurements of the H boson production modes in various kinematic regions, and to reduce the theoretical uncertainties that are folded into the measurements. It also allows for the use of advanced categorization techniques and provides a common scheme for combining measurements in different decay channels or by different experiments. The regions of phase space defined by this framework are referred to as production bins and are determined by using generator-level information for H bosons with rapidity $|y_{\text{H}}| < 2.5$. Generator-level jets are defined as anti-$k_{\text{T}}$ jets with a distance parameter of 0.4 and a $p_{\text{T}}$ threshold of 30 GeV; no requirement is placed on the generator-level leptons.

The STXS framework has been designed to complement the Run I measurements of the production signal strength modifiers and fiducial differential cross sections of the H boson by combining their advantages. The sensitivity to theoretical uncertainties in the signal strength modifier results is suppressed by excluding dominant theoretical uncertainties causing production bin migration effects from the STXS measurements. They are included only when comparing the results with the theoretical predictions. In contrast to the fiducial differential cross section measurements, in the STXS framework measurements are optimized for sensitivity by means

of event categories and matrix element discriminants. To account for the evolving experimental sensitivity, different stages of production bins with increasing granularity are developed.

The stage 0 production bins are called `ggH`, `qqH`, `VH-lep`, and `ttH` and are designed to closely match the main H boson production mechanisms. The `qqH` bin includes the EW production of the H boson in association with two quarks from either VBF or VH events with hadronic decays of the vector boson V. The `VH-lep` production bin includes VH events with leptonic decays of the vector boson V. The low rate $b\bar{b}H$ and $q_tH$ production processes are considered together with the `ggH` and `ttH` production bins, respectively. In this analysis, a modified version of the stage 0 production bins is also studied, where instead of `VH-lep` and `qqH` bins we define the `WH`, `ZH`, and `VBF` bins that map the H boson production mechanisms without the splitting of the VH events in leptonic and hadronic decays.

Stage 1 of the STXS framework was designed by further splitting the bins from the stage 0, one of the main motives being the enhanced sensitivity to possible signatures of physics beyond the SM. This is achieved by dividing stage 0 bins with additional requirements on generator-level quantities that include the transverse momentum of the H boson ($p_T^H$), the number of associated jets ($N^j$), the dijet invariant mass ($m_{jj}$), the transverse momentum of the H boson and the leading jet ($p_T^{Hj}$), and the transverse momentum of the H boson and the two leading jets ($p_T^{Hjj}$). These bins were designed in order to maximize sensitivity to new physics while also taking into account the current experimental sensitivity limited mostly by the amount of collected data. The most recent set of bins defined in the STXS framework is referred to as stage 1.2. This paper presents a first set of cross section measurements in the H $\rightarrow 4\ell$ channel for the stage 1.2 of the STXS framework. However, several stage 1.2 production bins are merged as the full set of bins cannot be measured with the current data sample. The merging scheme results in 19 production bins; it is illustrated in Fig. 1 and discussed in more detail below.

The `ggH` production process is split into events with $p_T^H < 200\,\text{GeV}$ and $p_T^H > 200\,\text{GeV}$. The events with $p_T^H > 200\,\text{GeV}$ are placed into one single production bin called `ggH/p_T > 200`. The events with $p_T^H < 200\,\text{GeV}$ are split in events with zero, one, and two or more jets. The events with zero or one jets are split into the following production bins according to the H boson $p_T$: `ggH-0j/p_T[0,10]`, `ggH-0j/p_T[10,200]`, `ggH-1j/p_T[0,60]`, `ggH-1j/p_T[60,120]`, and `ggH-1j/p_T[120,200]`. The events with two or more jets are split according to the dijet invariant mass as follows. The events with $m_{jj} < 350\,\text{GeV}$ are split into three production bins according to the H boson $p_T$: `ggH-2j/p_T[0,60]`, `ggH-2j/p_T[60,120]`, and `ggH-2j/p_T[120,200]`. The events with $m_{jj} > 350\,\text{GeV}$ are all placed into one production bin `ggH-2j/m_{jj} > 350`, which merges four bins originally suggested in stage 1.2 of the STXS framework.

The merging scheme of the electroweak `qqH` production bins is as follows. The events with zero jets, one jet, or with two or more jets with $m_{jj} < 60\,\text{GeV}$ or $120 < m_{jj} < 350\,\text{GeV}$ correspond to production bins with insufficient statistics; they are all merged into one bin called `qqH-rest`. The events with two or more jets and $60 < m_{jj} < 120\,\text{GeV}$ are placed in the `qqH-2j/m_{jj}[60,120]` bin. The events with two or more jets and $m_{jj} > 350\,\text{GeV}$ are split into events with $p_T^H < 200\,\text{GeV}$ and $p_T^H > 200\,\text{GeV}$. The events with $p_T^H > 200\,\text{GeV}$ are placed into one single production bin called `qqH-2j/p_T > 200`. The events with $p_T^H < 200\,\text{GeV}$ and $p_T^{Hjj} < 25\,\text{GeV}$ are split into two production bins, `qqH-2j/m_{jj}[350,700]` and `qqH-2j/m_{jj} > 700`, and otherwise if $p_T^{Hjj} > 25\,\text{GeV}$ are merged in a single bin called `qqH-3j/m_{jj} > 350`.

The three production processes $q\bar{q}' \rightarrow$ WH, gg $\rightarrow$ ZH, and $q\bar{q} \rightarrow$ ZH are combined to build
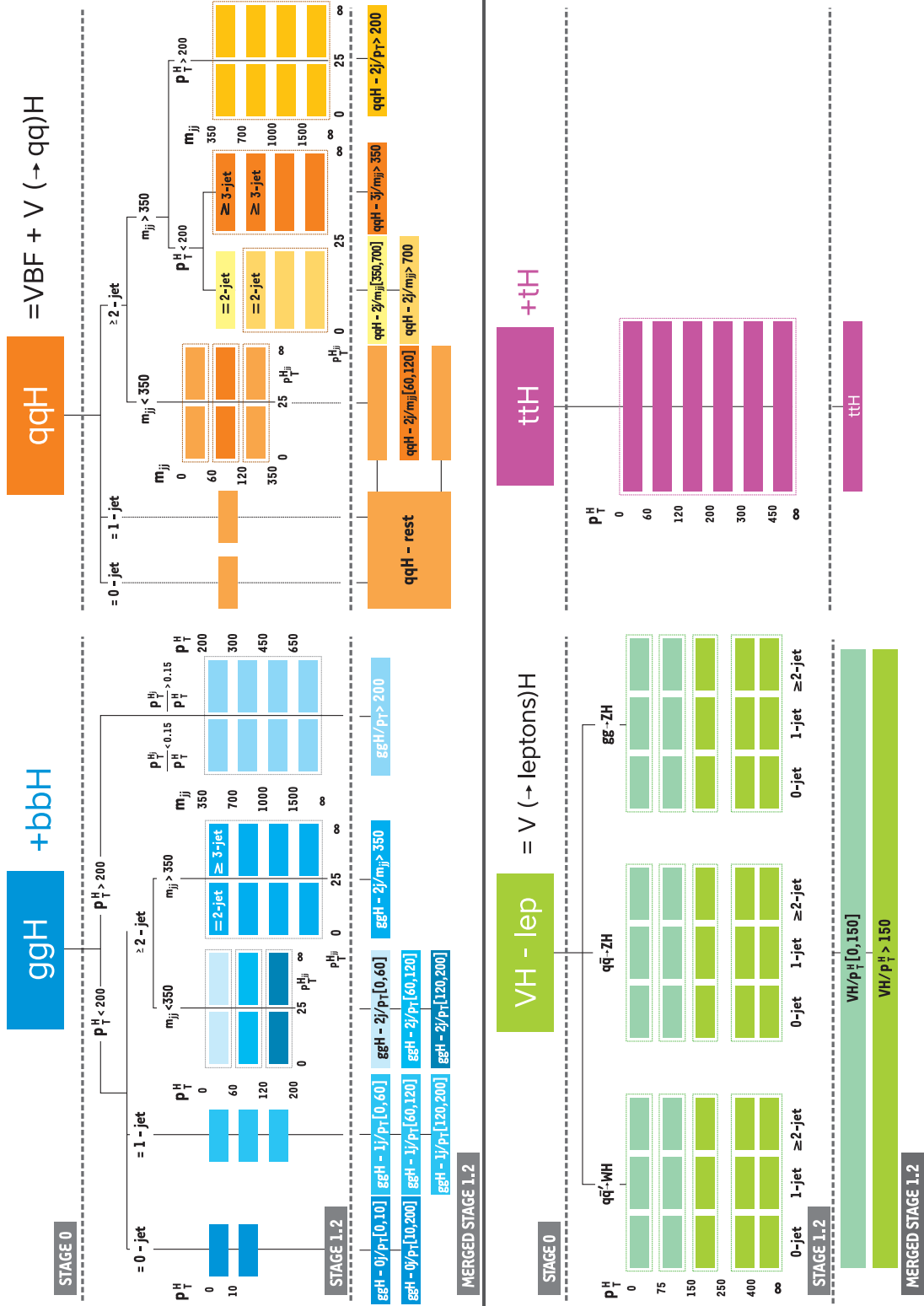
Figure 1: Binning of the gluon fusion production process, the electroweak production process (combines VBF and VH with hadronic V decay), the VH production process with leptonic V decay (combining WH, ZH, and gluon fusion ZH production), and the $t\bar{t}$H production process in the merged stage 1.2 of the STXS framework used in the H $\rightarrow$ ZZ $\rightarrow$ 4$\ell$ analysis.

`VH-lep` reduced stage 1.2 production bins. Several proposed production bins are merged into just two bins according to the $p_T$ of the H boson: `VH-lep`/$p_T^H$[0, 150] and `VH-lep`/$p_T^H > 150$.

In stage 1.2 of the STXS framework the `ttH` stage 0 production bin is split in five different bins according to the $p_T$ of the H boson. Because of the very low expected yields all these bins are merged into a single bin that includes the $q_tH$ production process as well.

Finally, in stage 1.2 the $b\bar{b}H$ production process, which has small cross section, is classified in the `ggH-0j`/$p_T$[10, 200] production bin.

## 6.2 Reconstructed event categories

In order to be sensitive to different production bins, the ZZ candidates that pass the event selection described in Section 4 are classified into several dedicated reconstructed event categories. The category definitions are based on the multiplicity of jets, $q_b$-tagged jets, and additional leptons in the event. Additional leptons are not involved in the ZZ candidate selection but, if present, should satisfy the identification, vertex compatibility, and isolation requirements. Requirements on the categorization discriminants described in Section 5, the invariant mass of the two leading jets, and the transverse momentum of the ZZ candidate are also exploited.

The event categorization is carried out in two steps. In the first step, the ZZ candidates are split into seven initial categories to target the main H boson production mechanisms corresponding to the stage 0 production bins. The first step of the categorization closely follows the analysis strategy from the previous publication [18]. To ensure exclusive categories, an event is considered for the subsequent category only if it does not satisfy the requirements of the previous one.

In the first categorization step, the following criteria are applied:

- The VBF-2jet-tagged category requires exactly 4 leptons. In addition there must be either 2 or 3 jets of which at most 1 is $q_b$-tagged, or at least 4 jets and no $q_b$-tagged jets. Finally, $\mathcal{D}_{2jet}^{VBF} > 0.5$ is required.
- The VH-hadronic-tagged category requires exactly 4 leptons. In addition there must be 2 or 3 jets with no $q_b$-tagging requirements, or at least 4 jets and no $q_b$-tagged jets. Finally, $\mathcal{D}_{2jet}^{VH} > 0.5$ is required.
- The VH-leptonic-tagged category requires no more than 3 jets and no $q_b$-tagged jets in the event, and exactly 1 additional lepton or 1 additional pair of opposite sign, same flavor leptons. This category also includes events with no jets and at least 1 additional lepton.
- The $t\bar{t}H$-hadronic-tagged category requires at least 4 jets, of which at least 1 is $q_b$-tagged, and no additional leptons.
- The $t\bar{t}H$-leptonic-tagged category requires at least 1 additional lepton in the event.
- The VBF-1jet-tagged category requires exactly 4 leptons, exactly 1 jet and $\mathcal{D}_{1jet}^{VBF} > 0.7$.
- The untagged category consists of the remaining events.

Reconstructed events are further subdivided in the second step of the categorization that is designed to closely match the merged stage 1.2 production bins described in the previous section. In the second categorization step, the untagged, VBF-2jet-tagged, VH-hadronic-tagged, and VH-leptonic-tagged categories are further split exploiting additional variables like the invari-

ant mass of the two leading jets and the transverse momentum of the ZZ candidate. A total number of twenty-two reconstructed event categories is defined and details of the categorization are presented in Table 2.

Table 2: Event categorization criteria of the H $\rightarrow 4\ell$ analysis targeting stage 1.2 STXS production bins. Events from the first step of the categorization are further classified based on the kinematical properties listed in the table. A dash indicates no requirement.

| Reconstructed event category | 1st categorization step | Number of jets | Kinematical requirements (GeV) | Targeted production bin |
|---|---|---|---|---|
| Untagged-0j-$p_T^{4\ell}[0,10]$ | Untagged | 0 | $0 < p_T^{4\ell} < 10$ | ggH-0j/$p_T[0,10]$ |
| Untagged-0j-$p_T^{4\ell}[10,200]$ | Untagged | 0 | $10 < p_T^{4\ell} < 200$ | ggH-0j/$p_T[10,200]$ |
| Untagged-1j-$p_T^{4\ell}[0,60]$ | Untagged | 1 | $0 < p_T^{4\ell} < 60$ | ggH-1j/$p_T[0,60]$ |
| Untagged-1j-$p_T^{4\ell}[60,120]$ | Untagged | 1 | $60 < p_T^{4\ell} < 120$ | ggH-1j/$p_T[60,120]$ |
| Untagged-1j-$p_T^{4\ell}[120,200]$ | Untagged | 1 | $120 < p_T^{4\ell} < 200$ | ggH-1j/$p_T[120,200]$ |
| Untagged-2j-$p_T^{4\ell}[0,60]$ | Untagged | 2 | $0 < p_T^{4\ell} < 60, m_{jj} < 350$ | ggH-2j/$p_T[0,60]$ |
| Untagged-2j-$p_T^{4\ell}[60,120]$ | Untagged | 2 | $60 < p_T^{4\ell} < 120, m_{jj} < 350$ | ggH-2j/$p_T[60,120]$ |
| Untagged-2j-$p_T^{4\ell}[120,200]$ | Untagged | 2 | $120 < p_T^{4\ell} < 200, m_{jj} < 350$ | ggH-2j/$p_T[120,200]$ |
| Untagged-$p_T^{4\ell} > 200$ | Untagged | — | $p_T^{4\ell} > 200$ | ggH/$p_T > 200$ |
| Untagged-2j-$m_{jj} > 350$ | Untagged | 2 | $m_{jj} > 350$ | ggH-2j/$m_{jj} > 350$ |
| VBF-1jet-tagged | VBF-1jet-tagged | — | — | qqH-rest |
| VBF-2jet-tagged-$m_{jj}[350,700]$ | VBF-2jet-tagged | — | $p_T^{4\ell} < 200, p_T^{4\ell jj} < 25, 350 < m_{jj} < 700$ | qqH-2j/$m_{jj}[350,700]$ |
| VBF-2jet-tagged-$m_{jj} > 700$ | VBF-2jet-tagged | — | $p_T^{4\ell} < 200, p_T^{4\ell jj} < 25, m_{jj} > 700$ | qqH-2j/$m_{jj} > 700$ |
| VBF-3jet-tagged-$m_{jj} > 350$ | VBF-2jet-tagged | — | $p_T^{4\ell} < 200, p_T^{4\ell jj} > 25, m_{jj} > 350$ | qqH-3j/$m_{jj} > 350$ |
| VBF-2jet-tagged-$p_T^{4\ell} > 200$ | VBF-2jet-tagged | — | $p_T^{4\ell} > 200, m_{jj} > 350$ | qqH-2j/$p_T > 200$ |
| VBF-rest | VBF-2jet-tagged | — | $m_{jj} < 350$ | qqH-rest |
| VH-hadronic-tagged-$m_{jj}[60,120]$ | VH-hadronic-tagged | — | $60 < m_{jj} < 120$ | qqH-2j/$m_{jj}[60,120]$ |
| VH-rest | VH-hadronic-tagged | — | $m_{jj} < 60$ or $m_{jj} > 120$ | qqH-rest |
| VH-leptonic-tagged-$p_T^{4\ell}[0,150]$ | VH-leptonic-tagged | — | $p_T^{4\ell} < 150$ | VH-lep/$p_T^H[0,150]$ |
| VH-leptonic-tagged-$p_T^{4\ell} > 150$ | VH-leptonic-tagged | — | $p_T^{4\ell} > 150$ | VH-lep/$p_T^H > 150$ |
| $t\bar{t}$H-leptonic-tagged | $t\bar{t}$H-leptonic-tagged | — | — | ttH |
| $t\bar{t}$H-hadronic-tagged | $t\bar{t}$H-hadronic-tagged | — | — | ttH |

# 7 Background estimation

## 7.1 Irreducible backgrounds

The irreducible background to the H boson signal in the $4\ell$ channel, which comes from the production of ZZ via $q\bar{q}$ annihilation or gluon fusion, is estimated using simulation. The fully differential cross section for the $q\bar{q} \rightarrow ZZ$ process is computed at NNLO [99], and the NNLO/NLO K factor as a function of $m_{ZZ}$ is applied to the POWHEG sample. This K factor varies from 1.0 to 1.2 and is 1.1 at $m_{ZZ} = 125$ GeV. Additional NLO electroweak corrections that depend on the initial state quark flavor and kinematics are also applied in the region $m_{ZZ} > 2m_Z$ following the prescription in Ref. [100].

The production of ZZ via gluon fusion contributes at NNLO in pQCD. It has been shown that the soft collinear approximation is able to describe the cross section for this process and the interference term at NNLO [101]. Further calculations also show that the K factors are very similar at NLO for signal and background [102] and at NNLO for signal and interference terms [103]. Therefore, the same K factor is used for signal and background [104]. The NNLO K factor for the signal is obtained as a function of $m_{ZZ}$ using the HNNLO v2 program [105–107] by calculating the NNLO and LO $gg \rightarrow H \rightarrow 2\ell2\ell'$ cross sections for the H boson decay width of 4.07 MeV and taking their ratios. The NNLO/LO K factor for $gg \rightarrow ZZ$ varies from $\approx$2.0 to 2.6 and is 2.27 at $m_{ZZ} = 125$ GeV; a systematic uncertainty of 10% is assigned to it when applied to the background process.

The triboson background processes ZZZ, WZZ, and WWZ, as well as $t\bar{t}Z$, $t\bar{t}WW$, and $t\bar{t}ZZ$ are also considered. These rare backgrounds are all estimated from simulation and are jointly

referred to as the EW backgrounds.

Simulated samples are used to obtain shapes of the four-lepton invariant mass that are later used to build the likelihood function. For each irreducible background contribution, events are divided in three final states ($4\mu$, $4e$, and $2e2\mu$) and 22 event sub-categories defined in Section 6.1. To extract the shape of the $m_{4\ell}$ distribution, expected yields are fitted to empirical functional forms built from a third order Bernstein polynomial. In sub-categories with not enough statistics to perform a fit, the shape is extracted from the inclusive distribution in the corresponding final state.

## 7.2 Reducible backgrounds

Additional backgrounds to the H boson signal in the $4\ell$ channel arise from processes in which decays of heavy-flavor hadrons, in-flight decays of light mesons within jets, or (for electrons) charged hadrons overlapping with $\pi^0$ decays are misidentified as leptons. The main processes leading to these backgrounds are Z+jets, $t\bar{t}$+jets, $Z\gamma$+jets, WW+jets, and WZ+jets production. We denote these reducible backgrounds as "Z+X" since they are dominated by the Z+jets process. The contribution from the reducible background is estimated with two independent methods, each with dedicated control regions in data. The control regions are defined by the presence of both a lepton pair satisfying all the requirements of a $Z_1$ candidate and two additional opposite sign (OS) or same sign (SS) leptons; the two additional leptons satisfy identification requirements looser than those used in the analysis. These four leptons are then required to pass the analysis ZZ candidate selection. The event yield in the signal region is obtained by weighting the control region events by the lepton misidentification probability $f_e$ ($f_\mu$), defined as the fraction of non-signal electrons (muons) that are identified by the analysis selection criteria. A detailed description of both methods can be found in Ref. [18].

The lepton misidentification rates $f_e$ and $f_\mu$ are measured as a function of $p_T^\ell$ and $\eta^\ell$ by means of a sample that includes a $Z_1$ candidate consisting of a pair of leptons, both passing the selection requirements used in the analysis, and exactly one additional lepton passing the relaxed selection. Furthermore, the $p_T^{miss}$ is required to be less than 25 GeV in order to suppress contamination from WZ and $t\bar{t}$ processes.

For the OS method, the mass of the $Z_1$ candidate is required to satisfy the condition $|Z_1 - m_Z| < 7$ GeV in order to reduce the contribution of (asymmetric) photon conversions, which is estimated separately. In the SS method, the contribution of photon conversions to the misidentification rate is estimated with dedicated samples.

The predicted yields of the reducible background from the two methods are in agreement within their uncertainties for each final state ($4\mu$, $4e$, and $2e2\mu$). The final yield used in the analysis is a weighted average of the two independent estimates. To extract the shape of the $m_{4\ell}$ distribution for the reducible background a maximum-likelihood fit is performed in each of the 22 event sub-categories defined in Section 6.1. For each sub-category, the expected "Z+X" yields from the OS and SS methods are binned as a function of $m_{4\ell}$ and fitted to empirical functional forms built from Landau distributions [108]. In sub-categories with not enough statistics to perform a fit, the shape is extracted from the inclusive distribution in the corresponding final state.

The dominant systematic uncertainty on the reducible background estimation arises from the difference in the composition of the sample from which the misidentification rate is computed and that of the control regions. It is determined from the MC simulation and is found to be around 30%, depending on the final state. Additional sources of systematic uncertainty arise

from the limited number of events in the control regions as well as in the region where the misidentification rates are computed.

# 8 Signal modeling

In order to generate an accurate signal model, the $p_T$ spectrum of the H boson, $p_T^H$, was tuned in the POWHEG simulation of the dominant gluon fusion production mode to better match the predictions from full phase space calculations implemented in the HRES generator [107, 109, 110].

In order to take advantage of the accuracy of the NNLOPS [111] simulation available for the ggH process, an event reweighting procedure is used. Events originating from the ggH process are subdivided into classes with 0, 1, 2, and $\geq 3$ jets; the jets with $p_T > 30\,\text{GeV}$ are clustered from all stable particles using the anti-$k_T$ algorithm with a distance parameter of 0.4, excluding the decay products of the H boson or associated vector bosons. The weights are obtained as the ratios of the $p_T^H$ distributions from the NNLOPS and the POWHEG generators for each event class; the sum of the weights in each sample is normalized to the inclusive cross section.

The signal shape is parametrized by means of a double-sided Crystal Ball function [112] around $m_H \approx 125\,\text{GeV}$. A Landau function is added in the total probability density function for the non-resonant part of the signal for the case of WH, ZH and t$\bar{\text{t}}$H production modes. The signal shape is parametrized as a function of $m_H$ by performing a simultaneous fit of several mass points for the ggH production mode in the 105 to 140 GeV mass range. Each parameter of the double-sided Crystal Ball function has a linear dependence on $m_H$, for a total of 12 free parameters. An examples of the fit is shown in Fig. 2.
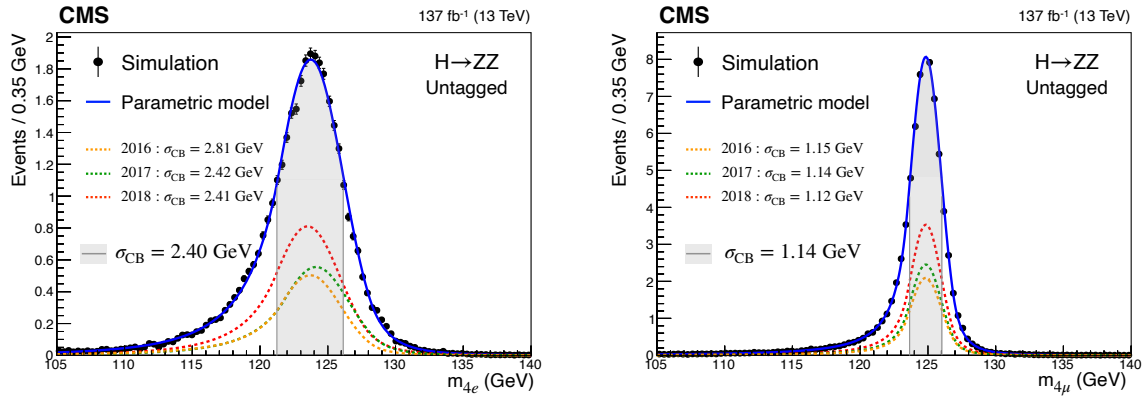


Figure 2: The shape of the parametric signal model for each year of simulated data, and for the sum of all years together. The black points represent weighted simulation events of the ggH production mechanism for $m_H = 125\,\text{GeV}$ and the blue line the corresponding model. Also shown is the $\sigma_{CB}$ value (half the width of the narrowest interval containing 68% of the invariant mass distribution) in the gray shaded area. The contribution of the signal model from each year of data-taking is illustrated with the dotted lines. The models are shown for the 4e (left) and 4$\mu$ (right) final states in the untagged event category.

# 9 Systematic uncertainties

The systematic uncertainties are divided into experimental and theoretical. The main experimental uncertainties originate from the imperfect knowledge of the detector; the dominant

sources are the uncertainties in the luminosity measurement, the lepton reconstruction and selection efficiency, the lepton and jet energy scale and resolution, the $q_b$ tagging efficiency, and the reducible background estimate. The theoretical uncertainties account for the uncertainties in the modeling of the signal and background processes.

Both types of uncertainties can affect the signal selection, cause migrations between the event categories, and affect the signal or background shapes used in the fit. All the uncertainties affecting this analysis are modeled as nuisance parameters (NPs) that are profiled in the maximum likelihood fit described in Section 10.

In the combination of the three data-taking periods, all theoretical uncertainties are treated as correlated across these periods. The experimental uncertainties related to reconstruction and selection efficiency, the lepton energy scale and resolution, and the $q_b$-tagging efficiency are also considered correlated across data-taking periods. Luminosity uncertainty is treated as partially correlated. All other experimental uncertainties are treated as uncorrelated. Correlated sources of uncertainty are assigned the same NP and uncorrelated sources have a dedicated NP in the likelihood fit described in Section 10.

The dominant sources of uncertainties and their effect on the analysis are discussed in detail in the following subsections. The impact of a NP on a parameter of interest (POI) is defined as the shift induced on POI when NP is varied by a $\pm 1$ standard deviation from its post-fit value, with all other parameters profiled as usual. The relative impact of the dominant systematic uncertainties on some of the measurements discussed in Section 10 is illustrated in Fig. 3.

## 9.1 Experimental uncertainties

The integrated luminosities of the 2016, 2017, and 2018 data-taking periods are individually known with uncertainties in the 2.3–2.5% range [41–43], while the total Run 2 (2016–2018) integrated luminosity has an uncertainty of 1.8%, the improvement in precision reflecting the (uncorrelated) time evolution of some systematic effects. The experimental uncertainty on the integrated luminosity measurement affects all final states, both signal and background. Another experimental uncertainty common to all final states is the uncertainty in the lepton reconstruction and selection efficiency. Here selection efficiency includes all the steps from trigger to impact parameter significance and finally identification and isolation requirements. The uncertainty ranges from 1 to 2.3% in the $4\mu$ channel and from 11 to 15.5% in the 4e channel. While for muon efficiency measurements in the low $p_T^\mu$ regions we rely on low mass di-muon resonances, the electron efficiency measurement relies solely on the Z boson resonance, resulting in a higher uncertainty in the low $p_T^e$ region.

Lepton momentum scale and resolution uncertainties are estimated from dedicated studies on the $Z \rightarrow \ell^+\ell^-$ mass distribution in data and simulation. Events are classified according to the $p_T$ and $\eta$ of one of the two leptons, determined randomly, and integrated over the other. The dilepton mass distributions are then fit by a Breit-Wigner parameterization convolved with the double-sided Crystal Ball function described in Section 8. The scale uncertainty is found to be 0.04% in the $4\mu$ channel and 0.3% in the 4e channel, while the resolution uncertainty is 20% for both channels. In both cases full correlation between the leptons in the event is assumed. Both scale and resolution uncertainties alter the signal shape by allowing the corresponding parameters of the double-sided Crystal Ball function to vary. The impact is found to be non-negligible only in the case of fiducial cross section measurements.

The effects of the jet energy corrections are studied in a similar manner. While jet energy scale and smearing do not alter signal selection efficiency, they cause event migrations between the
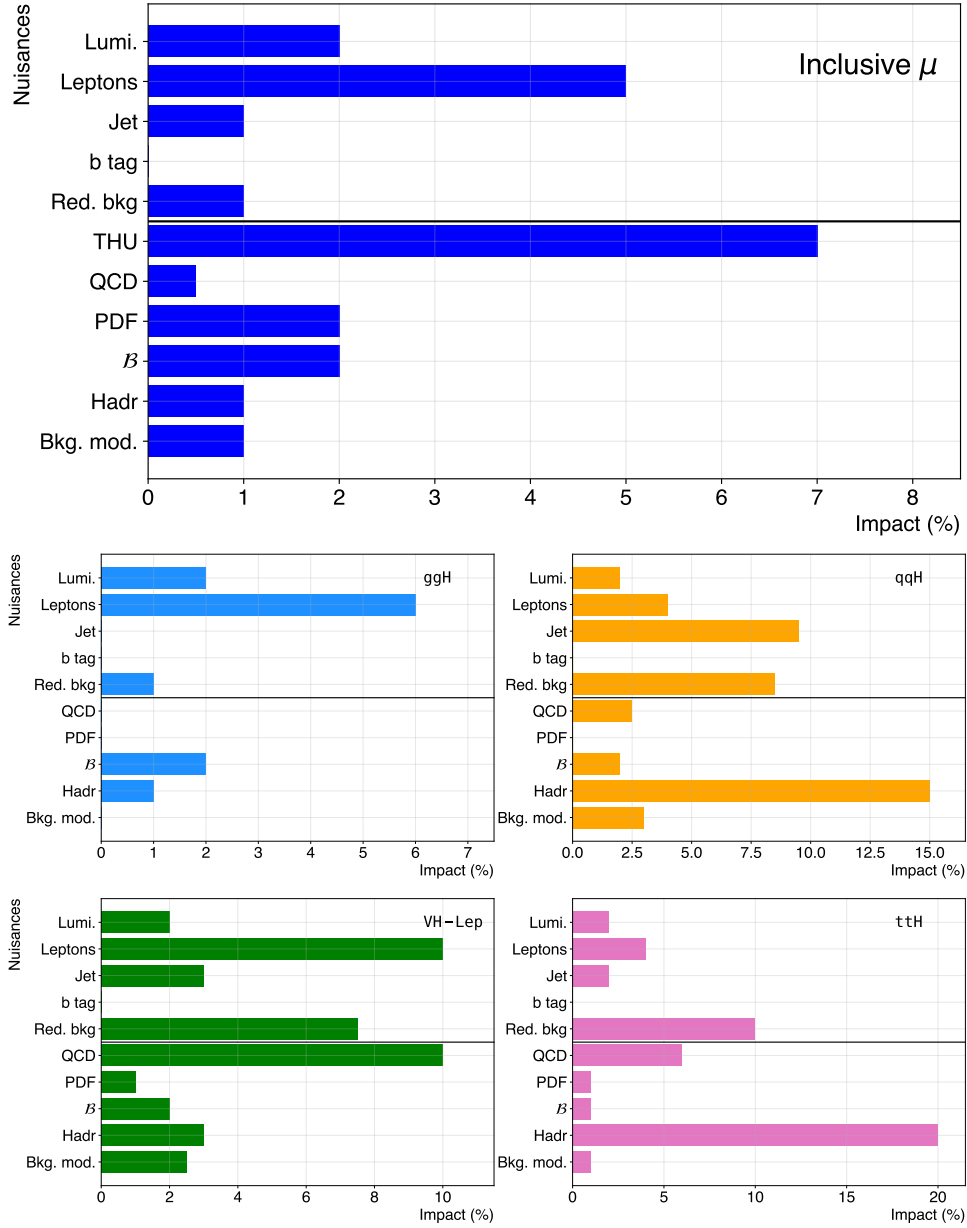
Figure 3: The impact of the dominant systematic uncertainties (in percent) on the inclusive signal strength $\mu$ and stage 0 production mode cross section described in Section 10. Impacts from different NPs are combined assuming no correlation. Only dominant experimental sources are presented: integrated luminosity uncertainty (Lumi.), lepton reconstruction and selection efficiency, scale and resolution (Leptons), jet energy scale and resolution (Jet), $q_b$-tagging efficiency (B-tag), and reducible background estimation uncertainty (Red. bkg). Only dominant theoretical sources are presented: ggH, VBF, and VH cross section theoretical uncertainty scheme (THU), renormalization and factorization scale (QCD), choice of the PDF set (PDF), the branching fraction of $H \rightarrow 4\ell$ ($\mathcal{B}$), modeling of hadronization and the underlying event (Hadr), and background modeling (Bkg. mod.). The THU uncertainty is not considered in the stage 0 cross section measurements. The uncertainties are rounded to the nearest 0.5%.

categories. They can also alter the shape of the discriminants, but the effect on the shape is negligible. The uncertainty in the jet energy scale ranges from 1% in the high jet $p_T$ range and increases up to 5% in the low jet $p_T$ range. The uncertainty in jet energy resolution ranges

from 1 to 2%. A detailed description of the determination of the jet energy scale and smearing uncertainties can be found in [113]. The effect on the analysis is studied in detail by propagating the uncertainties and estimating the effect on event migration in each of the 22 sub-categories. Their impact on the inclusive measurements is found to be negligible. However, the impact is significant in measurements of the VBF and VH production modes and differential cross section measurements as a function of jet kinematics, where it is one of the leading sources of uncertainty.

The uncertainty in the $q_b$-tagging efficiency is found to be 1% in the high jet $p_T$ range and increases up to 3% in the low jet $p_T$ range. The impact from the category migration is found to be negligible in all categories.

Finally, experimental uncertainties in the reducible background estimation, described in Section 7.2, originating from the background composition and misidentification rate uncertainties vary between 30 and 45% depending on the final state and category. However, the impact of this uncertainty on the measurements is found to be negligible.

Other sources of experimental uncertainties are also studied but their impact is negligible compared to the sources described above.

## 9.2 Theoretical uncertainties

Theoretical uncertainties that affect both the signal and background estimation include those related to the renormalization and factorization scales, and the choice of the PDF set. The uncertainty from the renormalization and factorization scales is determined by varying these scales between 0.5 and 2 times their nominal value, while keeping their ratio between 0.5 and 2. The uncertainty due to the PDF set is determined following the PDF4LHC recommendations by taking the root mean square of the variation of the results when using different replicas of the default NNPDF set [114, 115]. The uncertainties just described have an effect both on the signal and background yields, as well as on the migration of events between the categories. An additional 10% uncertainty in the K factor used for the gg $\rightarrow$ ZZ prediction is applied as described in Section 7.1. A systematic uncertainty of 2% [32] in the branching fraction of H $\rightarrow 4\ell$ only affects the signal yield.

Theoretical uncertainties that affect the predictions of the STXS production bins are described in Ref. [32]. From here on we will refer to these uncertainties as the theoretical uncertainty scheme (THU).

The THU for the ggH process includes 9 NPs, which account for uncertainties in the cross section prediction for exclusive jet bins (including the migration between the 0 and 1-jet, as well as between the 1 and $\geq$2-jet bins), the 2 jet and $\geq$3 jet VBF phase space, migrations around the $p_T^H$ bin boundaries at 10, 60, and 120 GeV, and the uncertainty in the $p_T^H$ distribution due to missing higher order finite top quark mass corrections.

In the THU uncertainties for VBF and VH production, additional sources are introduced to account for the uncertainty in the modeling of the $p_T^H$, $m_{jj}$ and $p_T^{Hjj}$ distributions, as well as that of the number of jets in the event. A total of 6 NPs account for the migrations of events across the $m_{jj}$ boundaries at 60, 120, 350, 700, 1000, and 1500 GeV. Two additional NPs account for migrations across the $p_T^H = 200$ GeV and $p_T^{Hjj} = 25$ GeV bin boundaries. Finally, a single source is introduced to account for migrations between the zero and one jet, as well as the the two or more jet bins. In each case, the uncertainty is computed by varying the renormalization and factorization scales and recalculating the fractional breakdown of the qqH STXS stage 1.2 cross

sections.

A set of THU uncertainties is considered as NPs in the likelihood fit when signal strength modifiers, rather than STXS, are measured. In the STXS framework, THU uncertainties only enter at the interpretation step and are thus applied only to the SM cross section predictions.

Additional theoretical effects that only cause migration of signal and background events between categories originate from the modeling of the hadronization and the underlying event. The underlying event modeling uncertainty is determined by varying initial- and final-state radiation scales between 0.25 and 4 times their nominal value. The effects of the modeling of hadronization are determined by simulating additional events with the variation of the nominal PYTHIA tune described in Section 3.

## 10 Results

The reconstructed four-lepton invariant mass distribution is shown in Fig. 4 for the 4e, 4$\mu$ and 2e2$\mu$ events together, and is compared with the expectations for signal and background processes. The error bars on the data points correspond to the intervals at 68% confidence level (CL) [116]. The observed distribution agrees with the expectation within the statistical uncertainties over the whole spectrum.
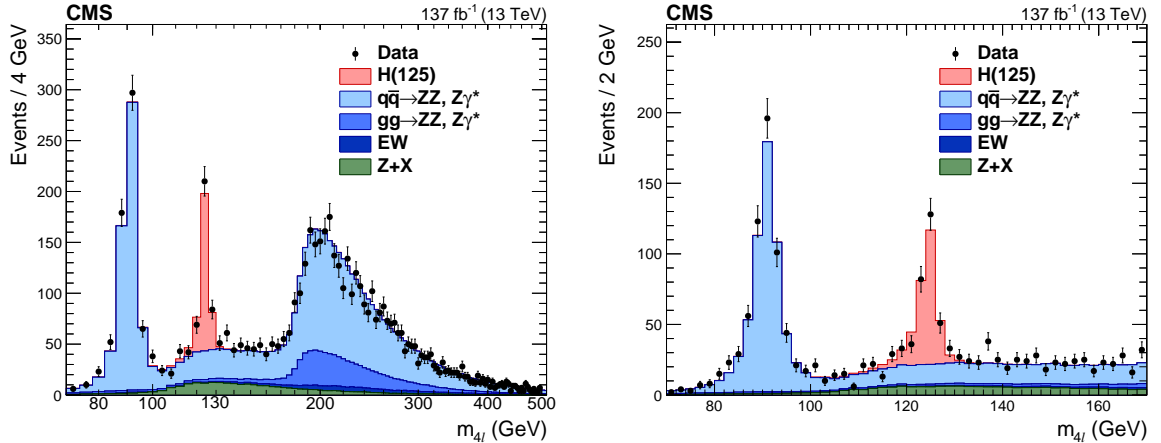


Figure 4: Four-lepton mass distribution, $m_{4\ell}$, up to 500 GeV with 4 GeV bin size (left) and in the low-mass range with 2 GeV bin size (right). Points with error bars represent the data and stacked histograms represent the expected distributions for the signal and background processes. The SM Higgs boson signal with $m_{\mathrm{H}} = 125$ GeV, denoted as H(125), the ZZ and rare electroweak backgrounds are normalized to the SM expectation, the Z+X background to the estimation from data.

The reconstructed four-lepton invariant mass distribution is shown in Fig. 5 for the three 4$\ell$ final states and is compared with the expectations from signal and background processes.

The number of candidates observed in the data and the expected yields for 137 fb$^{-1}$, for the backgrounds and H boson signal after the full event selection, are given in Table 3 for each of the 22 reconstructed event categories (described in Section 6.2) for the $105 < m_{4\ell} < 140$ GeV mass window around the Higgs boson peak. Figure 6 shows the number of expected and observed events for each of the categories.

The reconstructed invariant masses of the $Z_1$ and $Z_2$ dilepton systems are shown in Fig. 7 for $118 < m_{4\ell} < 130$ GeV, together with their 2D distribution in the $105 < m_{4\ell} < 140$ GeV
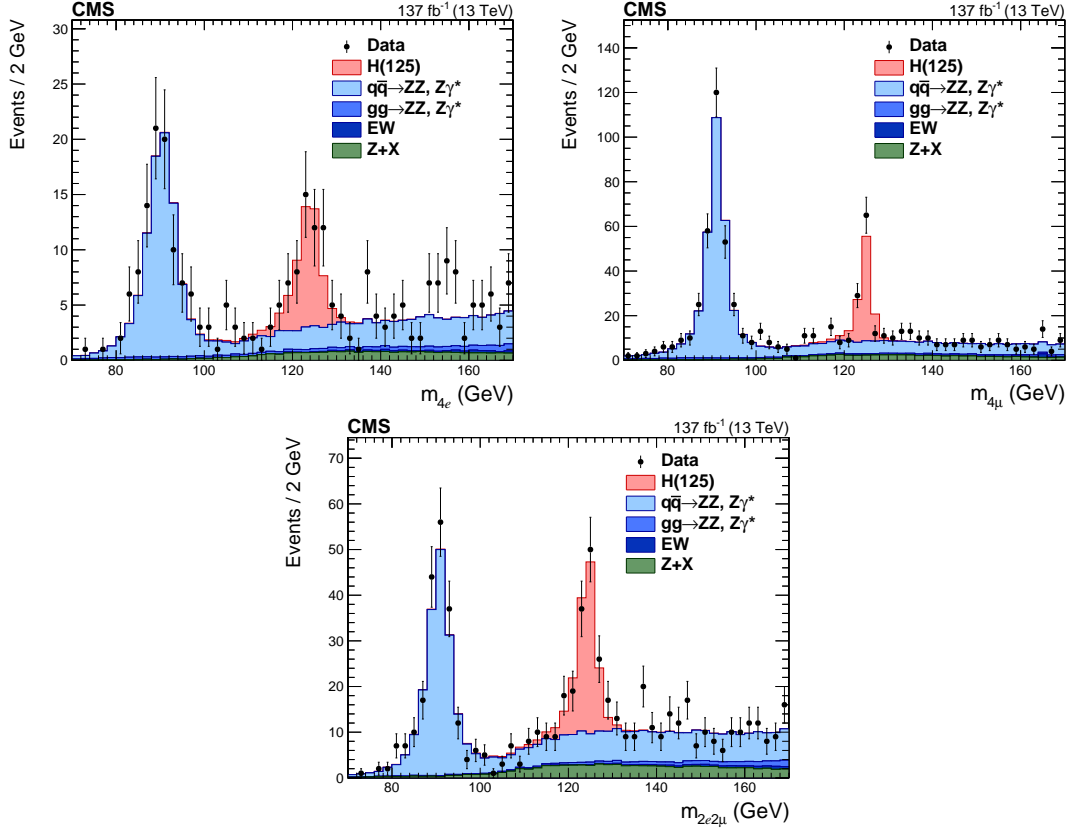
Figure 5: Four-lepton mass distribution in three final states: 4e upper left), 4μ (upper right), and 2e2μ (lower). Points with error bars represent the data and stacked histograms represent the expected distributions for the signal and background processes. The SM Higgs boson signal with $m_H = 125$ GeV, denoted as H(125), the ZZ and rare electroweak backgrounds are normalized to the SM expectation, the Z+X background to the estimation from data.

mass region. The distribution of the discriminants used for event categorization along with the corresponding working point values are shown in Fig. 8.

The results presented in Sections 10.1 and 10.2 are extracted with a two-dimensional likelihood fit that relies on two variables, the four-lepton invariant mass $m_{4\ell}$ and the matrix element kinematic discriminant $\mathcal{D}$. The fit is performed in the $105 < m_{4\ell} < 140$ GeV mass region. The parameters of interest (POIs) are estimated with their corresponding confidence intervals using a profile likelihood ratio test statistic [117, 118], in which the experimental and theoretical uncertainties are incorporated via NPs. The choice of the POIs depends on the specific measurement under consideration, while the remaining parameters are treated as NPs. All the POIs considered in the analysis are forced to be greater than or equal to zero; this reflects the fact that the signal yield is substantially larger than the background yield in the mass range studied. Negative POIs would imply negative signal strength modifiers and a negative probability density function (pdf). We define a two-dimensional pdf as the product of two one-dimensional pdfs:

$$f(m_{4\ell}, \mathcal{D}) = \mathcal{P}(m_{4\ell})\mathcal{P}(\mathcal{D}|m_{4\ell}). \tag{6}$$

The first term, $\mathcal{P}(m_{4\ell})$, is the unbinned analytical shape described in Section 8 for signals and Section 7 for backgrounds. The second term, $\mathcal{P}(\mathcal{D}|m_{4\ell})$, is a binned template of $\mathcal{D}$ that is conditional to $m_{4\ell}$. This is achieved by creating a two-dimensional template of $m_{4\ell}$ vs. $\mathcal{D}$ and normalizing it to 1 for each bin of $m_{4\ell}$.

Table 3: Number of expected background and signal events and number of observed candidates after full analysis selection, for each event category, in the mass range $105 < m_{4\ell} < 140\,\text{GeV}$ and for an integrated luminosity of $137\,\text{fb}^{-1}$. The yields are given for the different production modes. The uncertainties listed are statistical only. Signal is estimated from MC simulation at $m_H = 125\,\text{GeV}$, ZZ and rare electroweak backgrounds are also estimated from MC simulation, and Z+X is estimated from data.

| Reconstructed event category | Signal ggH | VBF | WH | ZH | t$\bar{\text{t}}$H | b$\bar{\text{b}}$H | q$_t$H | Background $q\bar{q} \to ZZ$ | $gg \to ZZ$ | EW | Z+X | Expected signal | total | Observed |
|---|---|---|---|---|---|---|---|---|---|---|---|---|---|---|
| Untagged-0j-$p_T^{4\ell}$[0,10] | 27.7 | 0.09 | 0.03 | 0.03 | 0.00 | 0.15 | 0.00 | 71.5 | 3.06 | 0.01 | 3.21 | 27.9±0.1 | 106±0 | 114 |
| Untagged-0j-$p_T^{4\ell}$[10,200] | 96.2 | 1.69 | 0.60 | 0.77 | 0.01 | 1.01 | 0.00 | 98.1 | 11.6 | 0.35 | 37.8 | 100±0 | 248±1 | 278 |
| Untagged-1j-$p_T^{4\ell}$[0,60] | 26.8 | 1.51 | 0.56 | 0.48 | 0.01 | 0.45 | 0.01 | 25.3 | 3.02 | 0.64 | 14.2 | 29.8±0.1 | 72.9±0.4 | 74 |
| Untagged-1j-$p_T^{4\ell}$[60,120] | 13.5 | 1.31 | 0.51 | 0.41 | 0.02 | 0.11 | 0.01 | 7.81 | 0.82 | 0.62 | 7.95 | 15.9±0.1 | 33.1±0.3 | 20 |
| Untagged-1j-$p_T^{4\ell}$[120,200] | 3.51 | 0.60 | 0.17 | 0.17 | 0.01 | 0.02 | 0.00 | 1.15 | 0.19 | 0.25 | 1.63 | 4.48±0.05 | 7.69±0.16 | 11 |
| Untagged-2j-$p_T^{4\ell}$[0,60] | 3.45 | 0.29 | 0.15 | 0.14 | 0.08 | 0.09 | 0.02 | 2.14 | 0.32 | 0.63 | 4.75 | 4.20±0.06 | 12.1±0.2 | 14 |
| Untagged-2j-$p_T^{4\ell}$[60,120] | 5.26 | 0.56 | 0.24 | 0.19 | 0.12 | 0.04 | 0.03 | 2.19 | 0.30 | 0.72 | 4.14 | 6.43±0.06 | 13.8±0.2 | 15 |
| Untagged-2j-$p_T^{4\ell}$[120,200] | 3.07 | 0.40 | 0.16 | 0.13 | 0.07 | 0.01 | 0.02 | 0.75 | 0.14 | 0.34 | 1.19 | 3.86±0.05 | 6.28±0.14 | 7 |
| Untagged-$p_T^{4\ell} > 200$ | 2.79 | 0.62 | 0.21 | 0.17 | 0.07 | 0.01 | 0.02 | 0.43 | 0.21 | 0.21 | 0.73 | 3.89±0.04 | 5.47±0.11 | 3 |
| Untagged-2j-$m_{jj} > 350$ | 0.77 | 0.16 | 0.06 | 0.04 | 0.05 | 0.01 | 0.01 | 0.34 | 0.06 | 0.31 | 1.71 | 1.12±0.02 | 3.54±0.14 | 3 |
| VBF-1jet-tagged | 15.5 | 3.29 | 0.22 | 0.16 | 0.00 | 0.13 | 0.01 | 6.85 | 1.53 | 0.20 | 2.44 | 19.3±0.1 | 30.3±0.2 | 27 |
| VBF-2jet-tagged-$m_{jj}$[350,700] | 0.83 | 1.19 | 0.01 | 0.01 | 0.00 | 0.01 | 0.00 | 0.19 | 0.07 | 0.11 | 0.14 | 2.05±0.03 | 2.55±0.05 | 2 |
| VBF-2jet-tagged-$m_{jj} > 700$ | 0.43 | 1.96 | 0.00 | 0.00 | 0.00 | 0.00 | 0.00 | 0.07 | 0.05 | 0.12 | 0.03 | 2.40±0.02 | 2.67±0.03 | 1 |
| VBF-3jet-tagged-$m_{jj} > 350$ | 2.52 | 2.35 | 0.06 | 0.06 | 0.03 | 0.03 | 0.05 | 0.62 | 0.21 | 0.64 | 2.43 | 5.11±0.05 | 9.01±0.17 | 12 |
| VBF-2jet-tagged-$p_T^{4\ell} > 200$ | 0.44 | 0.79 | 0.01 | 0.01 | 0.01 | 0.00 | 0.01 | 0.03 | 0.03 | 0.04 | 0.06 | 1.26±0.02 | 1.42±0.03 | 0 |
| VBF-rest | 2.48 | 0.94 | 0.13 | 0.09 | 0.04 | 0.04 | 0.01 | 0.98 | 0.20 | 0.39 | 2.18 | 3.74±0.05 | 7.49±0.17 | 5 |
| VH-hadronic-tagged-$m_{jj}$[60,120] | 4.11 | 0.25 | 1.09 | 0.96 | 0.13 | 0.06 | 0.02 | 1.69 | 0.22 | 0.52 | 2.93 | 6.62±0.06 | 12.0±0.2 | 12 |
| VH-rest | 0.57 | 0.03 | 0.09 | 0.06 | 0.03 | 0.01 | 0.00 | 0.16 | 0.02 | 0.06 | 0.33 | 0.79±0.02 | 1.36±0.06 | 0 |
| VH-leptonic-tagged-$p_T^{4\ell}$[0,150] | 0.33 | 0.04 | 0.85 | 0.26 | 0.10 | 0.03 | 0.03 | 2.16 | 0.36 | 0.19 | 1.11 | 1.64±0.02 | 5.47±0.13 | 10 |
| VH-leptonic-tagged-$p_T^{4\ell} > 150$ | 0.02 | 0.01 | 0.21 | 0.06 | 0.04 | 0.00 | 0.01 | 0.05 | 0.01 | 0.03 | 0.08 | 0.35±0.01 | 0.52±0.03 | 0 |
| t$\bar{\text{t}}$H-leptonic-tagged | 0.02 | 0.01 | 0.02 | 0.02 | 0.68 | 0.00 | 0.03 | 0.08 | 0.01 | 0.23 | 0.21 | 0.79±0.01 | 1.32±0.07 | 0 |
| t$\bar{\text{t}}$H-hadronic-tagged | 0.18 | 0.05 | 0.03 | 0.05 | 0.86 | 0.01 | 0.03 | 0.03 | 0.01 | 0.82 | 1.06 | 1.22±0.01 | 3.15±0.14 | 2 |

In almost all sub-categories we use a decay-only kinematic discriminant ($\mathcal{D} = \mathcal{D}_{\text{bkg}}^{\text{kin}}$) to separate the H boson signal from the background as defined in Eq. (3). Conversely, in the sub-categories of the VBF-2jet-tagged, the $\mathcal{D} = \mathcal{D}_{\text{bkg}}^{\text{VBF+dec}}$ discriminant (defined in Eq. (4)) is used, which is sensitive to the VBF production mechanism. Similarly, in two sub-categories of the VH-hadronic-tagged category, the $\mathcal{D} = \mathcal{D}_{\text{bkg}}^{\text{VH+dec}}$ discriminant (defined in Eq. (5)) is used.

The ggH, VBF, WH, ZH and t$\bar{\text{t}}$H samples are used to build different signal templates for each of the nineteen STXS production bins described in Section 6.1. Irreducible background templates are built starting from $q\bar{q} \to ZZ$ and $gg \to ZZ$ samples. Finally, reducible background templates are built using data driven methods described in Section 7.2. Following the described procedure, $\mathcal{P}(\mathcal{D}|m_{4\ell})$ templates are obtained for the twenty-two event categories and the three final states (4$\mu$, 4e, 2e2$\mu$).

The unbinned likelihood function, $\mathcal{L}(\vec{\mu})$, is defined as the product over $N$ observed events:

$$\mathcal{L}(\vec{\mu}) = \frac{1}{N} \prod_{\text{events}} \left( \sum_{i=1}^{19} \mu_i S_i^{jk} f_S^{ijk}(m_{4\ell}, \mathcal{D}) + B^{jk} f_B^{jk}(m_{4\ell}, \mathcal{D}) \right) e^{-\sum_i \mu_i S_i^{jk} + B^{jk}}, \qquad (7)$$

where $\mu_i$ is the signal strength modifier for the production bin $i$, $S_i^{jk}$ are the predicted SM rates of events in the production bin $i$ that are observed in the reconstructed event category $j$ and final state $k$, $B^{jk}$ are the predicted background rates in the reconstructed event category $j$ and final state $k$, $f_S^{ijk}(m_{4\ell}, \mathcal{D})$ are the pdfs for the signal, and $f_B^{jk}(m_{4\ell}, \mathcal{D})$ the pdfs for the background.

The correlation of the kinematic discriminants $\mathcal{D}_{\text{bkg}}^{\text{kin}}$, $\mathcal{D}_{\text{bkg}}^{\text{VBF+dec}}$, and $\mathcal{D}_{\text{bkg}}^{\text{VH+dec}}$ with the four-lepton invariant mass is shown in Fig. 9 for the mass interval $105 < m_{4\ell} < 140\,\text{GeV}$. Their distributions for the mass interval $118 < m_{4\ell} < 130\,\text{GeV}$ are shown in Fig. 10.
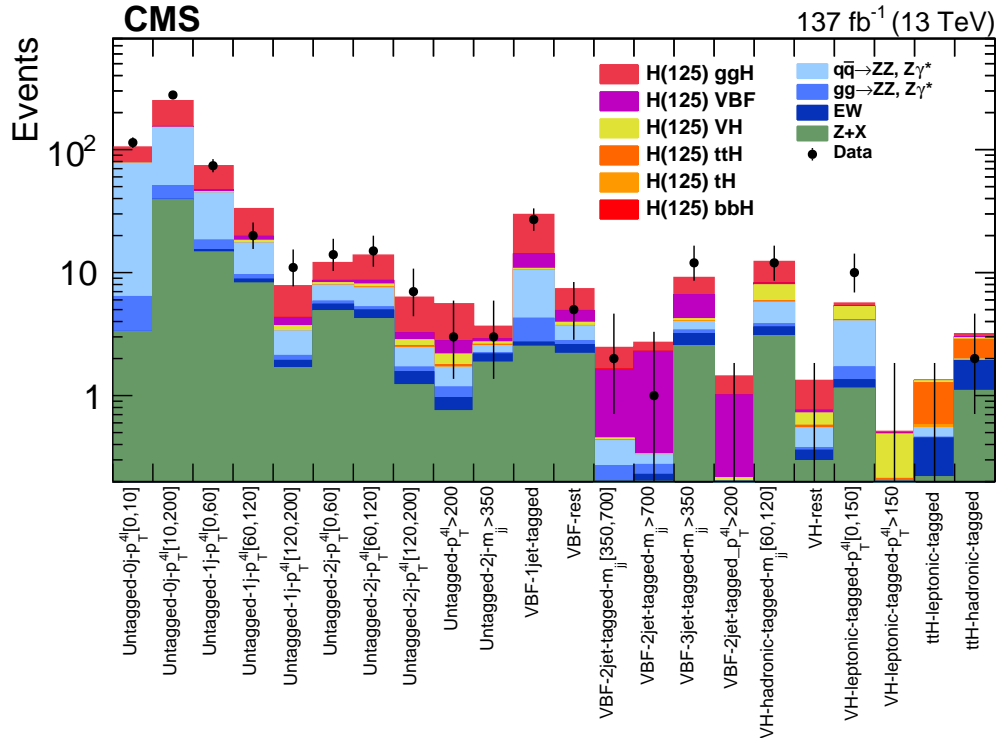
Figure 6: Distributions of the expected and observed number of events for the reconstructed event categories in the mass region $105 < m_{4\ell} < 140$ GeV. Points with error bars represent the data and stacked histograms represent the expected numbers of the signal and background events. The yields of the different H boson production mechanisms with $m_H = 125$ GeV, denoted as H(125), and those of the ZZ and rare electroweak backgrounds are normalized to the SM expectations, while the Z+X background yield is normalized to the estimate from the data.

## 10.1 Signal strength modifier

A simultaneous fit to all categories is performed to extract the signal strength modifier, defined as the ratio of the observed H boson yield in the H $\to 4\ell$ decay channel to the standard model expectation.

The combined measurement of the inclusive signal strength modifier is measured to be $\mu = 0.94^{+0.12}_{-0.11}$ or $\mu = 0.94 \pm 0.07\,\text{(stat)}^{+0.07}_{-0.06}\,\text{(theo)}^{+0.06}_{-0.05}\,\text{(exp)}$ at a fixed mass value $m_H = 125.38$ GeV, which is the current most precise measurement of the H boson mass published by the CMS Collaboration [119]. In all subsequent fits, $m_H$ is fixed to this value. The dominant experimental sources of systematic uncertainty are the uncertainties in the lepton identification efficiencies and luminosity measurement, while the dominant theoretical source is the uncertainty in the total gluon fusion cross section. The contributions to the total uncertainty from experimental and theoretical sources are found to be similar in magnitude. The signal strength modifiers are further studied in terms of the five main SM Higgs boson production mechanisms, namely ggH, VBF, ZH, WH, and $t\bar{t}$H. The contributions of the $b\bar{b}$H and $q_t$H production modes are also taken into account. The relative normalizations of the $b\bar{b}$H and the gluon fusion contributions are kept fixed in the fit, and so are the $q_t$H and $t\bar{t}$H ones. The results are shown in Fig. 11 for the observed and expected profile likelihood scans of the inclusive signal strength modifier and those for the signal strength modifiers of the five main SM Higgs boson production mechanisms. The corresponding numerical values, including the decomposition of the uncertainties
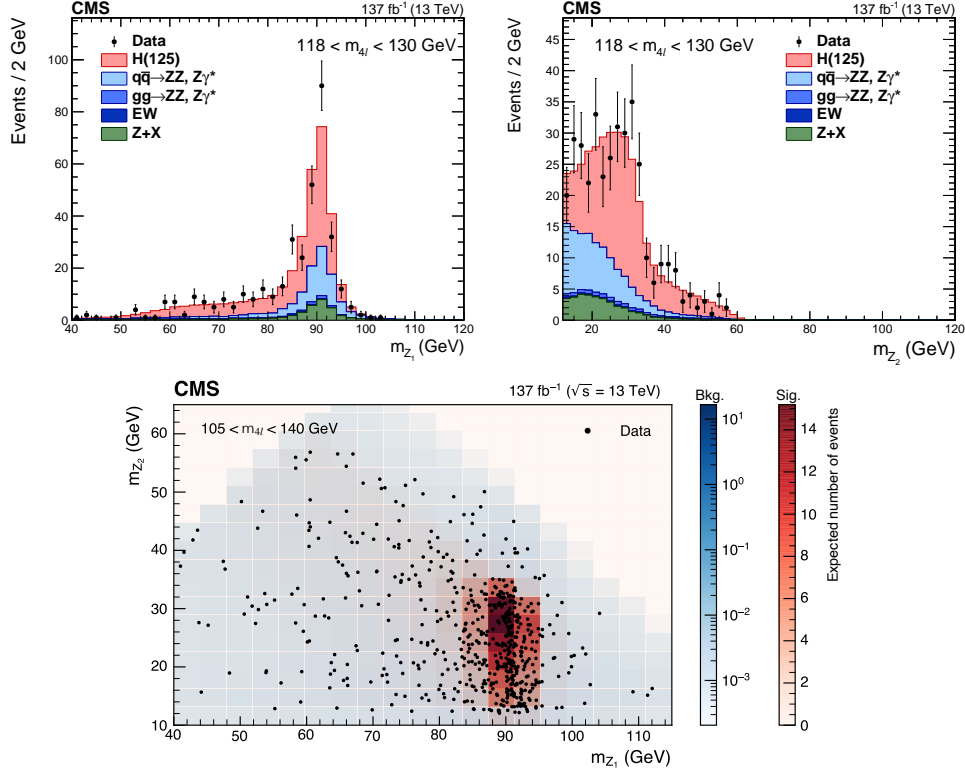
Figure 7: Distribution of the $Z_1$ (upper left) and $Z_2$ (upper right) reconstructed masses in the $118 < m_{4\ell} < 130$ GeV mass region and their 2D distribution (lower) in the $105 < m_{4\ell} < 140$ GeV mass region. The stacked histograms and the red and blue scales represent expected distributions of the signal and background processes and the points represent the data. The yields of the different H boson production mechanisms with $m_H = 125$ GeV, denoted as H(125), and those of the ZZ and rare electroweak backgrounds are normalized to the SM expectations, while the Z+X background yield is normalized to the estimate from the data.

into statistical and systematic components, as well as the expected uncertainties, are given in Table 4.

The dependence of the measured signal strengths on the profiling of $m_H$ is checked and found to have a small impact both on the inclusive results and those in terms of the five main H boson production mechanisms, well within the measurement uncertainties. The best fit signal value changes at most by 4% and the profiled value of the mass is found to be $m_H = 125.09^{+0.15}_{-0.14}$ (stat) GeV. It is important to note here that the precise determination of $m_H$ and the systematic uncertainties that enter its measurement are beyond the scope of this analysis.

Two signal strength modifiers, $\mu_f \equiv \mu_{ggH, t\bar{t}H, b\bar{b}H, q_t H}$ and $\mu_V \equiv \mu_{VBF, VH}$, are introduced for the fermion and vector-boson induced contributions to the expected SM cross section. A two-parameter fit is performed simultaneously to the events reconstructed in all categories, leading to $\mu_f = 0.96^{+0.14}_{-0.12}$ and $\mu_V = 0.82^{+0.36}_{-0.31}$. The expected values for $m_H = 125.38$ GeV are $\mu_f = 1.00^{+0.15}_{-0.13}$ and $\mu_V = 1.00^{+0.39}_{-0.33}$. The 68 and 95% CL contours in the $(\mu_f, \mu_V)$ plane are shown in Fig. 12 and the SM predictions lie within the 68% CL regions of this measurement.
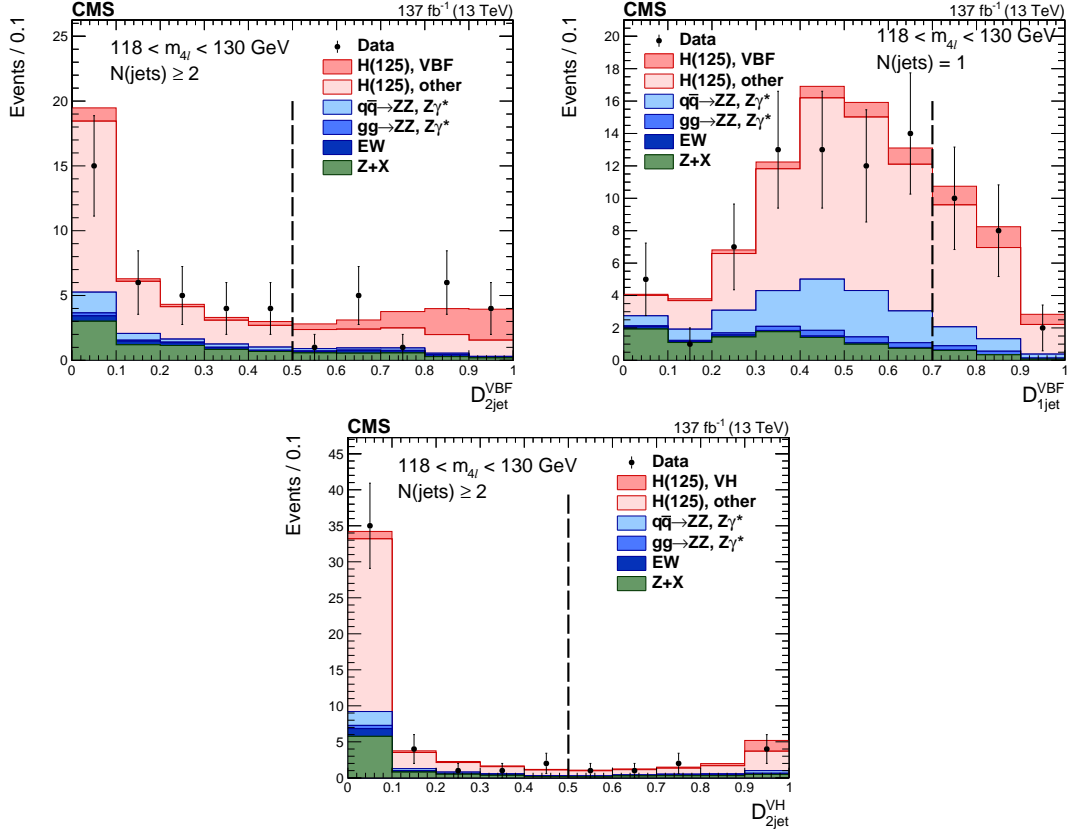
Figure 8: Distribution of categorization discriminants in the mass region $118 < m_{4\ell} < 130\,\text{GeV}$: $\mathcal{D}_{2\text{jet}}^{\text{VBF}}$ (upper left), $\mathcal{D}_{1\text{jet}}^{\text{VBF}}$ (upper right), $\mathcal{D}_{2\text{jet}}^{\text{VH}}$ (lower) = $\max(\mathcal{D}_{2\text{jet}}^{\text{WH}}, \mathcal{D}_{2\text{jet}}^{\text{ZH}})$. Points with error bars represent the data and stacked histograms represent expected distributions of the signal and background processes. The SM Higgs boson signal with $m_\text{H} = 125\,\text{GeV}$, denoted as H(125), and the ZZ backgrounds and rare electroweak backgrounds are normalized to the SM expectation, the Z+X background to the estimation from data. The vertical dashed lines denote the working points used in the event categorization. The SM H boson signal is separated into two components: the production mode which is targeted by the specific discriminant, and other production modes, where the gluon fusion process dominates.

## 10.2 Simplified template cross section

The results for the H boson product of cross section times branching fraction for $\text{H} \rightarrow \text{ZZ}$ decay, $(\sigma\mathcal{B})_\text{obs}$, and comparisons with the SM expectation, $(\sigma\mathcal{B})_\text{SM}$, for the stages of production bins defined in Section 6.1, are shown in Fig. 13 for the stage 0 and in Fig. 14 for the merged stage 1.2. The corresponding numerical values are given in Tables 5 and 6.

As discussed, the set of THU uncertainties described in Section 9.2 is not considered for the STXS measurements: THU uncertainties are model dependent and should be only considered in the interpretation of the results. Therefore, the THU uncertainties are included in the SM predictions of the cross section. The correlation matrices are shown in Fig. 15. The dominant experimental sources of systematic uncertainty are the same as for the signal strength modifiers measurement, while the dominant theoretical source is the uncertainty in the category migration for the ggH process.
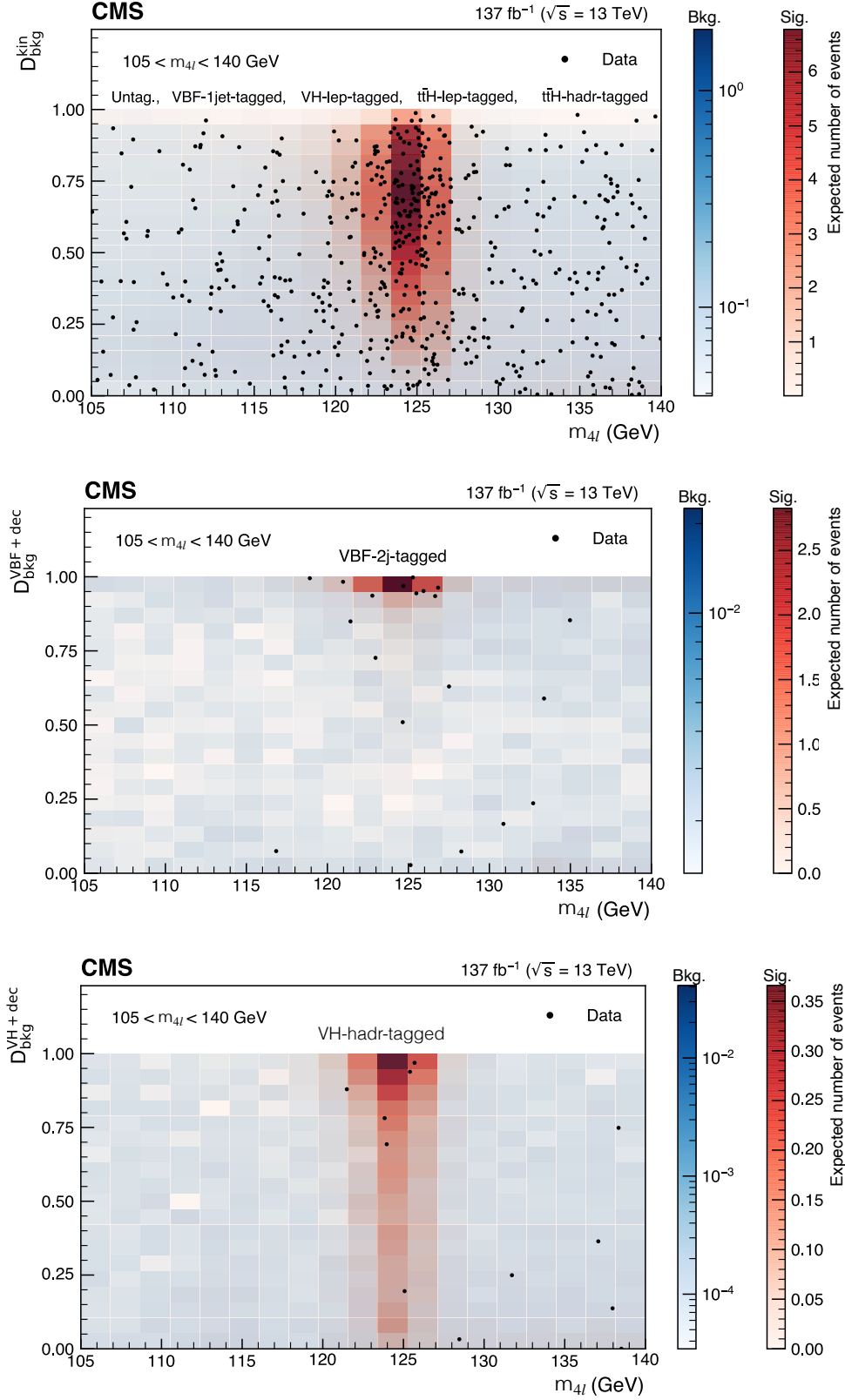
Figure 9: Distribution of three different kinematic discriminants versus $m_{4\ell}$: $\mathcal{D}_{bkg}^{kin}$ (upper), $\mathcal{D}_{bkg}^{VBF+dec}$ (middle) and $\mathcal{D}_{bkg}^{VH+dec}$ (lower) shown in the mass region $105 < m_{4\ell} < 140\,\mathrm{GeV}$. The blue scale represents the expected total number of ZZ, rare electroweak, and Z+X background events. The red scale represents the number of expected SM H boson signal events for $m_H = 125\,\mathrm{GeV}$. The points show the data from the categories listed in the legend.
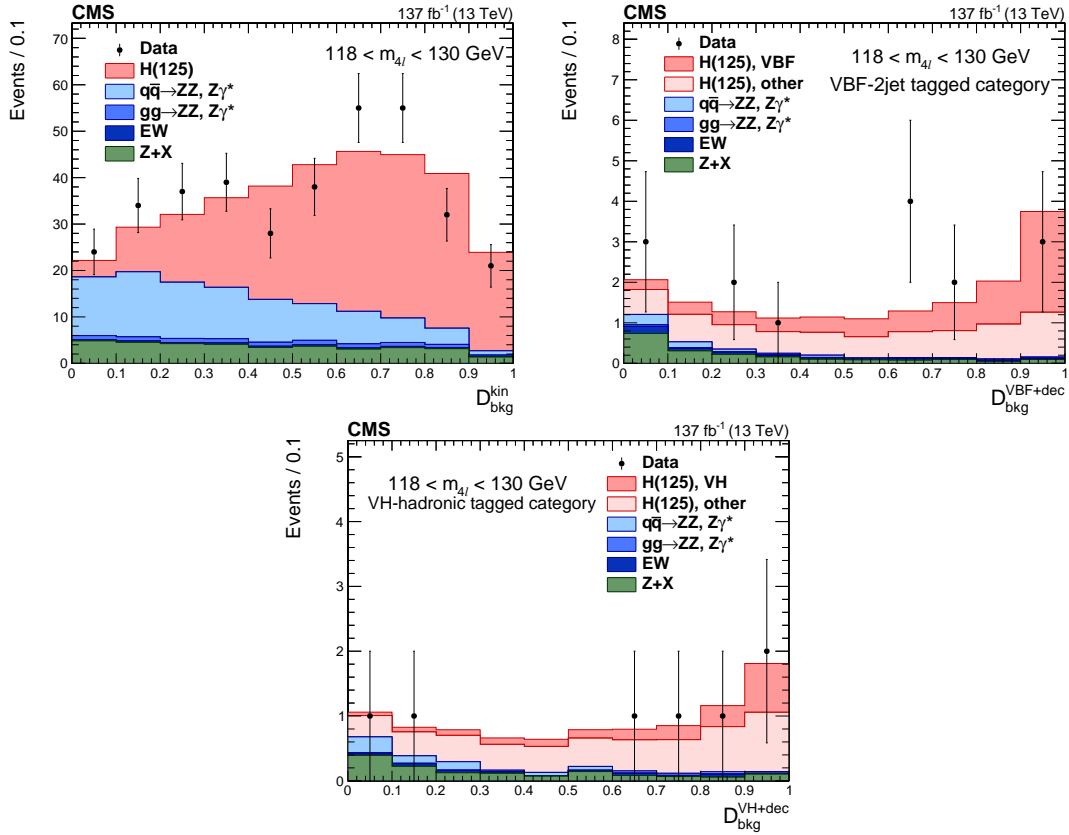
Figure 10: Distribution of kinematic discriminants in the mass region $118 < m_{4\ell} < 130\,\text{GeV}$: (upper left) $\mathcal{D}_{\text{bkg}}^{\text{kin}}$, (upper right) $\mathcal{D}_{\text{bkg}}^{\text{VBF+dec}}$, (lower) $\mathcal{D}_{\text{bkg}}^{\text{VH+dec}}$. Points with error bars represent the data and stacked histograms represent expected distributions of the signal and background processes. The yields of the different H boson production mechanisms with $m_{\text{H}} = 125\,\text{GeV}$, denoted as H(125), and those of the ZZ and rare electroweak backgrounds are normalized to the SM expectations, while the Z+X background yield is normalized to the estimate from the data. In the middle and right figures the SM H boson signal is separated into two components: the production mode which is targeted by the specific discriminant, and other production modes, where the gluon fusion process dominates.

## 10.3   Fiducial cross section

In this section the cross section measurement for the process $\text{pp} \to \text{H} \to 4\ell$ within a fiducial volume that closely matches the reconstruction level selection is presented. In particular, the integrated fiducial cross section is measured as well as differential cross sections as a function of the transverse momentum of the H boson ($p_{\text{T}}^{\text{H}}$), its rapidity ($|y^{\text{H}}|$), the number of associated jets ($N^{\text{j}}$), and the transverse momentum of the leading jet ($p_{\text{T}}^{\text{j}}$). These measurements are largely independent of the assumptions on the relative fractions and kinematic distributions of the individual production modes. The definition of the fiducial volume is based on generator-level quantities and is identical to that in Ref. [18]. In order to reduce the experimental uncertainties, only jets with $p_{\text{T}}^{\text{j}} > 30\,\text{GeV}$ and $|\eta^{\text{j}}| < 2.5$ are considered for the differential cross sections as a function of jet observables. An increase in model dependence compared to Ref. [25] is observed when using the ZZ candidate selection at reconstruction level where the candidate with the best $\mathcal{D}_{\text{bkg}}^{\text{kin}}$ discriminant value is chosen. Therefore, the fiducial cross section measurement is performed using the event selection algorithm in Ref. [25]. Specifically, the $\text{Z}_1$ candidate is chosen to be the one with $m(\text{Z}_1)$ closest to the nominal Z boson mass, and in cases where mul-
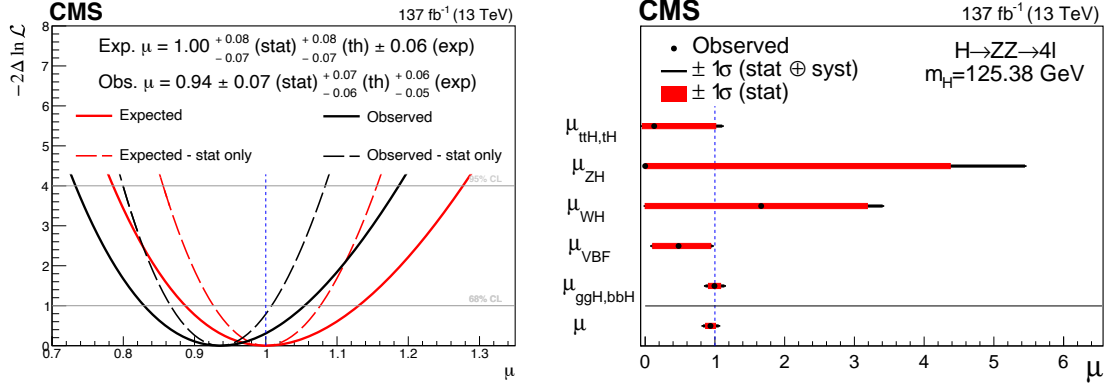
Figure 11: (left) The observed and expected profile likelihood scans of the inclusive signal strength modifier. The scans are shown both with (solid line) and without (dashed line) systematic uncertainties. (right) Results of likelihood scans for the signal strength modifiers corresponding to the five main SM H boson production mechanisms, compared to the SM prediction shown as a vertical dashed line. The thick black lines indicate the one standard deviation confidence intervals including both statistical and systematic sources. The thick red lines indicate the statistical uncertainties corresponding to the one standard deviation confidence intervals.

tiple $Z_2$ candidates satisfy all criteria, the pair of leptons with the largest sum of the transverse momenta magnitudes is chosen. The full fiducial volume definition is detailed in Table 7 and

Table 4: Best fit values and $\pm 1$ standard deviation uncertainties for the expected and observed signal strength modifiers at $m_H = 125.38\,\text{GeV}$. The statistical and systematic uncertainties are given separately.

|  | Expected | Observed |
|---|---|---|
| $\mu_{t\bar{t}H,q_tH}$ | $1.00^{+1.23}_{-0.77}\,\text{(stat)}^{+0.51}_{-0.06}\,\text{(syst)}$ | $0.17^{+0.88}_{-0.17}\,\text{(stat)}^{+0.42}_{-0.00}\,\text{(syst)}$ |
| $\mu_{WH}$ | $1.00^{+1.83}_{-1.00}\,\text{(stat)}^{+0.75}_{-0.00}\,\text{(syst)}$ | $1.66^{+1.52}_{-1.66}\,\text{(stat)}^{+0.85}_{-0.00}\,\text{(syst)}$ |
| $\mu_{ZH}$ | $1.00^{+4.79}_{-1.00}\,\text{(stat)}^{+6.76}_{-0.00}\,\text{(syst)}$ | $0.00^{+4.38}_{-0.00}\,\text{(stat)}^{+3.24}_{-0.00}\,\text{(syst)}$ |
| $\mu_{VBF}$ | $1.00^{+0.53}_{-0.44}\,\text{(stat)}^{+0.18}_{-0.12}\,\text{(syst)}$ | $0.48^{+0.46}_{-0.37}\,\text{(stat)}^{+0.14}_{-0.10}\,\text{(syst)}$ |
| $\mu_{ggH,b\bar{b}H}$ | $1.00 \pm 0.10\,\text{(stat)}^{+0.12}_{-0.10}\,\text{(syst)}$ | $0.99 \pm 0.09\,\text{(stat)}^{+0.11}_{-0.09}\,\text{(syst)}$ |
| $\mu$ | $1.00^{+0.08}_{-0.07}\,\text{(stat)}^{+0.10}_{-0.08}\,\text{(syst)}$ | $0.94 \pm 0.07\,\text{(stat)}^{+0.09}_{-0.08}\,\text{(syst)}$ |

Table 5: Best fit values and $\pm 1$ standard deviation uncertainties for the measured cross sections $(\sigma\mathcal{B})_{\text{obs}}$, the SM predictions $(\sigma\mathcal{B})_{\text{SM}}$, and their ratio for the stage 0 STXS production bins at $m_H = 125.38\,\text{GeV}$ for $H \to ZZ$ decay.

|  | $(\sigma\mathcal{B})_{\text{obs}}$ (fb) | $(\sigma\mathcal{B})_{\text{SM}}$ (fb) | $(\sigma\mathcal{B})_{\text{obs}}/(\sigma\mathcal{B})_{\text{SM}}$ |
|---|---|---|---|
| ttH | $3^{+16}_{-3}$ | $15.9 \pm 1.4$ | $0.16^{+0.98}_{-0.16}$ |
| VH-lep | $41^{+52}_{-35}$ | $25.9 \pm 0.8$ | $1.56^{+1.99}_{-1.34}$ |
| qqH | $61^{+53}_{-44}$ | $122 \pm 6$ | $0.50^{+0.44}_{-0.36}$ |
| ggH | $1214^{+135}_{-125}$ | $1192 \pm 95$ | $1.02^{+0.11}_{-0.10}$ |
| Inclusive | $1318^{+130}_{-122}$ | $1369 \pm 164$ | $0.96^{+0.10}_{-0.09}$ |
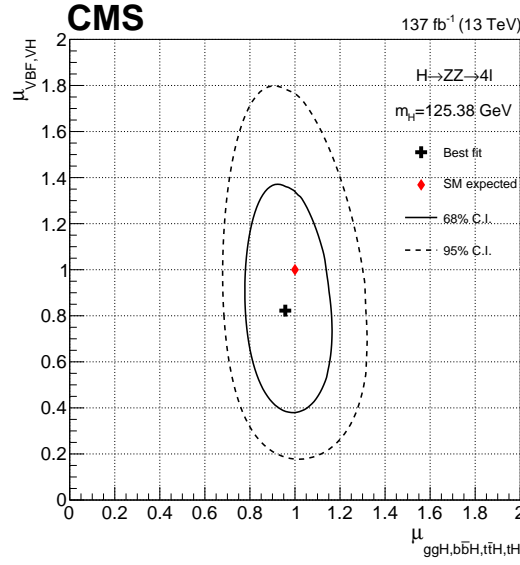
Figure 12: Result of the 2D likelihood scan for the $\mu_f \equiv \mu_{ggH,t\bar{t}H,b\bar{b}H,q_tH}$ and $\mu_V \equiv \mu_{VBF,VH}$ signal strength modifiers. The solid and dashed contours show the 68 and 95% CL regions, respectively. The cross indicates the best fit value, and the diamond represents the expected value for the SM Higgs boson.
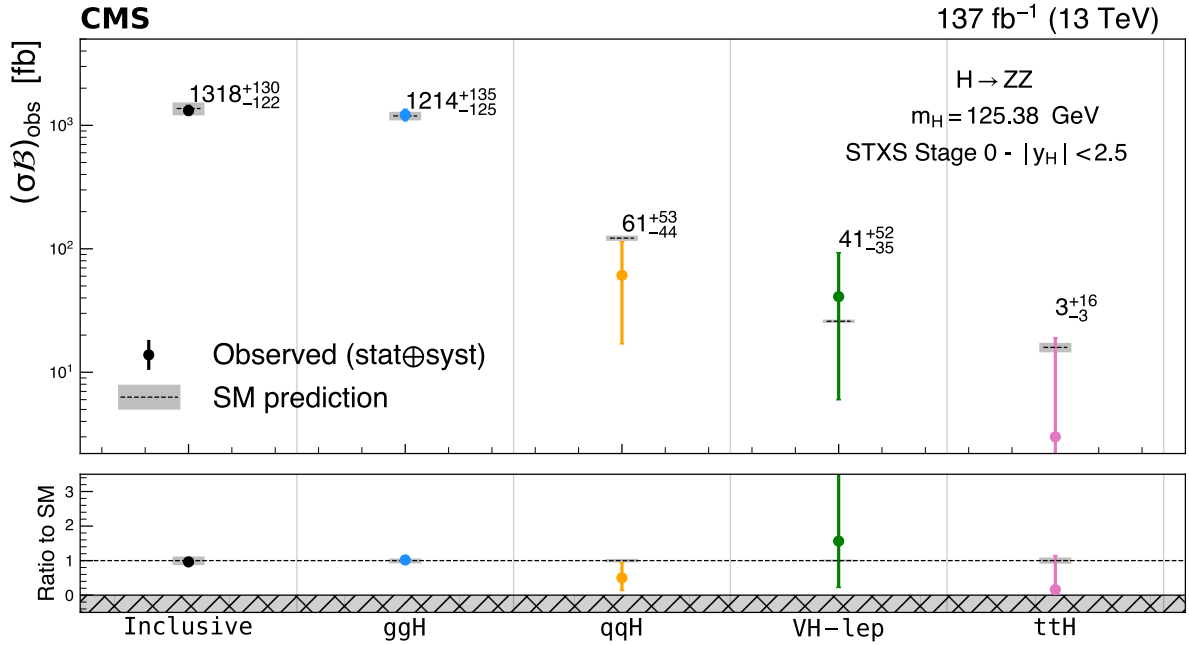


Figure 13: The measured product of cross section times branching fraction for $H \rightarrow ZZ$ decay $(\sigma\mathcal{B})_{obs}$ and the SM predictions $(\sigma\mathcal{B})_{SM}$ for the stage 0 STXS production bins and the inclusive measurement at $m_H = 125.38\,\text{GeV}$. Points with error bars represent measured values and black dashed lines with gray uncertainty bands represent the SM predictions. In the bottom panel ratios of the measured cross sections and the SM predictions are shown along with the uncertainties for each of the bins and the inclusive measurement.

the acceptance for various SM production modes is given in Table 8.

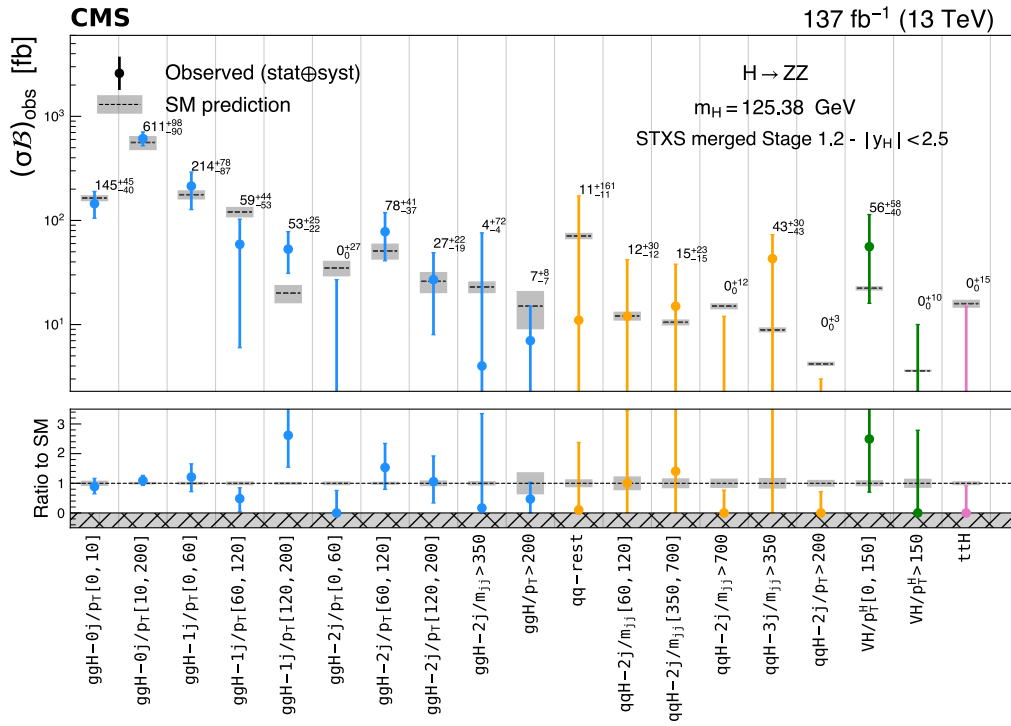A maximum likelihood fit of the signal and background parameterizations to the observed

Figure 14: The measured cross sections $(\sigma\mathcal{B})_{\mathrm{obs}}$ and the SM predictions $(\sigma\mathcal{B})_{\mathrm{SM}}$ for $\mathrm{H} \rightarrow \mathrm{ZZ}$ decay and the merged stage 1.2 STXS production bins at $m_{\mathrm{H}} = 125.38\,\mathrm{GeV}$. Points with error bars represent measured values and black dashed lines with gray uncertainty bands represent the SM predictions. In the bottom panel ratios of the measured cross sections and the SM predictions are shown with corresponding uncertainties for each of the bins.

$4\ell$ mass distribution, $N_{\mathrm{obs}}(m_{4\ell})$, is performed to extract the integrated fiducial cross section for the process pp $\rightarrow$ H $\rightarrow$ $4\ell$ ($\sigma_{\mathrm{fid}}$). The fit is carried out inclusively (i.e., without any event categorization) and does not use the $\mathcal{D}_{\mathrm{bkg}}^{\mathrm{kin}}$ observable in order to minimize the model dependence. The fit is performed simultaneously in all final states and assumes a H boson mass $m_{\mathrm{H}} = 125.38\,\mathrm{GeV}$, while the branching fractions of the H boson to different final states ($4e, 4\mu, 2e2\mu$) are free parameters in the fit. The systematic uncertainties described in Section 9 are included in the form of NPs and the results are obtained using an asymptotic approach [118] with a test statistic based on the profile likelihood ratio [117]. This procedure accounts for the unfolding of detector effects from the observed distributions and is the same as in Refs. [25] and [120].

The number of expected events in each final state $f$ and in each bin $i$ of a given observable is

Table 6: Best fit values and $\pm 1$ standard deviation uncertainties for the measured cross sections $(\sigma\mathcal{B})_{\mathrm{obs}}$, the SM predictions $(\sigma\mathcal{B})_{\mathrm{SM}}$, and their ratio for the merged stage 1.2 STXS production bins at $m_{\mathrm{H}} = 125.38\,\mathrm{GeV}$ for H $\rightarrow$ ZZ decay.

| | $(\sigma\mathcal{B})_{\mathrm{obs}}$ (fb) | $(\sigma\mathcal{B})_{\mathrm{SM}}$ (fb) | $(\sigma\mathcal{B})_{\mathrm{obs}}/(\sigma\mathcal{B})_{\mathrm{SM}}$ |
|---|---|---|---|
| ggH-0j/$p_{\mathrm{T}}[0,10]$ | $145^{+45}_{-40}$ | $164 \pm 11$ | $0.89^{+0.28}_{-0.24}$ |
| ggH-0j/$p_{\mathrm{T}}[10,200]$ | $611^{+98}_{-90}$ | $561 \pm 87$ | $1.09^{+0.17}_{-0.16}$ |
| ggH-1j/$p_{\mathrm{T}}[0,60]$ | $214^{+78}_{-87}$ | $177 \pm 18$ | $1.21^{+0.44}_{-0.49}$ |
| ggH-1j/$p_{\mathrm{T}}[60,120]$ | $59^{+44}_{-53}$ | $121 \pm 14$ | $0.48^{+0.37}_{-0.44}$ |
| ggH-1j/$p_{\mathrm{T}}[120,200]$ | $53^{+25}_{-22}$ | $20 \pm 4$ | $2.62^{+1.24}_{-1.08}$ |
| ggH-2j/$p_{\mathrm{T}}[0,60]$ | $0^{+27}_{-0}$ | $35 \pm 6$ | $0.00^{+0.76}_{-0.00}$ |
| ggH-2j/$p_{\mathrm{T}}[60,120]$ | $78^{+41}_{-37}$ | $51 \pm 9$ | $1.53^{+0.81}_{-0.73}$ |
| ggH-2j/$p_{\mathrm{T}}[120,200]$ | $27^{+22}_{-19}$ | $26 \pm 6$ | $1.06^{+0.87}_{-0.72}$ |
| ggH-2j/$m_{\mathrm{jj}} > 350$ | $4^{+72}_{-4}$ | $23 \pm 3$ | $0.17^{+3.2}_{-0.17}$ |
| ggH/$p_{\mathrm{T}} > 200$ | $7^{+8}_{-7}$ | $15 \pm 6$ | $0.47^{+0.56}_{-0.47}$ |
| qqH-rest | $11^{+161}_{-11}$ | $71 \pm 5$ | $0.15^{+2.27}_{-0.15}$ |
| qqH-2j/$m_{\mathrm{jj}}[60,120]$ | $12^{+30}_{-12}$ | $12.1 \pm 1.2$ | $1.01^{+2.45}_{-1.01}$ |
| qqH-2j/$m_{\mathrm{jj}}[350,700]$ | $15^{+23}_{-15}$ | $10.5 \pm 0.7$ | $1.41^{+2.21}_{-1.41}$ |
| qqH-2j/$m_{\mathrm{jj}} > 700$ | $0^{+12}_{-0}$ | $15 \pm 1$ | $0.00^{+0.77}_{-0.00}$ |
| qqH-3j/$m_{\mathrm{jj}} > 350$ | $43^{+30}_{-43}$ | $8.9 \pm 0.5$ | $4.84^{+3.38}_{-4.84}$ |
| qqH-2j/$p_{\mathrm{T}} > 200$ | $0^{+3}_{-0}$ | $4.2 \pm 0.2$ | $0.00^{+0.72}_{-0.00}$ |
| VH-lep/$p_{\mathrm{T}}^{\mathrm{H}}[0,150]$ | $56^{+58}_{-40}$ | $22.3 \pm 1.1$ | $2.49^{+2.60}_{-1.79}$ |
| VH-lep/$p_{\mathrm{T}}^{\mathrm{H}} > 150$ | $0^{+10}_{-0}$ | $3.6 \pm 0.1$ | $0.00^{+2.79}_{-0.00}$ |
| ttH | $0^{+15}_{-0}$ | $15.9 \pm 1.4$ | $0.00^{+0.91}_{-0.00}$ |
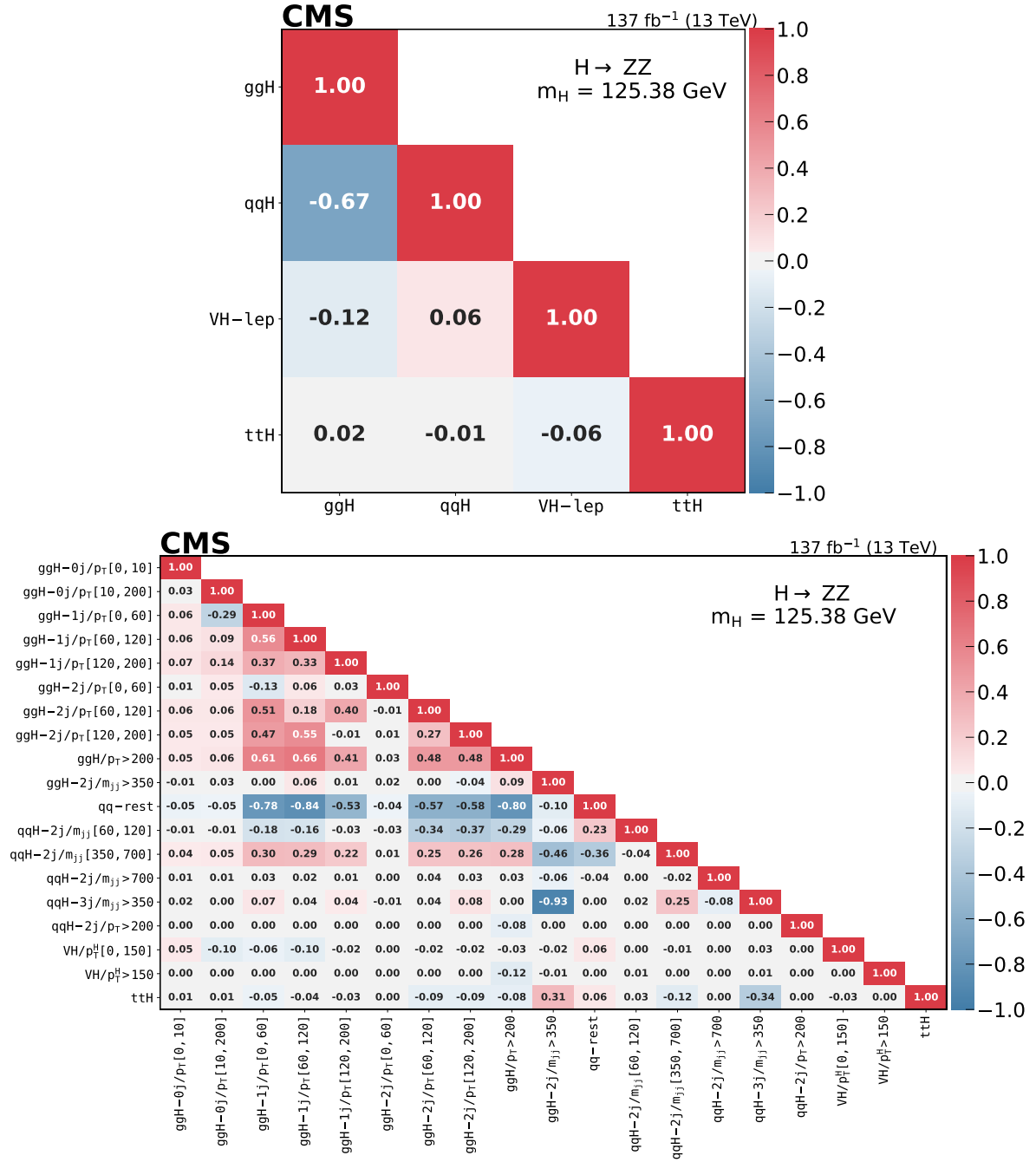
Figure 15: Correlation matrices between the measured cross sections for the stage 0 (upper) and the merged stage 1.2 (lower) for H $\rightarrow$ ZZ decay.

expressed as a function of $m_{4\ell}$ as:

$$
\begin{aligned}
N_{\text{exp}}^{f,i}(m_{4\ell}) &= N_{\text{fid}}^{f,i}(m_{4\ell}) + N_{\text{nonfid}}^{f,i}(m_{4\ell}) + N_{\text{nonres}}^{f,i}(m_{4\ell}) + N_{\text{bkg}}^{f,i}(m_{4\ell}) \\
&= \sum_j \epsilon_{i,j}^f \left( 1 + f_{\text{nonfid}}^{f,i} \right) \sigma_{\text{fid}}^{f,j} \mathcal{L} \mathcal{P}_{\text{res}}(m_{4\ell}) \\
&\quad + N_{\text{nonres}}^{f,i} \mathcal{P}_{\text{nonres}}(m_{4\ell}) + N_{\text{bkg}}^{f,i} \mathcal{P}_{\text{bkg}}(m_{4\ell}).
\end{aligned}
\tag{8}
$$

The shape of the resonant signal contribution, $\mathcal{P}_{\text{res}}(m_{4\ell})$, is described by a double-sided Crystal Ball function as discussed in Section 8, and the normalization is used to extract the fiducial cross

Table 7: Summary of requirements used in the definition of the fiducial phase space for the $H \to 4\ell$ cross section measurements.

| Requirements for the $H \to 4\ell$ fiducial phase space | |
| --- | --- |
| Lepton kinematics and isolation | |
| Leading lepton $p_T$ | $p_T > 20\,\mathrm{GeV}$ |
| Next-to-leading lepton $p_T$ | $p_T > 10\,\mathrm{GeV}$ |
| Additional electrons (muons) $p_T$ | $p_T > 7(5)\,\mathrm{GeV}$ |
| Pseudorapidity of electrons (muons) | $|\eta| < 2.5\,(2.4)$ |
| Sum of scalar $p_T$ of all stable particles within $\Delta R < 0.3$ from lepton | $< 0.35 p_T$ |
| Event topology | |
| Existence of at least two same-flavor OS lepton pairs, where leptons satisfy criteria above | |
| Inv. mass of the $Z_1$ candidate | $40 < m_{Z_1} < 120\,\mathrm{GeV}$ |
| Inv. mass of the $Z_2$ candidate | $12 < m_{Z_2} < 120\,\mathrm{GeV}$ |
| Distance between selected four leptons | $\Delta R(\ell_i, \ell_j) > 0.02$ for any $i \neq j$ |
| Inv. mass of any opposite sign lepton pair | $m_{\ell^+\ell^-} > 4\,\mathrm{GeV}$ |
| Inv. mass of the selected four leptons | $105 < m_{4\ell} < 140\,\mathrm{GeV}$ |

section. The non-resonant signal function, $\mathcal{P}_{\mathrm{nonres}}(m_{4\ell})$, is determined by the WH, ZH, and $t\bar{t}H$ contributions where one of the leptons from the H boson decay is lost or not selected. It is modeled by a Landau distribution with shape parameters constrained in the fit to be within a range determined from simulation. This contribution is referred to as the "combinatorial signal" and is treated as a background in this measurement.

The quantity $\epsilon_{i,j}^f$ represents the detector response matrix that maps the number of expected events in bin $j$ of a given observable at the fiducial level to the number of expected events in bin $i$ at the reconstruction level. This response matrix is determined using simulated signal samples and includes corrections for residual differences between data and simulation. In the case of the integrated fiducial cross section measurement, the response matrices become single numbers, which are listed in Table 8 for different SM production mechanism.

An additional resonant contribution arises from events which are accepted but do not originate from the fiducial phase space. These events are due to detector effects that cause differences between the quantities used for the fiducial phase space definition and the corresponding quantities at the reconstruction level. This contribution is treated as background and is referred to as the "non-fiducial signal" contribution. A simulated sample is used to verify that the shape of the distribution for these events is identical to that of the fiducial signal, and its normalization is fixed to the corresponding fraction of the fiducial signal. The value of this fraction, which we denote as $f_{\mathrm{nonfid}}$, is determined from simulation for each of the signal models studied. The value of $f_{\mathrm{nonfid}}$ for different signal models is shown in Table 8.

The integrated fiducial cross section is measured to be

$$\sigma_{\mathrm{fid}} = 2.84^{+0.34}_{-0.31} = 2.84^{+0.23}_{-0.22}\,(\mathrm{stat})^{+0.26}_{-0.21}\,(\mathrm{syst})\,\mathrm{fb}$$

at $m_H = 125.38\,\mathrm{GeV}$. This can be compared to the SM expectation $\sigma_{\mathrm{fid}}^{\mathrm{SM}} = 2.84 \pm 0.15\,\mathrm{fb}$. The measured inclusive fiducial cross sections in different final states and integrated as a function of center-of-mass energy are shown in Fig. 16. The corresponding numerical values, including the decomposition of the uncertainties into statistical and systematic components, and the corresponding expected uncertainties, are given in Table 9.

The measured differential cross sections as a function of the H boson transverse momentum

Table 8: Summary of the fraction of signal events for different SM signal production modes within the fiducial phase space (acceptance $\mathcal{A}_{\text{fid}}$), reconstruction efficiency ($\epsilon$) for signal events in the fiducial phase space, and ratio of the number of reconstructed events outside the fiducial phase space to that of the reconstructed events in the fiducial phase space ($f_{\text{nonfid}}$). For all production modes the values given are for $m_{\text{H}} = 125\,\text{GeV}$. Also shown in the last column is the factor $(1 + f_{\text{nonfid}})\epsilon$ which regulates the signal yield for a given fiducial cross section, as shown in Eq. (8). The uncertainties listed are statistical only. The theoretical uncertainty in $\mathcal{A}_{\text{fid}}$ for the SM is less than 1%.

| Signal process | $\mathcal{A}_{\text{fid}}$ | $\epsilon$ | $f_{\text{nonfid}}$ | $(1 + f_{\text{nonfid}})\epsilon$ |
|---|---|---|---|---|
| ggH (POWHEG) | $0.402 \pm 0.001$ | $0.598 \pm 0.002$ | $0.054 \pm 0.001$ | $0.631 \pm 0.002$ |
| VBF | $0.445 \pm 0.002$ | $0.615 \pm 0.002$ | $0.043 \pm 0.001$ | $0.641 \pm 0.003$ |
| WH | $0.329 \pm 0.002$ | $0.604 \pm 0.003$ | $0.078 \pm 0.002$ | $0.651 \pm 0.004$ |
| ZH | $0.340 \pm 0.003$ | $0.613 \pm 0.005$ | $0.082 \pm 0.004$ | $0.663 \pm 0.006$ |
| t$\bar{\text{t}}$H | $0.315 \pm 0.004$ | $0.588 \pm 0.007$ | $0.181 \pm 0.009$ | $0.694 \pm 0.010$ |
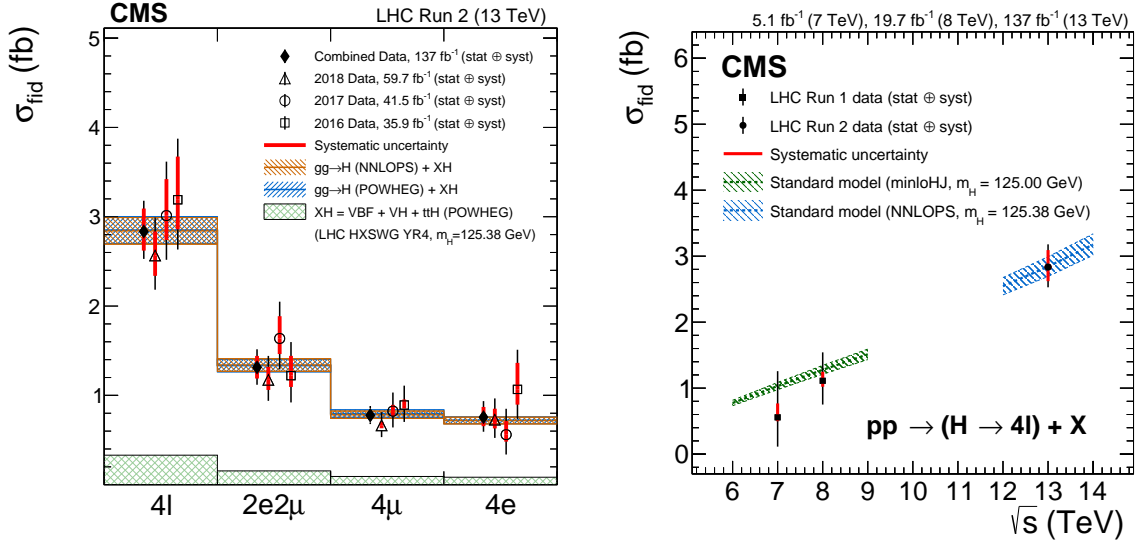


Figure 16: The measured inclusive fiducial cross section in different final states (left) and integrated as a function of $\sqrt{s}$ (right). The acceptance is calculated using POWHEG at $\sqrt{s} = 13\,\text{TeV}$ and HRES [107, 109] at $\sqrt{s} = 7$ and $8\,\text{TeV}$, and the total gluon fusion cross section and uncertainty are taken from Ref. [58]. The fiducial volume for $\sqrt{s} = 6$–$9\,\text{TeV}$ uses the lepton isolation definition from Ref. [25] and the SM predictions and measurements are calculated at $m_{\text{H}} = 125.0\,\text{GeV}$, while for $\sqrt{s} = 12$–$14\,\text{TeV}$ the definition described in the text is used and SM predictions and measurements are calculated at $m_{\text{H}} = 125.38\,\text{GeV}$.

and rapidity are shown in Fig. 17. The corresponding numerical values are given in Tables 10 and 11. Finally, the measured differential cross sections as a function of the number of associated jets and the transverse momentum of the leading jet are shown in Fig. 18. The corresponding numerical values are given in Tables 12 and 13.

For all the fiducial measurements the dominant systematic uncertainties are those on the lepton identification efficiencies and luminosity measurement, while the theoretical uncertainties are smaller. In order to assess the model dependence of the measurement, the unfolding procedure is repeated using different response matrices created by varying the relative fraction of each SM production mode within its experimental constraints. The uncertainty is negligible with respect to the experimental systematic uncertainties.

Table 9: The measured inclusive fiducial cross section and $\pm 1$ standard deviation uncertainties for different final states and data-taking periods at $m_\mathrm{H} = 125.38\,\mathrm{GeV}$. The statistical and systematic uncertainties are given separately for the inclusive measurements.

| | $2e2\mu$ (fb) | $4\mu$ (fb) | 4e (fb) | Inclusive (fb) |
|---|---|---|---|---|
| 2016 | $1.22^{+0.38}_{-0.30}$ | $0.89^{+0.22}_{-0.19}$ | $1.07^{+0.44}_{-0.33}$ | $3.19^{+0.68}_{-0.56} = 3.19^{+0.48}_{-0.45}$ (stat)$^{+0.48}_{-0.33}$ (syst) |
| 2017 | $1.64^{+0.41}_{-0.35}$ | $0.82^{+0.21}_{-0.18}$ | $0.56^{+0.29}_{-0.22}$ | $3.01^{+0.60}_{-0.50} = 3.01^{+0.44}_{-0.41}$ (stat)$^{+0.41}_{-0.27}$ (syst) |
| 2018 | $1.17^{+0.27}_{-0.24}$ | $0.66^{+0.15}_{-0.13}$ | $0.73^{+0.24}_{-0.20}$ | $2.57^{+0.42}_{-0.38} = 2.57^{+0.33}_{-0.31}$ (stat)$^{+0.27}_{-0.23}$ (syst) |
| 2016–2018 | $1.31^{+0.20}_{-0.19}$ | $0.78^{+0.10}_{-0.10}$ | $0.76^{+0.18}_{-0.16}$ | $2.84^{+0.34}_{-0.31} = 2.84^{+0.23}_{-0.22}$ (stat)$^{+0.26}_{-0.21}$ (syst) |
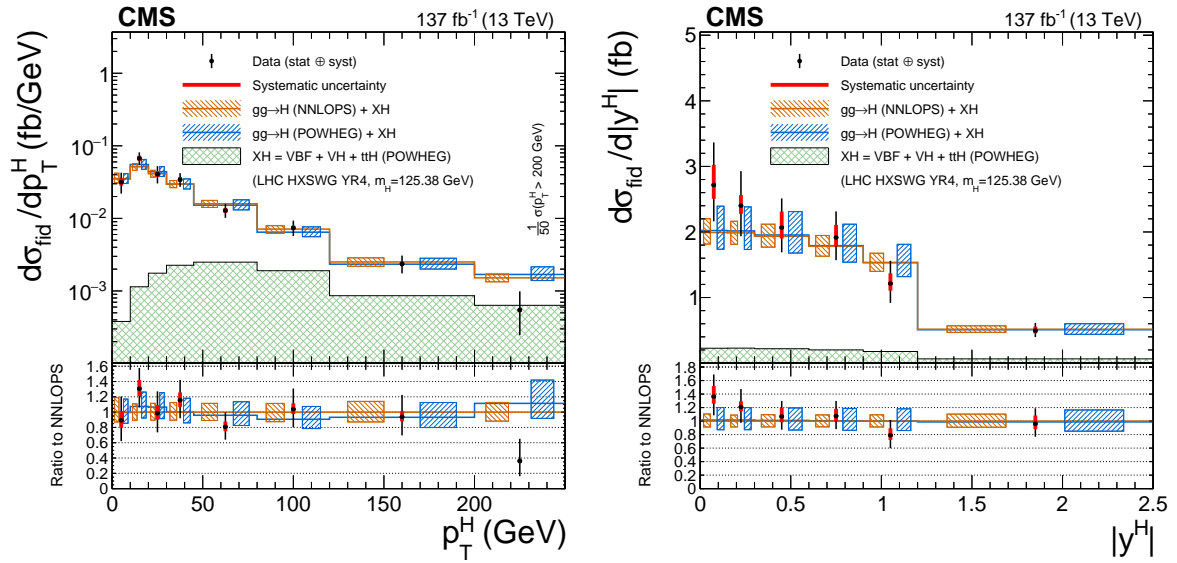


Figure 17: Differential cross sections as a function of $p_\mathrm{T}^\mathrm{H}$ (left) and $|y^\mathrm{H}|$ (right). The acceptance and theoretical uncertainties in the differential bins are calculated using POWHEG. The subdominant component of the signal (VBF + VH + t$\bar{\text{t}}$H) is denoted as XH.

Table 10: The measured differential fiducial cross section and $\pm 1$ standard deviation uncertainties for the $p_\mathrm{T}^\mathrm{H}$ observable at $m_\mathrm{H} = 125.38\,\mathrm{GeV}$. The breakdown of the total uncertainty (unc.) into statistical and systematic components is given.

| Bin range (GeV) | $d\sigma_\mathrm{fid}$ (fb) | unc. | (stat) | (syst) |
|---|---|---|---|---|
| 0–10 | 0.32 | $^{+0.11}_{-0.10}$ | $^{+0.10}_{-0.09}$ | $^{+0.04}_{-0.03}$ |
| 10–20 | 0.67 | $^{+0.14}_{-0.13}$ | $^{+0.13}_{-0.12}$ | $^{+0.06}_{-0.05}$ |
| 20–30 | 0.41 | $^{+0.12}_{-0.10}$ | $^{+0.11}_{-0.10}$ | $^{+0.04}_{-0.04}$ |
| 30–45 | 0.51 | $^{+0.12}_{-0.10}$ | $^{+0.11}_{-0.10}$ | $^{+0.04}_{-0.04}$ |
| 45–80 | 0.45 | $^{+0.10}_{-0.09}$ | $^{+0.10}_{-0.09}$ | $^{+0.04}_{-0.03}$ |
| 80–120 | 0.30 | $^{+0.08}_{-0.07}$ | $^{+0.07}_{-0.07}$ | $^{+0.02}_{-0.02}$ |
| 120–200 | 0.19 | $^{+0.06}_{-0.05}$ | $^{+0.06}_{-0.05}$ | $^{+0.01}_{-0.01}$ |
| 200–13000 | 0.03 | $^{+0.02}_{-0.02}$ | $^{+0.02}_{-0.01}$ | $^{+0.00}_{-0.00}$ |

Table 11: The measured differential fiducial cross section and $\pm 1$ standard deviation uncertainties for the $|y^{\mathrm{H}}|$ observable at $m_{\mathrm{H}} = 125.38\,\mathrm{GeV}$. The breakdown of the total uncertainty (unc.) into statistical and systematic components is given.

| Bin range | $\mathrm{d}\sigma_{\mathrm{fid}}$ (fb) | unc. | (stat) | (syst) |
|---|---|---|---|---|
| 0.0–0.15 | 0.41 | $+0.10$ $-0.08$ | $+0.09$ $-0.08$ | $+0.05$ $-0.03$ |
| 0.15–0.3 | 0.36 | $+0.08$ $-0.07$ | $+0.07$ $-0.07$ | $+0.03$ $-0.02$ |
| 0.3–0.6 | 0.62 | $+0.13$ $-0.11$ | $+0.11$ $-0.10$ | $+0.07$ $-0.05$ |
| 0.6–0.9 | 0.57 | $+0.12$ $-0.10$ | $+0.10$ $-0.10$ | $+0.06$ $-0.04$ |
| 0.9–1.2 | 0.36 | $+0.10$ $-0.09$ | $+0.09$ $-0.08$ | $+0.05$ $-0.03$ |
| 1.2–2.5 | 0.64 | $+0.15$ $-0.13$ | $+0.13$ $-0.12$ | $+0.08$ $-0.05$ |
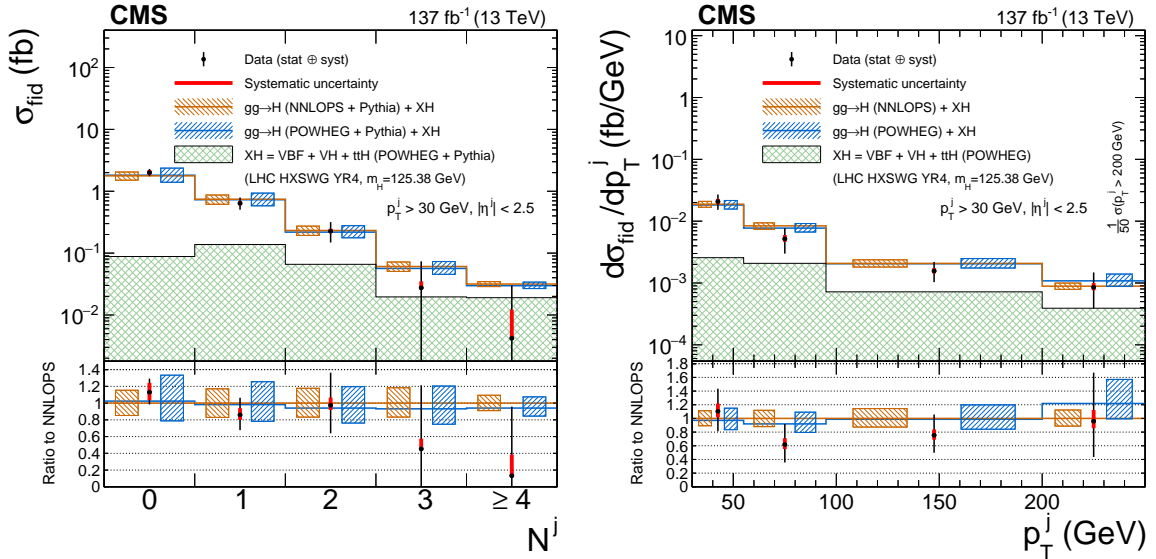


Figure 18: Differential cross sections as a function of the number of associated jets (left), and $p_{\mathrm{T}}$ of the leading jet (right). The acceptance and theoretical uncertainties in the differential bins are calculated using POWHEG. The sub-dominant component of the signal (VBF + VH + t$\bar{\mathrm{t}}$H) is denoted as XH.

Table 12: The measured differential fiducial cross section and $\pm 1$ standard deviation uncertainties for the $N^{\mathrm{j}}$ observable at $m_{\mathrm{H}} = 125.38\,\mathrm{GeV}$. The breakdown of the total uncertainty (unc.) into statistical and systematic components is given.

| Bin range | $\mathrm{d}\sigma_{\mathrm{fid}}$ (fb) | unc. | (stat) | (syst) |
|---|---|---|---|---|
| 0 | 2.00 | $+0.29$ $-0.26$ | $+0.21$ $-0.20$ | $+0.20$ $-0.17$ |
| 1 | 0.64 | $+0.15$ $-0.14$ | $+0.14$ $-0.13$ | $+0.06$ $-0.04$ |
| 2 | 0.23 | $+0.09$ $-0.08$ | $+0.09$ $-0.08$ | $+0.02$ $-0.01$ |
| 3 | 0.03 | $+0.05$ $-0.03$ | $+0.05$ $-0.03$ | $+0.01$ $-0.00$ |
| $\geq 4$ | 0.00 | $+0.03$ $-0.00$ | $+0.03$ $-0.00$ | $+0.01$ $-0.00$ |

Table 13: The measured differential fiducial cross section and $\pm 1$ standard deviation uncertainties for the $p_T^j$ observable at $m_H = 125.38\,\text{GeV}$. The breakdown of the total uncertainty (unc.) into statistical and systematic components is given.

| Bin range (GeV) | $d\sigma_\text{fid}$ (fb) | unc. | (stat) | (syst) |
|---|---|---|---|---|
| 0–10 | 0.32 | $+0.11$ $-0.10$ | $+0.10$ $-0.09$ | $+0.04$ $-0.03$ |
| 10–20 | 0.67 | $+0.14$ $-0.13$ | $+0.13$ $-0.12$ | $+0.06$ $-0.05$ |
| 20–30 | 0.41 | $+0.12$ $-0.10$ | $+0.11$ $-0.10$ | $+0.04$ $-0.04$ |
| 30–45 | 0.51 | $+0.12$ $-0.10$ | $+0.11$ $-0.10$ | $+0.04$ $-0.04$ |
| 45–80 | 0.45 | $+0.10$ $-0.09$ | $+0.10$ $-0.09$ | $+0.04$ $-0.03$ |
| 80–120 | 0.30 | $+0.08$ $-0.07$ | $+0.07$ $-0.07$ | $+0.02$ $-0.02$ |
| 120–200 | 0.19 | $+0.06$ $-0.05$ | $+0.06$ $-0.05$ | $+0.01$ $-0.01$ |
| 200–13000 | 0.03 | $+0.02$ $-0.02$ | $+0.02$ $-0.01$ | $+0.00$ $-0.00$ |

# 11  Summary

Several measurements of the Higgs boson production in the four-lepton final state at $\sqrt{s} = 13\,\text{TeV}$ have been presented, using data samples corresponding to an integrated luminosity of $137\,\text{fb}^{-1}$. Thanks to a large signal-to-background ratio and the complete reconstruction of the final state decay products, this channel enables a detailed study of the Higgs boson production properties. The measured signal strength modifier is $\mu = 0.94 \pm 0.07\,(\text{stat})^{+0.07}_{-0.06}\,(\text{theo})^{+0.06}_{-0.05}\,(\text{exp})$ and the integrated fiducial cross section is measured to be $\sigma_{\text{fid}} = 2.84^{+0.23}_{-0.22}\,(\text{stat})^{+0.26}_{-0.21}\,(\text{syst})\,\text{fb}$ with a standard model prediction of $2.84 \pm 0.15\,\text{fb}$ for the same fiducial region.. The signal strength modifiers for the main Higgs boson production modes are also reported. A new set of measurements, designed to quantify the different Higgs boson production processes in specific kinematical regions of phase space, have also been presented. The differential cross sections as a function of the transverse momentum and rapidity of the Higgs boson, the number of associated jets, and the transverse momentum of the leading associated jet are determined. All results are consistent, within their uncertainties, with the expectations for the standard model Higgs boson.

## Acknowledgments

# References

[1] ATLAS Collaboration, "Observation of a new particle in the search for the standard model Higgs boson with the ATLAS detector at the LHC", *Phys. Lett. B* **716** (2012) 1, `doi:10.1016/j.physletb.2012.08.020,arXiv:1207.7214.`

[2] CMS Collaboration, "Observation of a new boson at a mass of 125 GeV with the CMS experiment at the LHC", *Phys. Lett. B* **716** (2012) 30, `doi:10.1016/j.physletb.2012.08.021,arXiv:1207.7235.`

[3] CMS Collaboration, "Observation of a new boson with mass near 125 GeV in pp collisions at $\sqrt{s} = 7$ and 8 TeV", *JHEP* **06** (2013) 081, `doi:10.1007/JHEP06(2013)081,arXiv:1303.4571.`

[4] F. Englert and R. Brout, "Broken symmetry and the mass of gauge vector mesons", *Phys. Rev. Lett.* **13** (1964) 321, `doi:10.1103/PhysRevLett.13.321.`

[5] P. W. Higgs, "Broken symmetries, massless particles and gauge fields", *Phys. Lett.* **12** (1964) 132, `doi:10.1016/0031-9163(64)91136-9.`

[6] P. W. Higgs, "Broken symmetries and the masses of gauge bosons", *Phys. Rev. Lett.* **13** (1964) 508, `doi:10.1103/PhysRevLett.13.508.`

[7] G. S. Guralnik, C. R. Hagen, and T. W. B. Kibble, "Global conservation laws and massless particles", *Phys. Rev. Lett.* **13** (1964) 585, `doi:10.1103/PhysRevLett.13.585.`

[8] P. W. Higgs, "Spontaneous symmetry breakdown without massless bosons", *Phys. Rev.* **145** (1966) 1156, `doi:10.1103/PhysRev.145.1156.`

[9] T. W. B. Kibble, "Symmetry breaking in nonabelian gauge theories", *Phys. Rev.* **155** (1967) 1554, `doi:10.1103/PhysRev.155.1554.`

[10] ATLAS Collaboration, "Measurements of the Higgs boson production and decay rates and coupling strengths using $pp$ collision data at $\sqrt{s} = 7$ and 8 TeV in the ATLAS experiment", *Eur. Phys. J. C* **76** (2016) `doi:10.1140/epjc/s10052-015-3769-y,` `arXiv:1507.04548.`

[11] CMS Collaboration, "Precise determination of the mass of the Higgs boson and tests of compatibility of its couplings with the standard model predictions using proton collisions at 7 and 8 TeV", *Eur. Phys. J. C* **75** (2015) 212, `doi:10.1140/epjc/s10052-015-3351-7`, `arXiv:1412.8662`.

[12] ATLAS and CMS Collaborations, "Combined measurement of the Higgs boson mass in $pp$ collisions at $\sqrt{s} = 7$ and 8 TeV with the ATLAS and CMS experiments", *Phys. Rev. Lett.* **114** (2015) 191803, `doi:10.1103/PhysRevLett.114.191803`, `arXiv:1503.07589`.

[13] ATLAS and CMS Collaborations, "Measurements of the Higgs boson production and decay rates and constraints on its couplings from a combined ATLAS and CMS analysis of the LHC pp collision data at $\sqrt{s} = 7$ and 8 TeV", *JHEP* **08** (2016) 45, `doi:10.1007/JHEP08(2016)045`, `arXiv:1606.02266`.

[14] ATLAS Collaboration, "Measurements of Higgs boson production and couplings in the four-lepton channel in pp collisions at center-of-mass energies of 7 and 8 TeV with the ATLAS detector", *Phys. Rev. D* **91** (2015) 012006, `doi:10.1103/PhysRevD.91.012006`, `arXiv:1408.5191`.

[15] CMS Collaboration, "Measurement of the properties of a Higgs boson in the four-lepton final state", *Phys. Rev. D* **89** (2014) 092007, `doi:10.1103/PhysRevD.89.092007`, `arXiv:1312.5353`.

[16] CMS Collaboration, "Study of the mass and spin-parity of the Higgs boson candidate via its decays to Z boson pairs", *Phys. Rev. Lett.* **110** (2013) 081803, `doi:10.1103/PhysRevLett.110.081803`, `arXiv:1212.6639`.

[17] CMS Collaboration, "Constraints on the spin-parity and anomalous HVV couplings of the Higgs boson in proton collisions at 7 and 8 TeV", *Phys. Rev. D* **92** (2015) 012004, `doi:10.1103/PhysRevD.92.012004`, `arXiv:1411.3441`.

[18] CMS Collaboration, "Measurements of properties of the Higgs boson decaying into the four-lepton final state in pp collisions at $\sqrt{s} = 13$ TeV", *JHEP* **11** (2017) 047, `doi:10.1007/JHEP11(2017)047`, `arXiv:1706.09936`.

[19] ATLAS Collaboration, "Measurement of the Higgs boson coupling properties in the $H \to ZZ^* \to 4\ell$ decay channel at $\sqrt{s} = 13$ TeV with the ATLAS detector", *JHEP* **03** (2018) 095, `doi:10.1007/JHEP03(2018)095`, `arXiv:1712.02304`.

[20] CMS Collaboration, "Constraints on the Higgs boson width from off-shell production and decay to Z-boson pairs", *Phys. Lett. B* **736** (2014) 64, `doi:10.1016/j.physletb.2014.06.077`, `arXiv:1405.3455`.

[21] CMS Collaboration, "Limits on the Higgs boson lifetime and width from its decay to four charged leptons", *Phys. Rev. D* **92** (2015) 072010, `doi:10.1103/PhysRevD.92.072010`, `arXiv:1507.06656`.

[22] ATLAS Collaboration, "Constraints on the off-shell Higgs boson signal strength in the high-mass ZZ and WW final states with the ATLAS detector", *Eur. Phys. J. C* **75** (2015) 335, `doi:10.1140/epjc/s10052-015-3542-2`, `arXiv:1503.01060`.

[23] ATLAS Collaboration, "Constraints on off-shell Higgs boson production and the Higgs boson total width in $ZZ \to 4\ell$ and $ZZ \to 2\ell2\nu$ final states with the ATLAS detector", *Phys. Lett. B* **786** (2018) 223, `doi:10.1016/j.physletb.2018.09.048`, `arXiv:1808.01191`.

[24] ATLAS Collaboration, "Fiducial and differential cross sections of Higgs boson production measured in the four-lepton decay channel in $pp$ collisions at $\sqrt{s}$=8 TeV with the ATLAS detector", *Phys. Lett. B* **738** (2014) 234, `doi:10.1016/j.physletb.2014.09.054`, `arXiv:1408.3226`.

[25] CMS Collaboration, "Measurement of differential and integrated fiducial cross sections for Higgs boson production in the four-lepton decay channel in pp collisions at $\sqrt{s} = 7$ and 8 TeV", *JHEP* **04** (2016) 005, `doi:10.1007/JHEP04(2016)005`, `arXiv:1512.08377`.

[26] ATLAS Collaboration, "Measurement of inclusive and differential cross sections in the $H \to ZZ^* \to 4\ell$ decay channel in $pp$ collisions at $\sqrt{s} = 13$ TeV with the ATLAS detector", *JHEP* **10** (2017) 132, `doi:10.1007/JHEP10(2017)132`, `arXiv:1708.02810`.

[27] ATLAS Collaboration, "Higgs boson production cross-section measurements and their EFT interpretation in the $4\ell$ decay channel at $\sqrt{s} = 13$ TeV with the ATLAS detector", *Eur. Phys. J. C* **80** (2020) `doi:10.1140/epjc/s10052-020-8227-9`, `arXiv:2004.03447v2`.

[28] ATLAS Collaboration, "Measurements of the Higgs boson inclusive and differential fiducial cross sections in the $4\ell$ decay channel at $\sqrt{s} = 13$ TeV", *Eur. Phys. J. C* **80** (2020) `doi:10.1140/epjc/s10052-020-8223-0`, `arXiv:arXiv:2004.03969v3`.

[29] CMS Collaboration, "Constraints on anomalous Higgs boson couplings using production and decay information in the four-lepton final state", *Phys. Lett. B* **775** (2017) 1, `doi:10.1016/j.physletb.2017.10.021`, `arXiv:1707.00541`.

[30] CMS Collaboration, "Measurements of the Higgs boson width and anomalous HVV couplings from on-shell and off-shell production in the four-lepton final state", *Phys. Rev. D* **99** (2019) 112003, `doi:10.1103/PhysRevD.99.112003`, `arXiv:1901.00174`.

[31] J. Bendavid et al., eds., "Les Houches 2017: Physics at TeV Colliders Standard Model Working Group Report". (2018). `arXiv:1803.07977`.

[32] D. de Florian et al., "Handbook of LHC Higgs cross sections: 4. Deciphering the nature of the Higgs sector", CERN Report CERN-2017-002-M, 2016. `doi:10.23731/CYRM-2017-002`, `arXiv:1610.07922`.

[33] N. Berger et al., "Simplified template cross sections - stage 1.1", (2019). `arXiv:1906.02754`.

[34] CMS Collaboration, "Performance of the CMS Level-1 trigger in proton-proton collisions at $\sqrt{s} = 13$ TeV", *JINST* **15** (2020) P10017, `doi:10.1088/1748-0221/15/10/P10017`, `arXiv:2006.10165`.

[35] CMS Collaboration, "The CMS trigger system", *JINST* **12** (2017) P01020, `doi:10.1088/1748-0221/12/01/P01020`, `arXiv:1609.02366`.

[36] M. Cacciari, G. P. Salam, and G. Soyez, "The anti-$k_T$ jet clustering algorithm", *JHEP* **04** (2008) 063, `doi:10.1088/1126-6708/2008/04/063`, `arXiv:0802.1189`.

[37] M. Cacciari, G. P. Salam, and G. Soyez, "FastJet user manual", *Eur. Phys. J. C* **72** (2012) 1896, `doi:10.1140/epjc/s10052-012-1896-2`, `arXiv:1111.6097`.

[38] CMS Collaboration, "Performance of electron reconstruction and selection with the CMS detector in proton-proton collisions at $\sqrt{s} = 8$ TeV", *JINST* **10** (2015) P06005, `doi:10.1088/1748-0221/10/06/P06005`, `arXiv:1502.02701`.

[39] CMS Collaboration, "Performance of the CMS muon detector and muon reconstruction with proton-proton collisions at $\sqrt{s} = 13$ TeV", *JINST* **13** (2018) P06015, `doi:10.1088/1748-0221/13/06/P06015`, `arXiv:1804.04528`.

[40] CMS Collaboration, "The CMS experiment at the CERN LHC", *JINST* **3** (2008) S08004, `doi:10.1088/1748-0221/3/08/S08004`.

[41] CMS Collaboration, "CMS luminosity measurements for the 2016 data-taking period", CMS Physics Analysis Summary CMS-PAS-LUM-17-001, CERN, 2017.

[42] CMS Collaboration, "CMS luminosity measurement for the 2017 data-taking period at $\sqrt{s} = 13$ TeV", CMS Physics Analysis Summary CMS-PAS-LUM-17-004, CERN, 2017.

[43] CMS Collaboration, "CMS luminosity measurement for the 2018 data-taking period at $\sqrt{s} = 13$ TeV", CMS Physics Analysis Summary CMS-PAS-LUM-18-002, CERN, 2019.

[44] P. Nason, "A new method for combining NLO QCD with shower Monte Carlo algorithms", *JHEP* **11** (2004) 040, `doi:10.1088/1126-6708/2004/11/040`, `arXiv:hep-ph/0409146`.

[45] S. Frixione, P. Nason, and C. Oleari, "Matching NLO QCD computations with parton shower simulations: the POWHEG method", *JHEP* **11** (2007) 070, `doi:10.1088/1126-6708/2007/11/070`, `arXiv:0709.2092`.

[46] S. Alioli, P. Nason, C. Oleari, and E. Re, "A general framework for implementing NLO calculations in shower Monte Carlo programs: the POWHEG BOX", *JHEP* **06** (2010) 043, `doi:10.1007/JHEP06(2010)043`, `arXiv:1002.2581`.

[47] S. Alioli, P. Nason, C. Oleari, and E. Re, "NLO Higgs boson production via gluon fusion matched with shower in POWHEG", *JHEP* **04** (2009) 002, `doi:10.1088/1126-6708/2009/04/002`, `arXiv:0812.0578`.

[48] P. Nason and C. Oleari, "NLO Higgs boson production via vector-boson fusion matched with shower in POWHEG", *JHEP* **02** (2010) 037, `doi:10.1007/JHEP02(2010)037`, `arXiv:0911.5299`.

[49] G. Luisoni, P. Nason, C. Oleari, and F. Tramontano, "HW$^{\pm}$/HZ + 0 and 1 jet at NLO with the POWHEG BOX interfaced to GoSam and their merging within MiNLO", *JHEP* **10** (2013) 1, `doi:10.1007/JHEP10(2013)083`, `arXiv:1306.2542`.

[50] H. B. Hartanto, B. Jager, L. Reina, and D. Wackeroth, "Higgs boson production in association with top quarks in the POWHEG BOX", *Phys. Rev. D* **91** (2015) 094003, `doi:10.1103/PhysRevD.91.094003`, `arXiv:1501.04498`.

[51] Y. Gao et al., "Spin determination of single-produced resonances at hadron colliders", *Phys. Rev. D* **81** (2010) 075022, `doi:10.1103/PhysRevD.81.075022`, `arXiv:1001.3396`. [Erratum: `doi:10.1103/PhysRevD.81.079905`].

[52] S. Bolognesi et al., "On the spin and parity of a single-produced resonance at the LHC", *Phys. Rev. D* **86** (2012) 095031, `doi:10.1103/PhysRevD.86.095031`, `arXiv:1208.4018`.

[53] I. Anderson et al., "Constraining anomalous *HVV* interactions at proton and lepton colliders", *Phys. Rev. D* **89** (2014) 035007, `doi:10.1103/PhysRevD.89.035007`, `arXiv:1309.4819`.

[54] A. V. Gritsan, R. Röentsch, M. Schulze, and M. Xiao, "Constraining anomalous Higgs boson couplings to the heavy flavor fermions using matrix element techniques", *Phys. Rev. D* **94** (2016) 055023, `doi:10.1103/PhysRevD.94.055023`, `arXiv:1606.03107`.

[55] A. V. Gritsan et al., "New features in the JHU generator framework: constraining Higgs boson properties from on-shell and off-shell production", *Phys. Rev. D* **102** (2020) 056022, `doi:10.1103/PhysRevD.102.056022`, `arXiv:2002.09888`.

[56] J. Alwall et al., "The automated computation of tree-level and next-to-leading order differential cross sections, and their matching to parton shower simulations", *JHEP* **07** (2014) 079, `doi:10.1007/JHEP07(2014)079`, `arXiv:1405.0301`.

[57] C. Anastasiou et al., "Higgs boson gluon-fusion production in QCD at three loops", *Phys. Rev. Lett.* **114** (2015) 212001, `doi:10.1103/PhysRevLett.114.212001`, `arXiv:1503.06056`.

[58] C. Anastasiou et al., "High precision determination of the gluon fusion Higgs boson cross-section at the LHC", *JHEP* **05** (2016) 58, `doi:10.1007/JHEP05(2016)058`, `arXiv:1602.00695`.

[59] M. Ciccolini, A. Denner, and S. Dittmaier, "Strong and electroweak corrections to the production of a Higgs boson+2 jets via weak interactions at the Large Hadron Collider", *Phys. Rev. Lett.* **99** (2007) 161803, `doi:10.1103/PhysRevLett.99.161803`, `arXiv:0707.0381`.

[60] M. Ciccolini, A. Denner, and S. Dittmaier, "Electroweak and QCD corrections to Higgs production via vector-boson fusion at the LHC", *Phys. Rev. D* **77** (2008) 013002, `doi:10.1103/PhysRevD.77.013002`, `arXiv:0710.4749`.

[61] P. Bolzoni, F. Maltoni, S.-O. Moch, and M. Zaro, "Higgs production via vector-boson fusion at NNLO in QCD", *Phys. Rev. Lett.* **105** (2010) 011801, `doi:10.1103/PhysRevLett.105.011801`, `arXiv:1003.4451`.

[62] P. Bolzoni, F. Maltoni, S.-O. Moch, and M. Zaro, "Vector boson fusion at next-to-next-to-leading order in QCD: Standard model Higgs boson and beyond", *Phys. Rev. D* **85** (2012) 035002, `doi:10.1103/PhysRevD.85.035002`, `arXiv:1109.3717`.

[63] O. Brein, A. Djouadi, and R. Harlander, "NNLO QCD corrections to the Higgs-strahlung processes at hadron colliders", *Phys. Lett. B* **579** (2004) 149, `doi:10.1016/j.physletb.2003.10.112`, `arXiv:hep-ph/0307206`.

[64] M. L. Ciccolini, S. Dittmaier, and M. Krämer, "Electroweak radiative corrections to associated *WH* and *ZH* production at hadron colliders", *Phys. Rev. D* **68** (2003) 073003, `doi:10.1103/PhysRevD.68.073003`, `arXiv:hep-ph/0306234`.

[65] W. Beenakker et al., "Higgs radiation off top quarks at the Tevatron and the LHC", *Phys. Rev. Lett.* **87** (2001) 201805, `doi:10.1103/PhysRevLett.87.201805`, `arXiv:hep-ph/0107081`.

[66] W. Beenakker et al., "NLO QCD corrections to $t\bar{t}$ H production in hadron collisions.", *Nucl. Phys. B* **653** (2003) 151, `doi:10.1016/S0550-3213(03)00044-0`, `arXiv:hep-ph/0211352`.

[67] S. Dawson, L. H. Orr, L. Reina, and D. Wackeroth, "Associated top quark Higgs boson production at the LHC", *Phys. Rev. D* **67** (2003) 071503, `doi:10.1103/PhysRevD.67.071503`, `arXiv:hep-ph/0211438`.

[68] S. Dawson et al., "Associated Higgs production with top quarks at the Large Hadron Collider: NLO QCD corrections", *Phys. Rev. D* **68** (2003) 034022, `doi:10.1103/PhysRevD.68.034022`, `arXiv:hep-ph/0305087`.

[69] Z. Yu et al., "QCD NLO and EW NLO corrections to $t\bar{t}H$ production with top quark decays at hadron collider", *Phys. Lett. B* **738** (2014) 1, `doi:10.1016/j.physletb.2014.09.022`, `arXiv:1407.1110`.

[70] S. S. Frixione et al., "Weak corrections to Higgs hadroproduction in association with a top-quark pair", *JHEP* **09** (2014) 65, `doi:10.1007/JHEP09(2014)065`, `arXiv:1407.0823`.

[71] F. Demartin, F. Maltoni, K. Mawatari, and M. Zaro, "Higgs production in association with a single top quark at the LHC", *Eur. Phys. J. C* **75** (2015) 267, `doi:10.1140/epjc/s10052-015-3475-9`, `arXiv:1504.0611`.

[72] F. Demartin et al., "tWH associated production at the LHC", *Eur. Phys. J. C* **77** (2017) 34, `doi:10.1140/epjc/s10052-017-4601-7`, `arXiv:1607.05862`.

[73] A. Denner et al., "Standard model Higgs-boson branching ratios with uncertainties", *Eur. Phys. J. C* **71** (2011) 1753, `doi:10.1140/epjc/s10052-011-1753-8`, `arXiv:1107.5909`.

[74] A. Djouadi, J. Kalinowski, and M. Spira, "HDECAY: A program for Higgs boson decays in the standard model and its supersymmetric extension", *Comput. Phys. Commun.* **108** (1998) 56, `doi:10.1016/S0010-4655(97)00123-9`, `arXiv:hep-ph/9704448`.

[75] A. Djouadi, J. Kalinowski, M. Muhlleitner, and M. Spira, "An update of the program HDECAY", in *The Les Houches 2009 workshop on TeV colliders: The tools and Monte Carlo working group summary report*. 2010. `arXiv:1003.1643`.

[76] A. Bredenstein, A. Denner, S. Dittmaier, and M. M. Weber, "Precise predictions for the Higgs-boson decay H → WW/ZZ → 4 leptons", *Phys. Rev. D* **74** (2006) 013004, `doi:10.1103/PhysRevD.74.013004`, `arXiv:hep-ph/0604011`.

[77] A. Bredenstein, A. Denner, S. Dittmaier, and M. M. Weber, "Radiative corrections to the semileptonic and hadronic Higgs-boson decays H →WW/ZZ→ 4 fermions", *JHEP* **02** (2007) 80, `doi:10.1088/1126-6708/2007/02/080`, `arXiv:hep-ph/0611234`.

[78] S. Boselli et al., "Higgs boson decay into four leptons at NLOPS electroweak accuracy", *JHEP* **06** (2015) 23, `doi:10.1007/JHEP06(2015)023`, `arXiv:1503.07394`.

[79] S. Actis, G. Passarino, C. Sturm, and S. Uccirati, "NNLO computational techniques: the cases $H \to \gamma\gamma$ and $H \to gg$", *Nucl. Phys. B* **811** (2009) 182, `doi:10.1016/j.nuclphysb.2008.11.024`, `arXiv:0809.3667`.

[80] T. Melia, P. Nason, R. Rontsch, and G. Zanderighi, "W+W-, WZ and ZZ production in the POWHEG BOX", *JHEP* **11** (2011) 078, `doi:10.1007/JHEP11(2011)078`, `arXiv:1107.5051`.

[81] J. M. Campbell and R. K. Ellis, "MCFM for the Tevatron and the LHC", *Nucl. Phys. Proc. Suppl.* **205** (2010) 10, `doi:10.1016/j.nuclphysbps.2010.08.011`, `arXiv:1007.3492`.

[82] T. Sjöstrand et al., "An introduction to PYTHIA 8.2", *Comput. Phys. Commun.* **191** (2015) 159, `doi:10.1016/j.cpc.2015.01.024`, `arXiv:1410.3012`.

[83] CMS Collaboration, "Event generator tunes obtained from underlying event and multiparton scattering measurements", *Eur. Phys. J. C* **76** (2016) 155, `doi:10.1140/epjc/s10052-016-3988-x`, `arXiv:1512.00815`.

[84] CMS Collaboration, "Extraction and validation of a new set of CMS PYTHIA8 tunes from underlying-event measurements", *Eur. Phys. J. C* **80** (2020) 4, `doi:10.1140/epjc/s10052-019-7499-4`, `arXiv:1903.12179`.

[85] NNPDF Collaboration, "Parton distributions for the LHC Run II", *JHEP* **04** (2015) 040, `doi:10.1007/JHEP04(2015)040`, `arXiv:1410.8849`.

[86] GEANT4 Collaboration, "GEANT4: a simulation toolkit", *Nucl. Instrum. Meth. A* **506** (2003) 250, `doi:10.1016/S0168-9002(03)01368-8`.

[87] J. Allison et al., "Geant4 developments and applications", *IEEE Trans. Nucl. Sci.* **53** (2006) 270, `doi:10.1109/TNS.2006.869826`.

[88] CMS Collaboration, "Particle-flow reconstruction and global event description with the CMS detector", *JINST* **12** (2017) P10003, `doi:10.1088/1748-0221/12/10/P10003`, `arXiv:1706.04965`.

[89] CMS Collaboration, "Performance of missing transverse momentum reconstruction in proton-proton collisions at $\sqrt{s} = 13\,\text{TeV}$ using the CMS detector", *JINST* **14** (2019) P07004, `doi:10.1088/1748-0221/14/07/P07004`, `arXiv:1903.06078`.

[90] CMS Collaboration, "Performance of CMS muon reconstruction in $pp$ collision events at $\sqrt{s} = 7\,\text{TeV}$", *JINST* **7** (2012) P10002, `doi:10.1088/1748-0221/7/10/P10002`, `arXiv:1206.4071`.

[91] CMS Collaboration, "Pileup mitigation at CMS in 13 TeV data", *JINST* **15** (2020) P09018, `doi:10.1088/1748-0221/15/09/P09018`, `arXiv:2003.00503`.

[92] CMS Collaboration, "Electron and photon performance in CMS with the full 2017 data sample and additional highlights for the CALOR 2018 conference", CMS Detector Performance Summary CMS-DPS-2018/2017, 2018.

[93] T. Chen and C. Guestrin, "XGBoost: A scalable tree boosting system", (2016). `arXiv:1603.02754`.

[94] CMS Collaboration, "Measurement of the inclusive $W$ and $Z$ production cross sections in $pp$ collisions at $\sqrt{s} = 7$ TeV", *JHEP* **10** (2011) 132, `doi:10.1007/JHEP10(2011)132`, `arXiv:1107.4789`.

[95] CMS Collaboration, "Jet energy scale and resolution in the CMS experiment in pp collisions at 8 TeV", *JINST* **12** (2017) P02014, `doi:10.1088/1748-0221/12/02/P02014`, `arXiv:1607.03663`.

[96] CMS Collaboration, "Identification of heavy-flavour jets with the CMS detector in pp collisions at 13 TeV", *JINST* **13** (2018) P05011, `doi:10.1088/1748-0221/13/05/P05011`, `arXiv:1712.07158`.

[97] Particle Data Group, P. A. Zyla et al., "Review of particle physics", *Prog. Theor. Exp. Phys.* **2020** (2020) 083C01, `doi:10.1093/ptep/ptaa104`.

[98] CMS Collaboration, "Search for a Higgs boson in the mass range from 145 to 1000 GeV decaying to a pair of W or Z bosons", *JHEP* **10** (2015) 144, `doi:10.1007/JHEP10(2015)144`, `arXiv:1504.00936`.

[99] M. Grazzini, S. Kallweit, and D. Rathlev, "ZZ production at the LHC: Fiducial cross sections and distributions in NNLO QCD", *Phys. Lett. B* **750** (2015) 407, `doi:10.1016/j.physletb.2015.09.055`, `arXiv:1507.06257`.

[100] A. Bierweiler, T. Kasprzik, and J. H. Kuhn, "Vector-boson pair production at the LHC to $\mathcal{O}(\alpha^3)$ accuracy", *JHEP* **12** (2013) 071, `doi:10.1007/JHEP12(2013)071`, `arXiv:1305.5402`.

[101] M. Bonvini et al., "Signal-background interference effects in $gg \to H \to WW$ beyond leading order", *Phys. Rev. D* **88** (2013) 034032, `doi:10.1103/PhysRevD.88.034032`, `arXiv:1304.3053`.

[102] K. Melnikov and M. Dowling, "Production of two Z-bosons in gluon fusion in the heavy top quark approximation", *Phys. Lett. B* **744** (2015) 43, `doi:10.1016/j.physletb.2015.03.030`, `arXiv:1503.01274`.

[103] C. S. Li, H. T. Li, D. Y. Shao, and J. Wang, "Soft gluon resummation in the signal-background interference process of $gg(\to h^*) \to ZZ$", *JHEP* **08** (2015) 065, `doi:10.1007/JHEP08(2015)065`, `arXiv:1504.02388`.

[104] G. Passarino, "Higgs CAT", *Eur. Phys. J. C* **74** (2014) 2866, `doi:10.1140/epjc/s10052-014-2866-7`, `arXiv:1312.2397`.

[105] S. Catani and M. Grazzini, "An NNLO subtraction formalism in hadron collisions and its application to Higgs boson production at the LHC", *Phys. Rev. Lett.* **98** (2007) 222002, `doi:10.1103/PhysRevLett.98.222002`, `arXiv:hep-ph/0703012`.

[106] M. Grazzini, "NNLO predictions for the Higgs boson signal in the H $\to$ WW $\to \ell\nu\ell\nu$ and H$\to$ ZZ $\to 4\ell$ decay channels", *JHEP* **02** (2008) 043, `doi:10.1088/1126-6708/2008/02/043`, `arXiv:0801.3232`.

[107] M. Grazzini and H. Sargsyan, "Heavy-quark mass effects in Higgs boson production at the LHC", *JHEP* **09** (2013) 129, `doi:10.1007/JHEP09(2013)129`, `arXiv:1306.4581`.

[108] L. Landau, "On the energy loss of fast particles by ionization", *J. Phys. (USSR)* **8** (1944) 201.

[109] D. de Florian, G. Ferrera, M. Grazzini, and D. Tommasini, "Higgs boson production at the LHC: transverse momentum resummation effects in the $H \to \gamma\gamma$, $H \to WW \to \ell\nu\ell\nu$ and $H \to ZZ \to 4\ell$ decay modes", *JHEP* **06** (2012) 132, `doi:10.1007/JHEP06(2012)132`, `arXiv:1203.6321`.

[110] E. Bagnaschi, G. Degrassi, P. Slavich, and A. Vicini, "Higgs production via gluon fusion in the POWHEG approach in the SM and in the MSSM", *JHEP* **02** (2012) 088, `doi:10.1007/JHEP02(2012)088`, `arXiv:1111.2854`.

[111] K. Hamilton, P. Nason, E. Re, and G. Zanderighi, "NNLOPS simulation of Higgs boson production", *JHEP* **10** (2013) 222, `doi:10.1007/JHEP10(2013)222`, `arXiv:1309.0017`.

[112] M. J. Oreglia, "A study of the reactions $\psi' \to \gamma\gamma\psi$". PhD thesis, Stanford University, 1980. SLAC Report SLAC-R-236.

[113] CMS Collaboration, "Determination of jet energy calibration and transverse momentum resolution in CMS", *JINST* **6** (2011) P11002, `doi:10.1088/1748-0221/6/11/P11002`, `arXiv:1107.4277`.

[114] M. Botje et al., "The PDF4LHC working group interim recommendations", (2011). `arXiv:1101.0538`.

[115] S. Alekhin et al., "The PDF4LHC working group interim report", (2011). `arXiv:1101.0536`.

[116] F. Garwood, "Fiducial limits for the Poisson distribution", *Biometrika* **28** (1936) 437, `doi:10.1093/biomet/28.3-4.437`.

[117] G. Cowan, K. Cranmer, E. Gross, and O. Vitells, "Asymptotic formulae for likelihood-based tests of new physics", *Euro. Phys. J. C* **71** (2011) 1554, `doi:10.1140/epjc/s10052-011-1554-0`.

[118] The ATLAS Collaboration, The CMS Collaboration, The LHC Higgs Combination Group, "Procedure for the LHC Higgs boson search combination in Summer 2011", Technical Report CMS-NOTE-2011-005, ATL-PHYS-PUB-2011-11, 2011.

[119] CMS Collaboration, "A measurement of the Higgs boson mass in the diphoton decay channel", *Phys. Lett. B* **805** (2020) 135425, `doi:10.1016/j.physletb.2020.135425`, `arXiv:2002.06398`.

[120] CMS Collaboration, "Measurement of differential cross sections for Higg boson production in the diphoton decay channel in pp collisions at $\sqrt{s}$=8 TeV", *Eur. Phys. J. C* **76** (2015) 13, `doi:10.1140/epjc/s10052-015-3853-3`, `arXiv:1508.07819`.

# A  The CMS Collaboration

**Yerevan Physics Institute, Yerevan, Armenia**
A.M. Sirunyan[†], A. Tumasyan

**Institut für Hochenergiephysik, Wien, Austria**
W. Adam, J.W. Andrejkovic, T. Bergauer, S. Chatterjee, M. Dragicevic, A. Escalante Del Valle,
R. Frühwirth[1], M. Jeitler[1], N. Krammer, L. Lechner, D. Liko, I. Mikulec, F.M. Pitters, J. Schieck[1],
R. Schöfbeck, M. Spanring, S. Templ, W. Waltenberger, C.-E. Wulz[1]

**Institute for Nuclear Problems, Minsk, Belarus**
V. Chekhovsky, A. Litomin, V. Makarenko

**Universiteit Antwerpen, Antwerpen, Belgium**
M.R. Darwish[2], E.A. De Wolf, X. Janssen, T. Kello[3], A. Lelek, H. Rejeb Sfar, P. Van Mechelen,
S. Van Putte, N. Van Remortel

**Vrije Universiteit Brussel, Brussel, Belgium**
F. Blekman, E.S. Bols, J. D'Hondt, J. De Clercq, M. Delcourt, S. Lowette, S. Moortgat, A. Morton,
D. Müller, A.R. Sahasransu, S. Tavernier, W. Van Doninck, P. Van Mulders

**Université Libre de Bruxelles, Bruxelles, Belgium**
D. Beghin, B. Bilin, B. Clerbaux, G. De Lentdecker, L. Favart, A. Grebenyuk, A.K. Kalsi,
K. Lee, I. Makarenko, L. Moureaux, L. Pétré, A. Popov, N. Postiau, E. Starling, L. Thomas,
C. Vander Velde, P. Vanlaer, D. Vannerom, L. Wezenbeek

**Ghent University, Ghent, Belgium**
T. Cornelis, D. Dobur, M. Gruchala, G. Mestdach, M. Niedziela, C. Roskas, K. Skovpen,
M. Tytgat, W. Verbeke, B. Vermassen, M. Vit

**Université Catholique de Louvain, Louvain-la-Neuve, Belgium**
A. Bethani, G. Bruno, F. Bury, C. Caputo, P. David, C. Delaere, I.S. Donertas, A. Giammanco,
V. Lemaitre, K. Mondal, J. Prisciandaro, A. Taliercio, M. Teklishyn, P. Vischia, S. Wertz,
S. Wuyckens

**Centro Brasileiro de Pesquisas Fisicas, Rio de Janeiro, Brazil**
G.A. Alves, C. Hensel, A. Moraes

**Universidade do Estado do Rio de Janeiro, Rio de Janeiro, Brazil**
W.L. Aldá Júnior, M. Barroso Ferreira Filho, H. BRANDAO MALBOUISSON, W. Carvalho,
J. Chinellato[4], E.M. Da Costa, G.G. Da Silveira[5], D. De Jesus Damiao, S. Fonseca De Souza,
J. Martins[6], D. Matos Figueiredo, C. Mora Herrera, K. Mota Amarilo, L. Mundim, H. Nogima,
P. Rebello Teles, L.J. Sanchez Rosas, A. Santoro, S.M. Silva Do Amaral, A. Sznajder, M. Thiel,
F. Torres Da Silva De Araujo, A. Vilela Pereira

**Universidade Estadual Paulista [a], Universidade Federal do ABC [b], São Paulo, Brazil**
C.A. Bernardes[a,a], L. Calligaris[a], T.R. Fernandez Perez Tomei[a], E.M. Gregores[a,b], D.S. Lemos[a],
P.G. Mercadante[a,b], S.F. Novaes[a], Sandra S. Padula[a]

**Institute for Nuclear Research and Nuclear Energy, Bulgarian Academy of Sciences, Sofia, Bulgaria**
A. Aleksandrov, G. Antchev, I. Atanasov, R. Hadjiiska, P. Iaydjiev, M. Misheva, M. Rodozov,
M. Shopova, G. Sultanov

**University of Sofia, Sofia, Bulgaria**
A. Dimitrov, T. Ivanov, L. Litov, B. Pavlov, P. Petkov, A. Petrov

**Beihang University, Beijing, China**
T. Cheng, W. Fang[3], Q. Guo, T. Javaid[7], M. Mittal, H. Wang, L. Yuan

**Department of Physics, Tsinghua University, Beijing, China**
M. Ahmad, G. Bauer, C. Dozen[8], Z. Hu, Y. Wang, K. Yi[9,10]

**Institute of High Energy Physics, Beijing, China**
E. Chapon, G.M. Chen[7], H.S. Chen[7], M. Chen, A. Kapoor, D. Leggat, H. Liao, Z.-A. LIU[7], R. Sharma, A. Spiezia, J. Tao, J. Thomas-wilsker, J. Wang, H. Zhang, S. Zhang[7], J. Zhao

**State Key Laboratory of Nuclear Physics and Technology, Peking University, Beijing, China**
A. Agapitos, Y. Ban, C. Chen, Q. Huang, A. Levin, Q. Li, M. Lu, X. Lyu, Y. Mao, S.J. Qian, D. Wang, Q. Wang, J. Xiao

**Sun Yat-Sen University, Guangzhou, China**
Z. You

**Institute of Modern Physics and Key Laboratory of Nuclear Physics and Ion-beam Application (MOE) - Fudan University, Shanghai, China**
X. Gao[3], H. Okawa

**Zhejiang University, Hangzhou, China**
M. Xiao

**Universidad de Los Andes, Bogota, Colombia**
C. Avila, A. Cabrera, C. Florez, J. Fraga, A. Sarkar, M.A. Segura Delgado

**Universidad de Antioquia, Medellin, Colombia**
J. Jaramillo, J. Mejia Guisao, F. Ramirez, J.D. Ruiz Alvarez, C.A. Salazar González, N. Vanegas Arbelaez

**University of Split, Faculty of Electrical Engineering, Mechanical Engineering and Naval Architecture, Split, Croatia**
D. Giljanovic, N. Godinovic, D. Lelas, I. Puljak

**University of Split, Faculty of Science, Split, Croatia**
Z. Antunovic, M. Kovac, T. Sculac

**Institute Rudjer Boskovic, Zagreb, Croatia**
V. Brigljevic, D. Ferencek, D. Majumder, M. Roguljic, A. Starodumov[11], T. Susa

**University of Cyprus, Nicosia, Cyprus**
A. Attikis, E. Erodotou, A. Ioannou, G. Kole, M. Kolosova, S. Konstantinou, J. Mousa, C. Nicolaou, F. Ptochos, P.A. Razis, H. Rykaczewski, H. Saka

**Charles University, Prague, Czech Republic**
M. Finger[12], M. Finger Jr.[12], A. Kveton, J. Tomsa

**Escuela Politecnica Nacional, Quito, Ecuador**
E. Ayala

**Universidad San Francisco de Quito, Quito, Ecuador**
E. Carrera Jarrin

**Academy of Scientific Research and Technology of the Arab Republic of Egypt, Egyptian Network of High Energy Physics, Cairo, Egypt**
S. Abu Zeid[13], S. Khalil[14], E. Salama[15,13]

**Center for High Energy Physics (CHEP-FU), Fayoum University, El-Fayoum, Egypt**
M.A. Mahmoud, Y. Mohammed

**National Institute of Chemical Physics and Biophysics, Tallinn, Estonia**
S. Bhowmik, A. Carvalho Antunes De Oliveira, R.K. Dewanjee, K. Ehataht, M. Kadastik, J. Pata, M. Raidal, C. Veelken

**Department of Physics, University of Helsinki, Helsinki, Finland**
P. Eerola, L. Forthomme, H. Kirschenmann, K. Osterberg, M. Voutilainen

**Helsinki Institute of Physics, Helsinki, Finland**
E. Brücken, F. Garcia, J. Havukainen, V. Karimäki, M.S. Kim, R. Kinnunen, T. Lampén, K. Lassila-Perini, S. Lehti, T. Lindén, H. Siikonen, E. Tuominen, J. Tuominiemi

**Lappeenranta University of Technology, Lappeenranta, Finland**
P. Luukka, H. Petrow, T. Tuuva

**IRFU, CEA, Université Paris-Saclay, Gif-sur-Yvette, France**
C. Amendola, M. Besancon, F. Couderc, M. Dejardin, D. Denegri, J.L. Faure, F. Ferri, S. Ganjour, A. Givernaud, P. Gras, G. Hamel de Monchenault, P. Jarry, B. Lenzi, E. Locci, J. Malcles, J. Rander, A. Rosowsky, M.Ö. Sahin, A. Savoy-Navarro[16], M. Titov, G.B. Yu

**Laboratoire Leprince-Ringuet, CNRS/IN2P3, Ecole Polytechnique, Institut Polytechnique de Paris, Palaiseau, France**
S. Ahuja, F. Beaudette, M. Bonanomi, A. Buchot Perraguin, P. Busson, C. Charlot, O. Davignon, B. Diab, G. Falmagne, R. Granier de Cassagnac, A. Hakimi, I. Kucher, A. Lobanov, C. Martin Perez, M. Nguyen, C. Ochando, P. Paganini, J. Rembser, R. Salerno, J.B. Sauvan, Y. Sirois, A. Zabi, A. Zghiche

**Université de Strasbourg, CNRS, IPHC UMR 7178, Strasbourg, France**
J.-L. Agram[17], J. Andrea, D. Apparu, D. Bloch, G. Bourgatte, J.-M. Brom, E.C. Chabert, C. Collard, D. Darej, J.-C. Fontaine[17], U. Goerlach, C. Grimault, A.-C. Le Bihan, P. Van Hove

**Institut de Physique des 2 Infinis de Lyon (IP2I ), Villeurbanne, France**
E. Asilar, S. Beauceron, C. Bernet, G. Boudoul, C. Camen, A. Carle, N. Chanon, D. Contardo, P. Depasse, H. El Mamouni, J. Fay, S. Gascon, M. Gouzevitch, B. Ille, Sa. Jain, I.B. Laktineh, H. Lattaud, A. Lesauvage, M. Lethuillier, L. Mirabito, K. Shchablo, L. Torterotot, G. Touquet, M. Vander Donckt, S. Viret

**Georgian Technical University, Tbilisi, Georgia**
A. Khvedelidze[12], Z. Tsamalaidze[12]

**RWTH Aachen University, I. Physikalisches Institut, Aachen, Germany**
L. Feld, K. Klein, M. Lipinski, D. Meuser, A. Pauls, M.P. Rauch, J. Schulz, M. Teroerde

**RWTH Aachen University, III. Physikalisches Institut A, Aachen, Germany**
D. Eliseev, M. Erdmann, P. Fackeldey, B. Fischer, S. Ghosh, T. Hebbeker, K. Hoepfner, H. Keller, L. Mastrolorenzo, M. Merschmeyer, A. Meyer, G. Mocellin, S. Mondal, S. Mukherjee, D. Noll, A. Novak, T. Pook, A. Pozdnyakov, Y. Rath, H. Reithler, J. Roemer, A. Schmidt, S.C. Schuler, A. Sharma, S. Wiedenbeck, S. Zaleski

**RWTH Aachen University, III. Physikalisches Institut B, Aachen, Germany**
C. Dziwok, G. Flügge, W. Haj Ahmad[18], O. Hlushchenko, T. Kress, A. Nowack, C. Pistone, O. Pooth, D. Roy, H. Sert, A. Stahl[19], T. Ziemons

**Deutsches Elektronen-Synchrotron, Hamburg, Germany**

H. Aarup Petersen, M. Aldaya Martin, P. Asmuss, I. Babounikau, S. Baxter, O. Behnke, A. Bermúdez Martínez, A.A. Bin Anuar, K. Borras[20], V. Botta, D. Brunner, A. Campbell, A. Cardini, P. Connor, S. Consuegra Rodríguez, V. Danilov, M.M. Defranchis, L. Didukh, D. Domínguez Damiani, G. Eckerlin, D. Eckstein, L.I. Estevez Banos, E. Gallo[21], A. Geiser, A. Giraldi, A. Grohsjean, M. Guthoff, A. Harb, A. Jafari[22], N.Z. Jomhari, H. Jung, A. Kasem[20], M. Kasemann, H. Kaveh, C. Kleinwort, J. Knolle, D. Krücker, W. Lange, T. Lenz, J. Lidrych, K. Lipka, W. Lohmann[23], T. Madlener, R. Mankel, I.-A. Melzer-Pellmann, J. Metwally, A.B. Meyer, M. Meyer, J. Mnich, A. Mussgiller, V. Myronenko, Y. Otarid, D. Pérez Adán, S.K. Pflitsch, D. Pitzl, A. Raspereza, A. Saggio, A. Saibel, M. Savitskyi, V. Scheurer, C. Schwanenberger, A. Singh, R.E. Sosa Ricardo, N. Tonon, O. Turkot, A. Vagnerini, M. Van De Klundert, R. Walsh, D. Walter, Y. Wen, K. Wichmann, C. Wissing, S. Wuchterl, O. Zenaiev, R. Zlebcik

**University of Hamburg, Hamburg, Germany**

R. Aggleton, S. Bein, L. Benato, A. Benecke, K. De Leo, T. Dreyer, M. Eich, F. Feindt, A. Fröhlich, C. Garbers, E. Garutti, P. Gunnellini, J. Haller, A. Hinzmann, A. Karavdina, G. Kasieczka, R. Klanner, R. Kogler, V. Kutzner, J. Lange, T. Lange, A. Malara, A. Nigamova, K.J. Pena Rodriguez, O. Rieger, P. Schleper, M. Schröder, J. Schwandt, D. Schwarz, J. Sonneveld, H. Stadie, G. Steinbrück, A. Tews, B. Vormwald, I. Zoi

**Karlsruher Institut fuer Technologie, Karlsruhe, Germany**

J. Bechtel, T. Berger, E. Butz, R. Caspart, T. Chwalek, W. De Boer, A. Dierlamm, A. Droll, K. El Morabit, N. Faltermann, K. Flöh, M. Giffels, J.o. Gosewisch, A. Gottmann, F. Hartmann[19], C. Heidecker, U. Husemann, I. Katkov[24], P. Keicher, R. Koppenhöfer, S. Maier, M. Metzler, S. Mitra, Th. Müller, M. Musich, M. Neukum, G. Quast, K. Rabbertz, J. Rauser, D. Savoiu, D. Schäfer, M. Schnepf, D. Seith, I. Shvetsov, H.J. Simonis, R. Ulrich, J. Van Der Linden, R.F. Von Cube, M. Wassmer, M. Weber, S. Wieland, R. Wolf, S. Wozniewski, S. Wunsch

**Institute of Nuclear and Particle Physics (INPP), NCSR Demokritos, Aghia Paraskevi, Greece**

G. Anagnostou, P. Asenov, G. Daskalakis, T. Geralis, A. Kyriakis, D. Loukas, G. Paspalaki, A. Stakia

**National and Kapodistrian University of Athens, Athens, Greece**

M. Diamantopoulou, D. Karasavvas, G. Karathanasis, P. Kontaxakis, C.K. Koraka, A. Manousakis-katsikakis, A. Panagiotou, I. Papavergou, N. Saoulidou, K. Theofilatos, E. Tziaferi, K. Vellidis, E. Vourliotis

**National Technical University of Athens, Athens, Greece**

G. Bakas, K. Kousouris, I. Papakrivopoulos, G. Tsipolitis, A. Zacharopoulou

**University of Ioánnina, Ioánnina, Greece**

I. Evangelou, C. Foudas, P. Gianneios, P. Katsoulis, P. Kokkas, N. Manthos, I. Papadopoulos, J. Strologas

**MTA-ELTE Lendület CMS Particle and Nuclear Physics Group, Eötvös Loránd University, Budapest, Hungary**

M. Csanad, M.M.A. Gadallah[25], S. Lökös[26], P. Major, K. Mandal, A. Mehta, G. Pasztor, A.J. Rádl, O. Surányi, G.I. Veres

**Wigner Research Centre for Physics, Budapest, Hungary**

M. Bartók[27], G. Bencze, C. Hajdu, D. Horvath[28], F. Sikler, V. Veszpremi, G. Vesztergombi[†]

**Institute of Nuclear Research ATOMKI, Debrecen, Hungary**
S. Czellar, J. Karancsi[27], J. Molnar, Z. Szillasi, D. Teyssier

**Institute of Physics, University of Debrecen, Debrecen, Hungary**
P. Raics, Z.L. Trocsanyi[29], B. Ujvari

**Eszterhazy Karoly University, Karoly Robert Campus, Gyongyos, Hungary**
T. Csorgo[30], F. Nemes[30], T. Novak

**Indian Institute of Science (IISc), Bangalore, India**
S. Choudhury, J.R. Komaragiri, D. Kumar, L. Panwar, P.C. Tiwari

**National Institute of Science Education and Research, HBNI, Bhubaneswar, India**
S. Bahinipati[31], D. Dash, C. Kar, P. Mal, T. Mishra, V.K. Muraleedharan Nair Bindhu[32], A. Nayak[32], P. Saha, N. Sur, S.K. Swain

**Panjab University, Chandigarh, India**
S. Bansal, S.B. Beri, V. Bhatnagar, G. Chaudhary, S. Chauhan, N. Dhingra[33], R. Gupta, A. Kaur, S. Kaur, P. Kumari, M. Meena, K. Sandeep, J.B. Singh, A.K. Virdi

**University of Delhi, Delhi, India**
A. Ahmed, A. Bhardwaj, B.C. Choudhary, R.B. Garg, M. Gola, S. Keshri, A. Kumar, M. Naimuddin, P. Priyanka, K. Ranjan, A. Shah

**Saha Institute of Nuclear Physics, HBNI, Kolkata, India**
M. Bharti[34], R. Bhattacharya, S. Bhattacharya, D. Bhowmik, S. Dutta, S. Ghosh, B. Gomber[35], M. Maity[36], S. Nandan, P. Palit, P.K. Rout, G. Saha, B. Sahu, S. Sarkar, M. Sharan, B. Singh[34], S. Thakur[34]

**Indian Institute of Technology Madras, Madras, India**
P.K. Behera, S.C. Behera, P. Kalbhor, A. Muhammad, R. Pradhan, P.R. Pujahari, A. Sharma, A.K. Sikdar

**Bhabha Atomic Research Centre, Mumbai, India**
D. Dutta, V. Jha, V. Kumar, D.K. Mishra, K. Naskar[37], P.K. Netrakanti, L.M. Pant, P. Shukla

**Tata Institute of Fundamental Research-A, Mumbai, India**
T. Aziz, S. Dugad, G.B. Mohanty, U. Sarkar

**Tata Institute of Fundamental Research-B, Mumbai, India**
S. Banerjee, S. Bhattacharya, R. Chudasama, M. Guchait, S. Karmakar, S. Kumar, G. Majumder, K. Mazumdar, S. Mukherjee, D. Roy

**Indian Institute of Science Education and Research (IISER), Pune, India**
S. Dube, B. Kansal, S. Pandey, A. Rane, A. Rastogi, S. Sharma

**Department of Physics, Isfahan University of Technology, Isfahan, Iran**
H. Bakhshiansohi[38], M. Zeinali[39]

**Institute for Research in Fundamental Sciences (IPM), Tehran, Iran**
S. Chenarani[40], S.M. Etesami, M. Khakzad, M. Mohammadi Najafabadi

**University College Dublin, Dublin, Ireland**
M. Felcini, M. Grunewald

**INFN Sezione di Bari $^a$, Università di Bari $^b$, Politecnico di Bari $^c$, Bari, Italy**
M. Abbrescia$^{a,b}$, R. Aly$^{a,b,41}$, C. Aruta$^{a,b}$, A. Colaleo$^a$, D. Creanza$^{a,c}$, N. De Filippis$^{a,c}$,

M. De Palma[a,b], A. Di Florio[a,b], A. Di Pilato[a,b], W. Elmetenawee[a,b], L. Fiore[a], A. Gelmi[a,b], M. Gul[a], G. Iaselli[a,c], M. Ince[a,b], S. Lezki[a,b], G. Maggi[a,c], M. Maggi[a], I. Margjeka[a,b], V. Mastrapasqua[a,b], J.A. Merlin[a], S. My[a,b], S. Nuzzo[a,b], A. Pompili[a,b], G. Pugliese[a,c], A. Ranieri[a], G. Selvaggi[a,b], L. Silvestris[a], F.M. Simone[a,b], R. Venditti[a], P. Verwilligen[a]

**INFN Sezione di Bologna** [a], **Università di Bologna** [b], **Bologna, Italy**
G. Abbiendi[a], C. Battilana[a,b], D. Bonacorsi[a,b], L. Borgonovi[a], S. Braibant-Giacomelli[a,b], L. Brigliadori[a], R. Campanini[a,b], P. Capiluppi[a,b], A. Castro[a,b], F.R. Cavallo[a], C. Ciocca[a], M. Cuffiani[a,b], G.M. Dallavalle[a], T. Diotalevi[a,b], F. Fabbri[a], A. Fanfani[a,b], E. Fontanesi[a,b], P. Giacomelli[a], L. Giommi[a,b], C. Grandi[a], L. Guiducci[a,b], F. Iemmi[a,b], S. Lo Meo[a,42], S. Marcellini[a], G. Masetti[a], F.L. Navarria[a,b], A. Perrotta[a], F. Primavera[a,b], A.M. Rossi[a,b], T. Rovelli[a,b], G.P. Siroli[a,b], N. Tosi[a]

**INFN Sezione di Catania** [a], **Università di Catania** [b], **Catania, Italy**
S. Albergo[a,b,43], S. Costa[a,b,43], A. Di Mattia[a], R. Potenza[a,b], A. Tricomi[a,b,43], C. Tuve[a,b]

**INFN Sezione di Firenze** [a], **Università di Firenze** [b], **Firenze, Italy**
G. Barbagli[a], A. Cassese[a], R. Ceccarelli[a,b], V. Ciulli[a,b], C. Civinini[a], R. D'Alessandro[a,b], F. Fiori[a,b], E. Focardi[a,b], G. Latino[a,b], P. Lenzi[a,b], M. Lizzo[a,b], M. Meschini[a], S. Paoletti[a], R. Seidita[a,b], G. Sguazzoni[a], L. Viliani[a]

**INFN Laboratori Nazionali di Frascati, Frascati, Italy**
L. Benussi, S. Bianco, D. Piccolo

**INFN Sezione di Genova** [a], **Università di Genova** [b], **Genova, Italy**
M. Bozzo[a,b], F. Ferro[a], R. Mulargia[a,b], E. Robutti[a], S. Tosi[a,b]

**INFN Sezione di Milano-Bicocca** [a], **Università di Milano-Bicocca** [b], **Milano, Italy**
A. Benaglia[a], F. Brivio[a,b], F. Cetorelli[a,b], V. Ciriolo[a,b,19], F. De Guio[a,b], M.E. Dinardo[a,b], P. Dini[a], S. Gennai[a], A. Ghezzi[a,b], P. Govoni[a,b], L. Guzzi[a,b], M. Malberti[a], S. Malvezzi[a], A. Massironi[a], D. Menasce[a], F. Monti[a,b], L. Moroni[a], M. Paganoni[a,b], D. Pedrini[a], S. Ragazzi[a,b], N. Redaelli[a], T. Tabarelli de Fatis[a,b], D. Valsecchi[a,b,19], D. Zuolo[a,b]

**INFN Sezione di Napoli** [a], **Università di Napoli 'Federico II'** [b], **Napoli, Italy, Università della Basilicata** [c], **Potenza, Italy, Università G. Marconi** [d], **Roma, Italy**
S. Buontempo[a], N. Cavallo[a,c], A. De Iorio[a,b], F. Fabozzi[a,c], A.O.M. Iorio[a,b], L. Lista[a,b], S. Meola[a,d,19], P. Paolucci[a,19], B. Rossi[a], C. Sciacca[a,b]

**INFN Sezione di Padova** [a], **Università di Padova** [b], **Padova, Italy, Università di Trento** [c], **Trento, Italy**
P. Azzi[a], N. Bacchetta[a], D. Bisello[a,b], P. Bortignon[a], A. Bragagnolo[a,b], R. Carlin[a,b], P. Checchia[a], P. De Castro Manzano[a], T. Dorigo[a], F. Gasparini[a,b], U. Gasparini[a,b], S.Y. Hoh[a,b], L. Layer[a,44], M. Margoni[a,b], A.T. Meneguzzo[a,b], M. Presilla[a,b], P. Ronchese[a,b], R. Rossin[a,b], F. Simonetto[a,b], G. Strong[a], M. Tosi[a,b], H. YARAR[a,b], M. Zanetti[a,b], P. Zotto[a,b], A. Zucchetta[a,b], G. Zumerle[a,b]

**INFN Sezione di Pavia** [a], **Università di Pavia** [b], **Pavia, Italy**
C. Aime'[a,b], A. Braghieri[a], S. Calzaferri[a,b], D. Fiorina[a,b], P. Montagna[a,b], S.P. Ratti[a,b], V. Re[a], M. Ressegotti[a,b], C. Riccardi[a,b], P. Salvini[a], I. Vai[a], P. Vitulo[a,b]

**INFN Sezione di Perugia** [a], **Università di Perugia** [b], **Perugia, Italy**
G.M. Bilei[a], D. Ciangottini[a,b], L. Fanò[a,b], P. Lariccia[a,b], G. Mantovani[a,b], V. Mariani[a,b], M. Menichelli[a], F. Moscatelli[a], A. Piccinelli[a,b], A. Rossi[a,b], A. Santocchia[a,b], D. Spiga[a], T. Tedeschi[a,b]

**INFN Sezione di Pisa [a], Università di Pisa [b], Scuola Normale Superiore di Pisa [c], Pisa Italy, Università di Siena [d], Siena, Italy**

P. Azzurri[a], G. Bagliesi[a], V. Bertacchi[a,c], L. Bianchini[a], T. Boccali[a], E. Bossini, R. Castaldi[a], M.A. Ciocci[a,b], R. Dell'Orso[a], M.R. Di Domenico[a,d], S. Donato[a], A. Giassi[a], M.T. Grippo[a], F. Ligabue[a,c], E. Manca[a,c], G. Mandorli[a,c], A. Messineo[a,b], F. Palla[a], G. Ramirez-Sanchez[a,c], A. Rizzi[a,b], G. Rolandi[a,c], S. Roy Chowdhury[a,c], A. Scribano[a], N. Shafiei[a,b], P. Spagnolo[a], R. Tenchini[a], G. Tonelli[a,b], N. Turini[a,d], A. Venturi[a], P.G. Verdini[a]

**INFN Sezione di Roma [a], Sapienza Università di Roma [b], Rome, Italy**

F. Cavallari[a], M. Cipriani[a,b], D. Del Re[a,b], E. Di Marco[a], M. Diemoz[a], E. Longo[a,b], P. Meridiani[a], G. Organtini[a,b], F. Pandolfi[a], R. Paramatti[a,b], C. Quaranta[a,b], S. Rahatlou[a,b], C. Rovelli[a], F. Santanastasio[a,b], L. Soffi[a,b], R. Tramontano[a,b]

**INFN Sezione di Torino [a], Università di Torino [b], Torino, Italy, Università del Piemonte Orientale [c], Novara, Italy**

N. Amapane[a,b], R. Arcidiacono[a,c], S. Argiro[a,b], M. Arneodo[a,c], N. Bartosik[a], R. Bellan[a,b], A. Bellora[a,b], J. Berenguer Antequera[a,b], C. Biino[a], A. Cappati[a,b], N. Cartiglia[a], S. Cometti[a], M. Costa[a,b], R. Covarelli[a,b], N. Demaria[a], B. Kiani[a,b], F. Legger[a], C. Mariotti[a], S. Maselli[a], E. Migliore[a,b], V. Monaco[a,b], E. Monteil[a,b], M. Monteno[a], M.M. Obertino[a,b], G. Ortona[a], L. Pacher[a,b], N. Pastrone[a], M. Pelliccioni[a], G.L. Pinna Angioni[a,b], M. Ruspa[a,c], R. Salvatico[a,b], K. Shchelina[a,b], F. Siviero[a,b], V. Sola[a], A. Solano[a,b], D. Soldi[a,b], A. Staiano[a], M. Tornago[a,b], D. Trocino[a,b]

**INFN Sezione di Trieste [a], Università di Trieste [b], Trieste, Italy**

S. Belforte[a], V. Candelise[a,b], M. Casarsa[a], F. Cossutti[a], A. Da Rold[a,b], G. Della Ricca[a,b], F. Vazzoler[a,b]

**Kyungpook National University, Daegu, Korea**

S. Dogra, C. Huh, B. Kim, D.H. Kim, G.N. Kim, J. Lee, S.W. Lee, C.S. Moon, Y.D. Oh, S.I. Pak, B.C. Radburn-Smith, S. Sekmen, Y.C. Yang

**Chonnam National University, Institute for Universe and Elementary Particles, Kwangju, Korea**

H. Kim, D.H. Moon

**Hanyang University, Seoul, Korea**

B. Francois, T.J. Kim, J. Park

**Korea University, Seoul, Korea**

S. Cho, S. Choi, Y. Go, B. Hong, K. Lee, K.S. Lee, J. Lim, J. Park, S.K. Park, J. Yoo

**Kyung Hee University, Department of Physics, Seoul, Republic of Korea**

J. Goh, A. Gurtu

**Sejong University, Seoul, Korea**

H.S. Kim, Y. Kim

**Seoul National University, Seoul, Korea**

J. Almond, J.H. Bhyun, J. Choi, S. Jeon, J. Kim, J.S. Kim, S. Ko, H. Kwon, H. Lee, S. Lee, B.H. Oh, M. Oh, S.B. Oh, H. Seo, U.K. Yang, I. Yoon

**University of Seoul, Seoul, Korea**

D. Jeon, J.H. Kim, B. Ko, J.S.H. Lee, I.C. Park, Y. Roh, D. Song, I.J. Watson

**Yonsei University, Department of Physics, Seoul, Korea**
S. Ha, H.D. Yoo

**Sungkyunkwan University, Suwon, Korea**
Y. Choi, Y. Jeong, H. Lee, Y. Lee, I. Yu

**College of Engineering and Technology, American University of the Middle East (AUM), Egaila, Kuwait**
T. Beyrouthy, Y. Maghrbi

**Riga Technical University, Riga, Latvia**
V. Veckalns[45]

**Vilnius University, Vilnius, Lithuania**
M. Ambrozas, A. Juodagalvis, A. Rinkevicius, G. Tamulaitis, A. Vaitkevicius

**National Centre for Particle Physics, Universiti Malaya, Kuala Lumpur, Malaysia**
W.A.T. Wan Abdullah, M.N. Yusli, Z. Zolkapli

**Universidad de Sonora (UNISON), Hermosillo, Mexico**
J.F. Benitez, A. Castaneda Hernandez, J.A. Murillo Quijada, L. Valencia Palomo

**Centro de Investigacion y de Estudios Avanzados del IPN, Mexico City, Mexico**
G. Ayala, H. Castilla-Valdez, E. De La Cruz-Burelo, I. Heredia-De La Cruz[46], R. Lopez-Fernandez, C.A. Mondragon Herrera, D.A. Perez Navarro, A. Sanchez-Hernandez

**Universidad Iberoamericana, Mexico City, Mexico**
S. Carrillo Moreno, C. Oropeza Barrera, M. Ramirez-Garcia, F. Vazquez Valencia

**Benemerita Universidad Autonoma de Puebla, Puebla, Mexico**
I. Pedraza, H.A. Salazar Ibarguen, C. Uribe Estrada

**University of Montenegro, Podgorica, Montenegro**
J. Mijuskovic[47], N. Raicevic

**University of Auckland, Auckland, New Zealand**
D. Krofcheck

**University of Canterbury, Christchurch, New Zealand**
S. Bheesette, P.H. Butler

**National Centre for Physics, Quaid-I-Azam University, Islamabad, Pakistan**
A. Ahmad, M.I. Asghar, A. Awais, M.I.M. Awan, H.R. Hoorani, W.A. Khan, S. Qazi, M.A. Shah, M. Shoaib

**AGH University of Science and Technology Faculty of Computer Science, Electronics and Telecommunications, Krakow, Poland**
V. Avati, L. Grzanka, M. Malawski

**National Centre for Nuclear Research, Swierk, Poland**
H. Bialkowska, M. Bluj, B. Boimska, T. Frueboes, M. Górski, M. Kazana, M. Szleper, P. Traczyk, P. Zalewski

**Institute of Experimental Physics, Faculty of Physics, University of Warsaw, Warsaw, Poland**
K. Bunkowski, K. Doroba, A. Kalinowski, M. Konecki, J. Krolikowski, M. Walczak

**Laboratório de Instrumentação e Física Experimental de Partículas, Lisboa, Portugal**
M. Araujo, P. Bargassa, D. Bastos, A. Boletti, P. Faccioli, M. Gallinaro, J. Hollar, N. Leonardo,
T. Niknejad, J. Seixas, O. Toldaiev, J. Varela

**Joint Institute for Nuclear Research, Dubna, Russia**
S. Afanasiev, D. Budkouski, P. Bunin, M. Gavrilenko, I. Golutvin, I. Gorbunov, A. Kamenev,
V. Karjavine, A. Lanev, A. Malakhov, V. Matveev[48,49], V. Palichik, V. Perelygin, M. Savina,
D. Seitova, V. Shalaev, S. Shmatov, S. Shulha, V. Smirnov, O. Teryaev, N. Voytishin, A. Zarubin,
I. Zhizhin

**Petersburg Nuclear Physics Institute, Gatchina (St. Petersburg), Russia**
G. Gavrilov, V. Golovtcov, Y. Ivanov, V. Kim[50], E. Kuznetsova[51], V. Murzin, V. Oreshkin,
I. Smirnov, D. Sosnov, V. Sulimov, L. Uvarov, S. Volkov, A. Vorobyev

**Institute for Nuclear Research, Moscow, Russia**
Yu. Andreev, A. Dermenev, S. Gninenko, N. Golubev, A. Karneyeu, M. Kirsanov, N. Krasnikov,
A. Pashenkov, G. Pivovarov, D. Tlisov[+], A. Toropin

**Institute for Theoretical and Experimental Physics named by A.I. Alikhanov of NRC
'Kurchatov Institute', Moscow, Russia**
V. Epshteyn, V. Gavrilov, N. Lychkovskaya, A. Nikitenko[52], V. Popov, G. Safronov,
A. Spiridonov, A. Stepennov, M. Toms, E. Vlasov, A. Zhokin

**Moscow Institute of Physics and Technology, Moscow, Russia**
T. Aushev

**National Research Nuclear University 'Moscow Engineering Physics Institute' (MEPhI),
Moscow, Russia**
R. Chistov[53], M. Danilov[54], A. Oskin, P. Parygin, S. Polikarpov[54]

**P.N. Lebedev Physical Institute, Moscow, Russia**
V. Andreev, M. Azarkin, I. Dremin, M. Kirakosyan, A. Terkulov

**Skobeltsyn Institute of Nuclear Physics, Lomonosov Moscow State University, Moscow,
Russia**
A. Belyaev, E. Boos, V. Bunichev, M. Dubinin[55], L. Dudko, A. Gribushin, V. Klyukhin,
O. Kodolova, I. Lokhtin, S. Obraztsov, M. Perfilov, S. Petrushanko, V. Savrin

**Novosibirsk State University (NSU), Novosibirsk, Russia**
V. Blinov[56], T. Dimova[56], L. Kardapoltsev[56], I. Ovtin[56], Y. Skovpen[56]

**Institute for High Energy Physics of National Research Centre 'Kurchatov Institute',
Protvino, Russia**
I. Azhgirey, I. Bayshev, V. Kachanov, A. Kalinin, D. Konstantinov, V. Petrov, R. Ryutin, A. Sobol,
S. Troshin, N. Tyurin, A. Uzunian, A. Volkov

**National Research Tomsk Polytechnic University, Tomsk, Russia**
A. Babaev, V. Okhotnikov, L. Sukhikh

**Tomsk State University, Tomsk, Russia**
V. Borchsh, V. Ivanchenko, E. Tcherniaev

**University of Belgrade: Faculty of Physics and VINCA Institute of Nuclear Sciences,
Belgrade, Serbia**
P. Adzic[57], M. Dordevic, P. Milenovic, J. Milosevic, V. Milosevic

**Centro de Investigaciones Energéticas Medioambientales y Tecnológicas (CIEMAT), Madrid, Spain**

M. Aguilar-Benitez, J. Alcaraz Maestre, A. Álvarez Fernández, I. Bachiller, M. Barrio Luna, Cristina F. Bedoya, C.A. Carrillo Montoya, M. Cepeda, M. Cerrada, N. Colino, B. De La Cruz, A. Delgado Peris, J.P. Fernández Ramos, J. Flix, M.C. Fouz, O. Gonzalez Lopez, S. Goy Lopez, J.M. Hernandez, M.I. Josa, J. León Holgado, D. Moran, Á. Navarro Tobar, A. Pérez-Calero Yzquierdo, J. Puerta Pelayo, I. Redondo, L. Romero, S. Sánchez Navas, M.S. Soares, L. Urda Gómez, C. Willmott

**Universidad Autónoma de Madrid, Madrid, Spain**

J.F. de Trocóniz, R. Reyes-Almanza

**Universidad de Oviedo, Instituto Universitario de Ciencias y Tecnologías Espaciales de Asturias (ICTEA), Oviedo, Spain**

B. Alvarez Gonzalez, J. Cuevas, C. Erice, J. Fernandez Menendez, S. Folgueras, I. Gonzalez Caballero, E. Palencia Cortezon, C. Ramón Álvarez, J. Ripoll Sau, V. Rodríguez Bouza, A. Trapote

**Instituto de Física de Cantabria (IFCA), CSIC-Universidad de Cantabria, Santander, Spain**

J.A. Brochero Cifuentes, I.J. Cabrillo, A. Calderon, B. Chazin Quero, J. Duarte Campderros, M. Fernandez, C. Fernandez Madrazo, P.J. Fernández Manteca, A. García Alonso, G. Gomez, C. Martinez Rivero, P. Martinez Ruiz del Arbol, F. Matorras, J. Piedra Gomez, C. Prieels, F. Ricci-Tam, T. Rodrigo, A. Ruiz-Jimeno, L. Scodellaro, N. Trevisani, I. Vila, J.M. Vizan Garcia

**University of Colombo, Colombo, Sri Lanka**

MK Jayananda, B. Kailasapathy[58], D.U.J. Sonnadara, DDC Wickramarathna

**University of Ruhuna, Department of Physics, Matara, Sri Lanka**

W.G.D. Dharmaratna, K. Liyanage, N. Perera, N. Wickramage

**CERN, European Organization for Nuclear Research, Geneva, Switzerland**

T.K. Aarrestad, D. Abbaneo, J. Alimena, E. Auffray, G. Auzinger, J. Baechler, P. Baillon, A.H. Ball, D. Barney, J. Bendavid, N. Beni, M. Bianco, A. Bocci, E. Brondolin, T. Camporesi, M. Capeans Garrido, G. Cerminara, S.S. Chhibra, L. Cristella, D. d'Enterria, A. Dabrowski, N. Daci, A. David, A. De Roeck, M. Deile, R. Di Maria, M. Dobson, M. Dünser, N. Dupont, A. Elliott-Peisert, N. Emriskova, F. Fallavollita[59], D. Fasanella, S. Fiorendi, A. Florent, G. Franzoni, J. Fulcher, W. Funk, S. Giani, D. Gigi, K. Gill, F. Glege, L. Gouskos, M. Haranko, J. Hegeman, Y. Iiyama, V. Innocente, T. James, P. Janot, J. Kaspar, J. Kieseler, M. Komm, N. Kratochwil, C. Lange, S. Laurila, P. Lecoq, K. Long, C. Lourenço, L. Malgeri, S. Mallios, M. Mannelli, F. Meijers, S. Mersi, E. Meschi, F. Moortgat, M. Mulders, S. Orfanelli, L. Orsini, F. Pantaleo[19], L. Pape, E. Perez, M. Peruzzi, A. Petrilli, G. Petrucciani, A. Pfeiffer, M. Pierini, M. Pitt, H. Qu, T. Quast, D. Rabady, A. Racz, M. Rieger, M. Rovere, H. Sakulin, J. Salfeld-Nebgen, S. Scarfi, C. Schäfer, C. Schwick, M. Selvaggi, A. Sharma, P. Silva, W. Snoeys, P. Sphicas[60], S. Summers, V.R. Tavolaro, D. Treille, A. Tsirou, G.P. Van Onsem, M. Verzetti, K.A. Wozniak, W.D. Zeuner

**Paul Scherrer Institut, Villigen, Switzerland**

L. Caminada[61], A. Ebrahimi, W. Erdmann, R. Horisberger, Q. Ingram, H.C. Kaestli, D. Kotlinski, U. Langenegger, M. Missiroli, T. Rohe

**ETH Zurich - Institute for Particle Physics and Astrophysics (IPA), Zurich, Switzerland**

K. Androsov[62], M. Backhaus, P. Berger, A. Calandri, N. Chernyavskaya, A. De Cosa, G. Dissertori, M. Dittmar, M. Donegà, C. Dorfer, T. Gadek, T.A. Gómez Espinosa, C. Grab,

D. Hits, W. Lustermann, A.-M. Lyon, R.A. Manzoni, M.T. Meinhard, F. Micheli, F. Nessi-Tedaldi, J. Niedziela, F. Pauss, V. Perovic, G. Perrin, S. Pigazzini, M.G. Ratti, M. Reichmann, C. Reissel, T. Reitenspiess, B. Ristic, D. Ruini, D.A. Sanz Becerra, M. Schönenberger, V. Stampf, J. Steggemann[62], R. Wallny, D.H. Zhu

**Universität Zürich, Zurich, Switzerland**
C. Amsler[63], C. Botta, D. Brzhechko, M.F. Canelli, A. De Wit, R. Del Burgo, J.K. Heikkilä, M. Huwiler, A. Jofrehei, B. Kilminster, S. Leontsinis, A. Macchiolo, P. Meiring, V.M. Mikuni, U. Molinatti, I. Neutelings, G. Rauco, A. Reimers, P. Robmann, S. Sanchez Cruz, K. Schweiger, Y. Takahashi

**National Central University, Chung-Li, Taiwan**
C. Adloff[64], C.M. Kuo, W. Lin, A. Roy, T. Sarkar[36], S.S. Yu

**National Taiwan University (NTU), Taipei, Taiwan**
L. Ceard, P. Chang, Y. Chao, K.F. Chen, P.H. Chen, W.-S. Hou, Y.y. Li, R.-S. Lu, E. Paganis, A. Psallidas, A. Steen, E. Yazgan, P.r. Yu

**Chulalongkorn University, Faculty of Science, Department of Physics, Bangkok, Thailand**
B. Asavapibhop, C. Asawatangtrakuldee, N. Srimanobhas

**Çukurova University, Physics Department, Science and Art Faculty, Adana, Turkey**
F. Boran, S. Damarseckin[65], Z.S. Demiroglu, F. Dolek, I. Dumanoglu[66], E. Eskut, G. Gokbulut, Y. Guler, E. Gurpinar Guler[67], I. Hos[68], C. Isik, E.E. Kangal[69], O. Kara, A. Kayis Topaksu, U. Kiminsu, G. Onengut, K. Ozdemir[70], A. Polatoz, A.E. Simsek, B. Tali[71], U.G. Tok, S. Turkcapar, I.S. Zorbakir, C. Zorbilmez

**Middle East Technical University, Physics Department, Ankara, Turkey**
B. Isildak[72], G. Karapinar[73], K. Ocalan[74], M. Yalvac[75]

**Bogazici University, Istanbul, Turkey**
B. Akgun, I.O. Atakisi, E. Gülmez, M. Kaya[76], O. Kaya[77], Ö. Özçelik, S. Tekten[78], E.A. Yetkin[79]

**Istanbul Technical University, Istanbul, Turkey**
A. Cakir, K. Cankocak[66], Y. Komurcu, S. Sen[80]

**Istanbul University, Istanbul, Turkey**
F. Aydogmus Sen, S. Cerci[71], B. Kaynak, S. Ozkorucuklu, D. Sunar Cerci[71]

**Institute for Scintillation Materials of National Academy of Science of Ukraine, Kharkov, Ukraine**
B. Grynyov

**National Scientific Center, Kharkov Institute of Physics and Technology, Kharkov, Ukraine**
L. Levchuk

**University of Bristol, Bristol, United Kingdom**
E. Bhal, S. Bologna, J.J. Brooke, A. Bundock, E. Clement, D. Cussans, H. Flacher, J. Goldstein, G.P. Heath, H.F. Heath, L. Kreczko, B. Krikler, S. Paramesvaran, T. Sakuma, S. Seif El Nasr-Storey, V.J. Smith, N. Stylianou[81], J. Taylor, A. Titterton

**Rutherford Appleton Laboratory, Didcot, United Kingdom**
K.W. Bell, A. Belyaev[82], C. Brew, R.M. Brown, D.J.A. Cockerill, K.V. Ellis, K. Harder, S. Harper, J. Linacre, K. Manolopoulos, D.M. Newbold, E. Olaiya, D. Petyt, T. Reis, T. Schuh, C.H. Shepherd-Themistocleous, A. Thea, I.R. Tomalin, T. Williams

**Imperial College, London, United Kingdom**
R. Bainbridge, P. Bloch, S. Bonomally, J. Borg, S. Breeze, O. Buchmuller, V. Cepaitis, G.S. Chahal[83], D. Colling, P. Dauncey, G. Davies, M. Della Negra, S. Fayer, G. Fedi, G. Hall, M.H. Hassanshahi, G. Iles, J. Langford, L. Lyons, A.-M. Magnan, S. Malik, A. Martelli, J. Nash[84], V. Palladino, M. Pesaresi, D.M. Raymond, A. Richards, A. Rose, E. Scott, C. Seez, A. Shtipliyski, A. Tapper, K. Uchida, T. Virdee[19], N. Wardle, S.N. Webb, D. Winterbottom, A.G. Zecchinelli

**Brunel University, Uxbridge, United Kingdom**
J.E. Cole, A. Khan, P. Kyberd, C.K. Mackay, I.D. Reid, L. Teodorescu, S. Zahid

**Baylor University, Waco, USA**
S. Abdullin, A. Brinkerhoff, B. Caraway, J. Dittmann, K. Hatakeyama, A.R. Kanuganti, B. McMaster, N. Pastika, S. Sawant, C. Smith, C. Sutantawibul, J. Wilson

**Catholic University of America, Washington, DC, USA**
R. Bartek, A. Dominguez, R. Uniyal, A.M. Vargas Hernandez

**The University of Alabama, Tuscaloosa, USA**
A. Buccilli, O. Charaf, S.I. Cooper, D. Di Croce, S.V. Gleyzer, C. Henderson, C.U. Perez, P. Rumerio, C. West

**Boston University, Boston, USA**
A. Akpinar, A. Albert, D. Arcaro, C. Cosby, Z. Demiragli, D. Gastler, J. Rohlf, K. Salyer, D. Sperka, D. Spitzbart, I. Suarez, S. Yuan, D. Zou

**Brown University, Providence, USA**
G. Benelli, B. Burkle, X. Coubez[20], D. Cutts, Y.t. Duh, M. Hadley, U. Heintz, J.M. Hogan[85], K.H.M. Kwok, E. Laird, G. Landsberg, K.T. Lau, J. Lee, J. Luo, M. Narain, S. Sagir[86], E. Usai, W.Y. Wong, X. Yan, D. Yu, W. Zhang

**University of California, Davis, Davis, USA**
C. Brainerd, R. Breedon, M. Calderon De La Barca Sanchez, M. Chertok, J. Conway, P.T. Cox, R. Erbacher, F. Jensen, O. Kukral, R. Lander, M. Mulhearn, D. Pellett, D. Taylor, M. Tripathi, Y. Yao, F. Zhang

**University of California, Los Angeles, USA**
M. Bachtis, R. Cousins, A. Dasgupta, A. Datta, D. Hamilton, J. Hauser, M. Ignatenko, M.A. Iqbal, T. Lam, N. Mccoll, W.A. Nash, S. Regnard, D. Saltzberg, C. Schnaible, B. Stone, V. Valuev

**University of California, Riverside, Riverside, USA**
K. Burt, Y. Chen, R. Clare, J.W. Gary, G. Hanson, G. Karapostoli, O.R. Long, N. Manganelli, M. Olmedo Negrete, W. Si, S. Wimpenny, Y. Zhang

**University of California, San Diego, La Jolla, USA**
J.G. Branson, P. Chang, S. Cittolin, S. Cooperstein, N. Deelen, J. Duarte, R. Gerosa, L. Giannini, D. Gilbert, J. Guiang, V. Krutelyov, R. Lee, J. Letts, M. Masciovecchio, S. May, S. Padhi, M. Pieri, B.V. Sathia Narayanan, V. Sharma, M. Tadel, A. Vartak, F. Würthwein, Y. Xiang, A. Yagil

**University of California, Santa Barbara - Department of Physics, Santa Barbara, USA**
N. Amin, C. Campagnari, M. Citron, A. Dorsett, V. Dutta, J. Incandela, M. Kilpatrick, B. Marsh, H. Mei, A. Ovcharova, M. Quinnan, J. Richman, U. Sarica, D. Stuart, S. Wang

**California Institute of Technology, Pasadena, USA**
A. Bornheim, O. Cerri, I. Dutta, J.M. Lawhorn, N. Lu, J. Mao, H.B. Newman, J. Ngadiuba, T.Q. Nguyen, M. Spiropulu, J.R. Vlimant, C. Wang, S. Xie, Z. Zhang, R.Y. Zhu

**Carnegie Mellon University, Pittsburgh, USA**
J. Alison, M.B. Andrews, T. Ferguson, T. Mudholkar, M. Paulini, I. Vorobiev

**University of Colorado Boulder, Boulder, USA**
J.P. Cumalat, W.T. Ford, E. MacDonald, R. Patel, A. Perloff, K. Stenson, K.A. Ulmer, S.R. Wagner

**Cornell University, Ithaca, USA**
J. Alexander, Y. Cheng, J. Chu, D.J. Cranshaw, K. Mcdermott, J. Monroy, J.R. Patterson, D. Quach, A. Ryd, W. Sun, S.M. Tan, Z. Tao, J. Thom, P. Wittich, M. Zientek

**Fermi National Accelerator Laboratory, Batavia, USA**
M. Albrow, M. Alyari, G. Apollinari, A. Apresyan, A. Apyan, S. Banerjee, L.A.T. Bauerdick, A. Beretvas, D. Berry, J. Berryhill, P.C. Bhat, K. Burkett, J.N. Butler, A. Canepa, G.B. Cerati, H.W.K. Cheung, F. Chlebana, M. Cremonesi, K.F. Di Petrillo, V.D. Elvira, J. Freeman, Z. Gecse, L. Gray, D. Green, S. Grünendahl, O. Gutsche, R.M. Harris, R. Heller, T.C. Herwig, J. Hirschauer, B. Jayatilaka, S. Jindariani, M. Johnson, U. Joshi, P. Klabbers, T. Klijnsma, B. Klima, M.J. Kortelainen, S. Lammel, D. Lincoln, R. Lipton, T. Liu, J. Lykken, C. Madrid, K. Maeshima, C. Mantilla, D. Mason, P. McBride, P. Merkel, S. Mrenna, S. Nahn, V. O'Dell, V. Papadimitriou, K. Pedro, C. Pena[55], O. Prokofyev, F. Ravera, A. Reinsvold Hall, L. Ristori, B. Schneider, E. Sexton-Kennedy, N. Smith, A. Soha, L. Spiegel, S. Stoynev, J. Strait, L. Taylor, S. Tkaczyk, N.V. Tran, L. Uplegger, E.W. Vaandering, H.A. Weber, A. Woodard

**University of Florida, Gainesville, USA**
D. Acosta, P. Avery, D. Bourilkov, L. Cadamuro, V. Cherepanov, F. Errico, R.D. Field, D. Guerrero, B.M. Joshi, M. Kim, J. Konigsberg, A. Korytov, K.H. Lo, K. Matchev, N. Menendez, G. Mitselmakher, D. Rosenzweig, K. Shi, J. Sturdy, J. Wang, E. Yigitbasi, X. Zuo

**Florida State University, Tallahassee, USA**
T. Adams, A. Askew, D. Diaz, R. Habibullah, S. Hagopian, V. Hagopian, K.F. Johnson, R. Khurana, T. Kolberg, G. Martinez, H. Prosper, C. Schiber, R. Yohay, J. Zhang

**Florida Institute of Technology, Melbourne, USA**
M.M. Baarmand, S. Butalla, T. Elkafrawy[13], M. Hohlmann, R. Kumar Verma, D. Noonan, M. Rahmani, M. Saunders, F. Yumiceva

**University of Illinois at Chicago (UIC), Chicago, USA**
M.R. Adams, L. Apanasevich, H. Becerril Gonzalez, R. Cavanaugh, X. Chen, S. Dittmer, O. Evdokimov, C.E. Gerber, D.A. Hangal, D.J. Hofman, C. Mills, G. Oh, T. Roy, M.B. Tonjes, N. Varelas, J. Viinikainen, X. Wang, Z. Wu, Z. Ye

**The University of Iowa, Iowa City, USA**
M. Alhusseini, K. Dilsiz[87], S. Durgut, R.P. Gandrajula, M. Haytmyradov, V. Khristenko, O.K. Köseyan, J.-P. Merlo, A. Mestvirishvili[88], A. Moeller, J. Nachtman, H. Ogul[89], Y. Onel, F. Ozok[90], A. Penzo, C. Snyder, E. Tiras[91], J. Wetzel

**Johns Hopkins University, Baltimore, USA**
O. Amram, B. Blumenfeld, L. Corcodilos, J. Davis, M. Eminizer, A.V. Gritsan, S. Kyriacou, P. Maksimovic, J. Roskes, M. Swartz, T.Á. Vámi

**The University of Kansas, Lawrence, USA**
C. Baldenegro Barrera, P. Baringer, A. Bean, A. Bylinkin, T. Isidori, S. Khalil, J. King,

G. Krintiras, A. Kropivnitskaya, C. Lindsey, N. Minafra, M. Murray, C. Rogan, C. Royon, S. Sanders, E. Schmitz, J.D. Tapia Takaki, Q. Wang, J. Williams, G. Wilson

**Kansas State University, Manhattan, USA**
S. Duric, A. Ivanov, K. Kaadze, D. Kim, Y. Maravin, T. Mitchell, A. Modak, K. Nam

**Lawrence Livermore National Laboratory, Livermore, USA**
F. Rebassoo, D. Wright

**University of Maryland, College Park, USA**
E. Adams, A. Baden, O. Baron, A. Belloni, S.C. Eno, Y. Feng, N.J. Hadley, S. Jabeen, R.G. Kellogg, T. Koeth, A.C. Mignerey, S. Nabili, M. Seidel, A. Skuja, S.C. Tonwar, L. Wang, K. Wong

**Massachusetts Institute of Technology, Cambridge, USA**
D. Abercrombie, R. Bi, S. Brandt, W. Busza, I.A. Cali, Y. Chen, M. D'Alfonso, G. Gomez Ceballos, M. Goncharov, P. Harris, M. Hu, M. Klute, D. Kovalskyi, J. Krupa, Y.-J. Lee, B. Maier, A.C. Marini, C. Mironov, C. Paus, D. Rankin, C. Roland, G. Roland, Z. Shi, G.S.F. Stephans, K. Tatar, J. Wang, Z. Wang, B. Wyslouch

**University of Minnesota, Minneapolis, USA**
R.M. Chatterjee, A. Evans, P. Hansen, J. Hiltbrand, Sh. Jain, M. Krohn, Y. Kubota, Z. Lesko, J. Mans, M. Revering, R. Rusack, R. Saradhy, N. Schroeder, N. Strobbe, M.A. Wadud

**University of Mississippi, Oxford, USA**
J.G. Acosta, S. Oliveros

**University of Nebraska-Lincoln, Lincoln, USA**
K. Bloom, M. Bryson, S. Chauhan, D.R. Claes, C. Fangmeier, L. Finco, F. Golf, J.R. González Fernández, C. Joo, I. Kravchenko, J.E. Siado, G.R. Snow[†], W. Tabb, F. Yan

**State University of New York at Buffalo, Buffalo, USA**
G. Agarwal, H. Bandyopadhyay, L. Hay, I. Iashvili, A. Kharchilava, C. McLean, D. Nguyen, J. Pekkanen, S. Rappoccio, A. Williams

**Northeastern University, Boston, USA**
G. Alverson, E. Barberis, C. Freer, Y. Haddad, A. Hortiangtham, J. Li, G. Madigan, B. Marzocchi, D.M. Morse, V. Nguyen, T. Orimoto, A. Parker, L. Skinnari, A. Tishelman-Charny, T. Wamorkar, B. Wang, A. Wisecarver, D. Wood

**Northwestern University, Evanston, USA**
S. Bhattacharya, J. Bueghly, Z. Chen, A. Gilbert, T. Gunter, K.A. Hahn, N. Odell, M.H. Schmitt, K. Sung, M. Velasco

**University of Notre Dame, Notre Dame, USA**
R. Band, R. Bucci, N. Dev, R. Goldouzian, M. Hildreth, K. Hurtado Anampa, C. Jessop, K. Lannon, N. Loukas, N. Marinelli, I. Mcalister, F. Meng, K. Mohrman, Y. Musienko[48], R. Ruchti, P. Siddireddy, M. Wayne, A. Wightman, M. Wolf, M. Zarucki, L. Zygala

**The Ohio State University, Columbus, USA**
B. Bylsma, B. Cardwell, L.S. Durkin, B. Francis, C. Hill, A. Lefeld, B.L. Winer, B.R. Yates

**Princeton University, Princeton, USA**
F.M. Addesa, B. Bonham, P. Das, G. Dezoort, P. Elmer, A. Frankenthal, B. Greenberg, N. Haubrich, S. Higginbotham, A. Kalogeropoulos, G. Kopp, S. Kwan, D. Lange, M.T. Lucchini, D. Marlow, K. Mei, I. Ojalvo, J. Olsen, C. Palmer, D. Stickland, C. Tully

**University of Puerto Rico, Mayaguez, USA**
S. Malik, S. Norberg

**Purdue University, West Lafayette, USA**
A.S. Bakshi, V.E. Barnes, R. Chawla, S. Das, L. Gutay, M. Jones, A.W. Jung, S. Karmarkar, M. Liu, G. Negro, N. Neumeister, C.C. Peng, S. Piperov, A. Purohit, J.F. Schulte, M. Stojanovic[16], J. Thieman, F. Wang, R. Xiao, W. Xie

**Purdue University Northwest, Hammond, USA**
J. Dolen, N. Parashar

**Rice University, Houston, USA**
A. Baty, S. Dildick, K.M. Ecklund, S. Freed, F.J.M. Geurts, A. Kumar, W. Li, B.P. Padley, R. Redjimi, J. Roberts[†], W. Shi, A.G. Stahl Leiton

**University of Rochester, Rochester, USA**
A. Bodek, P. de Barbaro, R. Demina, J.L. Dulemba, C. Fallon, T. Ferbel, M. Galanti, A. Garcia-Bellido, O. Hindrichs, A. Khukhunaishvili, E. Ranken, R. Taus

**Rutgers, The State University of New Jersey, Piscataway, USA**
B. Chiarito, J.P. Chou, A. Gandrakota, Y. Gershtein, E. Halkiadakis, A. Hart, M. Heindl, E. Hughes, S. Kaplan, O. Karacheban[23], I. Laflotte, A. Lath, R. Montalvo, K. Nash, M. Osherson, S. Salur, S. Schnetzer, S. Somalwar, R. Stone, S.A. Thayil, S. Thomas, H. Wang

**University of Tennessee, Knoxville, USA**
H. Acharya, A.G. Delannoy, S. Spanier

**Texas A&M University, College Station, USA**
O. Bouhali[92], M. Dalchenko, A. Delgado, R. Eusebi, J. Gilmore, T. Huang, T. Kamon[93], H. Kim, S. Luo, S. Malhotra, R. Mueller, D. Overton, D. Rathjens, A. Safonov

**Texas Tech University, Lubbock, USA**
N. Akchurin, J. Damgov, V. Hegde, S. Kunori, K. Lamichhane, S.W. Lee, T. Mengke, S. Muthumuni, T. Peltola, S. Undleeb, I. Volobouev, Z. Wang, A. Whitbeck

**Vanderbilt University, Nashville, USA**
E. Appelt, S. Greene, A. Gurrola, W. Johns, C. Maguire, A. Melo, H. Ni, K. Padeken, F. Romeo, P. Sheldon, S. Tuo, J. Velkovska

**University of Virginia, Charlottesville, USA**
M.W. Arenton, B. Cox, G. Cummings, J. Hakala, R. Hirosky, M. Joyce, A. Ledovskoy, A. Li, C. Neu, B. Tannenwald, E. Wolfe

**Wayne State University, Detroit, USA**
P.E. Karchin, N. Poudyal, P. Thapa

**University of Wisconsin - Madison, Madison, WI, USA**
K. Black, T. Bose, J. Buchanan, C. Caillol, S. Dasu, I. De Bruyn, P. Everaerts, F. Fienga, C. Galloni, H. He, M. Herndon, A. Hervé, U. Hussain, A. Lanaro, A. Loeliger, R. Loveless, J. Madhusudanan Sreekala, A. Mallampalli, A. Mohammadi, D. Pinna, A. Savin, V. Shang, V. Sharma, W.H. Smith, D. Teague, S. Trembath-reichert, W. Vetens

†: Deceased
1: Also at Vienna University of Technology, Vienna, Austria
2: Also at Institute of Basic and Applied Sciences, Faculty of Engineering, Arab Academy for Science, Technology and Maritime Transport, Alexandria, Egypt, Alexandria, Egypt

3: Also at Université Libre de Bruxelles, Bruxelles, Belgium
4: Also at Universidade Estadual de Campinas, Campinas, Brazil
5: Also at Federal University of Rio Grande do Sul, Porto Alegre, Brazil
6: Also at UFMS, Nova Andradina, Brazil
7: Also at University of Chinese Academy of Sciences, Beijing, China
8: Also at Department of Physics, Tsinghua University, Beijing, China, Beijing, China
9: Also at Nanjing Normal University Department of Physics, Nanjing, China
10: Now at The University of Iowa, Iowa City, USA
11: Also at Institute for Theoretical and Experimental Physics named by A.I. Alikhanov of NRC 'Kurchatov Institute', Moscow, Russia
12: Also at Joint Institute for Nuclear Research, Dubna, Russia
13: Also at Ain Shams University, Cairo, Egypt
14: Also at Zewail City of Science and Technology, Zewail, Egypt
15: Also at British University in Egypt, Cairo, Egypt
16: Also at Purdue University, West Lafayette, USA
17: Also at Université de Haute Alsace, Mulhouse, France
18: Also at Erzincan Binali Yildirim University, Erzincan, Turkey
19: Also at CERN, European Organization for Nuclear Research, Geneva, Switzerland
20: Also at RWTH Aachen University, III. Physikalisches Institut A, Aachen, Germany
21: Also at University of Hamburg, Hamburg, Germany
22: Also at Department of Physics, Isfahan University of Technology, Isfahan, Iran, Isfahan, Iran
23: Also at Brandenburg University of Technology, Cottbus, Germany
24: Also at Skobeltsyn Institute of Nuclear Physics, Lomonosov Moscow State University, Moscow, Russia
25: Also at Physics Department, Faculty of Science, Assiut University, Assiut, Egypt
26: Also at Eszterhazy Karoly University, Karoly Robert Campus, Gyongyos, Hungary
27: Also at Institute of Physics, University of Debrecen, Debrecen, Hungary, Debrecen, Hungary
28: Also at Institute of Nuclear Research ATOMKI, Debrecen, Hungary
29: Also at MTA-ELTE Lendület CMS Particle and Nuclear Physics Group, Eötvös Loránd University, Budapest, Hungary, Budapest, Hungary
30: Also at Wigner Research Centre for Physics, Budapest, Hungary
31: Also at IIT Bhubaneswar, Bhubaneswar, India, Bhubaneswar, India
32: Also at Institute of Physics, Bhubaneswar, India
33: Also at G.H.G. Khalsa College, Punjab, India
34: Also at Shoolini University, Solan, India
35: Also at University of Hyderabad, Hyderabad, India
36: Also at University of Visva-Bharati, Santiniketan, India
37: Also at Indian Institute of Technology (IIT), Mumbai, India
38: Also at Deutsches Elektronen-Synchrotron, Hamburg, Germany
39: Also at Sharif University of Technology, Tehran, Iran
40: Also at Department of Physics, University of Science and Technology of Mazandaran, Behshahr, Iran
41: Now at INFN Sezione di Bari [a], Università di Bari [b], Politecnico di Bari [c], Bari, Italy
42: Also at Italian National Agency for New Technologies, Energy and Sustainable Economic Development, Bologna, Italy
43: Also at Centro Siciliano di Fisica Nucleare e di Struttura Della Materia, Catania, Italy
44: Also at Università di Napoli 'Federico II', NAPOLI, Italy

45: Also at Riga Technical University, Riga, Latvia, Riga, Latvia

46: Also at Consejo Nacional de Ciencia y Tecnología, Mexico City, Mexico

47: Also at IRFU, CEA, Université Paris-Saclay, Gif-sur-Yvette, France

48: Also at Institute for Nuclear Research, Moscow, Russia

49: Now at National Research Nuclear University 'Moscow Engineering Physics Institute' (MEPhI), Moscow, Russia

50: Also at St. Petersburg State Polytechnical University, St. Petersburg, Russia

51: Also at University of Florida, Gainesville, USA

52: Also at Imperial College, London, United Kingdom

53: Also at Moscow Institute of Physics and Technology, Moscow, Russia, Moscow, Russia

54: Also at P.N. Lebedev Physical Institute, Moscow, Russia

55: Also at California Institute of Technology, Pasadena, USA

56: Also at Budker Institute of Nuclear Physics, Novosibirsk, Russia

57: Also at Faculty of Physics, University of Belgrade, Belgrade, Serbia

58: Also at Trincomalee Campus, Eastern University, Sri Lanka, Nilaveli, Sri Lanka

59: Also at INFN Sezione di Pavia $^a$, Università di Pavia $^b$, Pavia, Italy, Pavia, Italy

60: Also at National and Kapodistrian University of Athens, Athens, Greece

61: Also at Universität Zürich, Zurich, Switzerland

62: Also at Ecole Polytechnique Fédérale Lausanne, Lausanne, Switzerland

63: Also at Stefan Meyer Institute for Subatomic Physics, Vienna, Austria, Vienna, Austria

64: Also at Laboratoire d'Annecy-le-Vieux de Physique des Particules, IN2P3-CNRS, Annecy-le-Vieux, France

65: Also at Şırnak University, Sirnak, Turkey

66: Also at Near East University, Research Center of Experimental Health Science, Nicosia, Turkey

67: Also at Konya Technical University, Konya, Turkey

68: Also at Istanbul University - Cerraphasa, Faculty of Engineering, Istanbul, Turkey

69: Also at Mersin University, Mersin, Turkey

70: Also at Piri Reis University, Istanbul, Turkey

71: Also at Adiyaman University, Adiyaman, Turkey

72: Also at Ozyegin University, Istanbul, Turkey

73: Also at Izmir Institute of Technology, Izmir, Turkey

74: Also at Necmettin Erbakan University, Konya, Turkey

75: Also at Bozok Universitetesi Rektörlügü, Yozgat, Turkey, Yozgat, Turkey

76: Also at Marmara University, Istanbul, Turkey

77: Also at Milli Savunma University, Istanbul, Turkey

78: Also at Kafkas University, Kars, Turkey

79: Also at Istanbul Bilgi University, Istanbul, Turkey

80: Also at Hacettepe University, Ankara, Turkey

81: Also at Vrije Universiteit Brussel, Brussel, Belgium

82: Also at School of Physics and Astronomy, University of Southampton, Southampton, United Kingdom

83: Also at IPPP Durham University, Durham, United Kingdom

84: Also at Monash University, Faculty of Science, Clayton, Australia

85: Also at Bethel University, St. Paul, Minneapolis, USA, St. Paul, USA

86: Also at Karamanoğlu Mehmetbey University, Karaman, Turkey

87: Also at Bingol University, Bingol, Turkey

88: Also at Georgian Technical University, Tbilisi, Georgia

89: Also at Sinop University, Sinop, Turkey